CALIFORNIA INSTITUTE OF TECHNOLOGY

EARTHQUAKE ENGINEERING RESEARCH LABORATORY

EXPERIMENTAL INVESTIGATION OF THE NONLINEAR SEISMIC RESPONSE OF CONCRETE GRAVITY DAMS

By

William P. Donlon, Jr.

Report No. EERL 89-01

A Report on Research Supported by Grants
from the National Science Foundation,
a Grant from Bechtel Corporation,
and by the Earthquake Research Affiliates
of the California Institute of Technology

Pasadena, California

1989

This investigation was sponsored by Grant Nos. CEE83-17257 and CES-8619908 from the National Science Foundation, a grant from Bechtel Corporation, and by the Earthquake Research Affiliates of the California Institute of Technology under the supervision of John F. Hall. Any opinions, findings, conclusions or recommendations expressed in this publication are those of the author and do not necessarily reflect the views of the National Science Foundation.

Experimental Investigation of the Nonlinear Seismic Response of Concrete Gravity Dams

Thesis by

William P. Donlon, Jr.

In partial Fulfillment of the Requirements
for the Degree of
Doctor of Philosophy

California Institute of Technology
Pasadena, California
1989
(Submitted January 9, 1989)

To my parents

Acknowledgements

I'll start by thanking my advisor, John Hall, for his patience, encouragement, and friendship. His willingness to devote the time and thought required by these experiments will not be forgotten. I'd also like to thank Professors Hall, Jim Beck, and Paul Jennings, who took the time to counsel me when I was hesitant in the pursuit of this degree. Much of the equipment used in these experiments belongs to the soil mechanics department at Caltech. I'd like to thank Professor Ron Scott, who gave me complete access to that equipment. A special thanks to the James Irvine Foundation, which provided the money needed to build the shaking table facility.

All of the people I've been fortunate enough to develop friendships with while at Caltech have been understanding and supportive. Their friendship made this all worthwhile. In particular, I'd like to thank Janet Blume, Murty Challa, Mike Dowling, Zee and Suzanne Duron, Bahaa El-Aidi, Paul and Linda Nowak, John Riedl, Kris and Laurie Wood, and George Yates. A special thanks to my roommates during my graduate school career: Bill Richards, Sy Shimabukuro, Stewart Silling, and Greg Weidekamp. Thanks also to the Civil Engineering Staff at Caltech, particularly Raul Relles.

There are five people without whom this work could not have been done. This degree is as much theirs as it is mine. My mother, Jeanne, is a source of silent support and is never far from my thoughts. My stepmother, Rita, has provided the love only a mother can give her son. My father's intellectual

curiosity motivated my graduate career, and his encouragement has helped me through the many rough spots. My sister Patricia has supported my independence without condition or hesitation. Mary Pat Sitlington has helped me realize that the people on these pages are the most important thing in my life.

Abstract

The nonlinear seismic response of concrete gravity dams is investigated experimentally through the use of small-scale models. Of primary interest is crack formation, crack opening and closing, and sliding along crack planes. Also of concern is the stability of the structure after cracking. Three small-scale models (length scale = 115) of a single monolith of Pine Flat Dam are tested to determine the extent of such behavior and its effect on structural stability. The models are constructed of one polymer-based and two plaster-based materials developed for these experiments. The plaster-based materials fulfill the strength, stiffness, and density requirements established by the laws of similitude, while the polymer-based material fulfills only the stiffness and density requirements and is used only in the lower part of the dam where cracking is not expected. The excitation is a modified version of the N00E component of the 1940 Imperial Valley earthquake, applied to each model's base in the stream direction through a vibration table with high-frequency capability. Tests are performed with and without water in the reservoir. The response of each earthquake test is presented in the form of acceleration and displacement time histories, Fourier spectra, and frames taken from high-speed films of the model's response. The results of the experiments indicate that the neck region of a concrete gravity dam is most susceptible to cracking, although crack profiles can differ as a result of variations in excitation, material properties, and construction techniques. These results also indicate alternate design techniques

which could improve the seismic stability of a cracked gravity dam.

Table of Contents

Chapter Four

TEST RESULTS

Chapter Five

SUMMARY AND CONCLUSIONS

Chapter 1

Introduction

The consequences of a structural failure of a concrete gravity dam are quite serious. Of primary importance is the possibly large loss of life associated with such a catastrophe. Secondary concerns include the destruction of nearby property, depletion of the area's water supply, and cost of repair attendant with the failure. These consequences demand that this type of structure be designed to safely withstand the most severe loading conditions possible.

Gravity dams built in seismically active areas present a difficult problem. While evidence indicates that a gravity dam can survive moderate earthquake motions, little is known about the response of the dam to severe levels of excitation. Of most concern is cracking of the concrete with subsequent opening and closing of the cracks and sliding along the cracks. Additional damage can be caused by high compressive stresses resulting from impacts during crack closure and from small contact zones during maximum crack opening. It should be mentioned that the occurrence of cracks does not imply complete failure, as demonstrated by the survival of the 338 ft. high Koyna Dam during a magnitude 6.5 earthquake in 1967 (1, 2). The peak ground acceleration in the stream direction reached 0.49g; the duration of strong shaking lasted about 4 seconds; and the water level stood 37 ft. below the crest. After the earthquake, a major crack was noted at a level 120 ft. below the crest, which coincided with the level of slope change on the

downstream face. Seepage from this crack indicated that it extended all the way through the dam. The only other concrete dam known to have suffered cracking as the result of an earthquake is Hsinfengkiang Dam (3), a 344 ft. high buttress dam.

The absence of experience for concrete gravity dams subjected to severe ground motions (say, from a nearby magnitude 7.5 to 8.0 earthquake) has motivated a number of attempts to mathematically model the nonlinear response in order to determine whether or not a gravity dam could remain stable and retain the impounded water during such an excitation. These analyses used a two-dimensional finite element idealization and either a smeared crack representation (4, 5, 6, 7, 8) or a discrete one (9, 10, 11). A summary of this work appears in (8), and the point to be emphasized here is the large amount of variation in the computed behavior of the dam regarding predicted crack locations, orientations, and extents. The implication is that nonlinear earthquake analysis of a concrete gravity dam is not straightforward and is highly uncertain, which motivates, along with the absence of field data, laboratory experiments on small-scale models.

Just two shaking table tests on concrete dam models have been conducted in the U.S. (12, 13), both on a single gravity dam monolith. Only in (12) was attention given to developing a model material which maintained similitude with the prototype. Previous experimental modeling of concrete dams in the U.S. considered only linear response under static loading, and the major requirement of the model material was that it be soft enough to facilitate the measurement of strains and displacements. A plaster-based material with a water-plaster ratio by weight of about 2:1 sufficed (14). Dynamic nonlinear models, on the other hand, require similitude for stiffness, strength, and density and generally must be much softer than those used for static tests, requiring a water-plaster ratio by weight of,

say, 8:1. In addition to (12), information about materials for dynamic nonlinear models of concrete dams ,although sparse, can be found in references from Japan (15, 16), Italy (17, 18), and Russia (19, 20, 21).

The tests performed in (12) were carried out on a single model of a monolith of Koyna Dam and are described in detail in that reference and in (22). With a full reservoir, the model remained stable in the presence of a crack which propagated all the way through the upper section of the dam. Table accelerations exceeded 1g. Most of the foreign tests have been carried out on arch dams (15, 16, 18, 21, 23), with the exception of a three-dimensional model of a concrete gravity dam in a centrifuge (20) and a series of tests on individual gravity dam monoliths in which horizontal construction joints were represented (19). The descriptions of the results from the foreign tests in the listed references are all lacking in detail.

Purposes of the present investigation are to perform more of the tests of the type described in (12) in order to extend the data set, and to improve the experimental technique, such as by the use of a shaking table with better high-frequency capability, by capturing crack propagation with a high-speed camera, and by developing new model materials.

Chapter 2 details the requirements on the model materials established by the laws of similitude, the properties of the system to be modeled, and the model construction technique.

Chapter 3 describes the equipment and procedures used for testing.

Chapter 4 presents the test results.

A summary of the major conclusions and details of possible future work are included in Chapter 5.

Chapter 2

Model Development

2.1 Introduction

Small-scale modeling of the nonlinear dynamic response of concrete gravity dams places unusual demands on the properties of the model material. Although a recipe for a plaster-based material was available (12), difficulty was encountered in reproducing the desired properties. Therefore, a new material development program was carried out, which resulted in three useful model materials. Because the plaster-based materials were prone to shrinkage, construction of the model proved to be difficult and two construction methods were employed. Details of these efforts are described in this chapter.

2.2 Laws of Similitude and Material Development

In order for the behavior of a small-scale model to accurately represent the corresponding behavior of its prototype, or full-scale structure, the model must follow certain laws of similitude. These laws, which are determined by a dimensional analysis of the problem under investigation, are relationships among the dimensionless ratios formed by corresponding parameters of the prototype and model structures. They establish requirements for the materials used to construct the

model and the loading used to excite it.

Physical models are classified as either linear or nonlinear. A linear model simulates the behavior of its prototype structure in the linearly elastic response range only. Consequently, properties such as the compressive and tensile strengths and the associated failure strains do not have to be scaled. The nonlinear model should simulate the response of its prototype through failure. As a result, the stress-strain relations of the model material must be properly scaled from those of the prototype material. In order to model the failure of a concrete gravity dam subjected to earthquake excitation, neglecting foundation interaction but including the reservoir fluid, the following system parameters must be considered: length L, time T, the ground acceleration A, the stress-strain relations of the dam material (represented here by the elastic modulus E_d, the tensile and compressive strengths σ_u^t and σ_u^c, and the tensile and compressive failure strains ϵ_u^t and ϵ_u^c), the bulk modulus of the reservoir fluid E_f, the mass densities of the dam and the reservoir fluid ρ_d and ρ_f, the vapor pressure of the reservoir fluid P_f, the gravitational acceleration g, and the atmospheric pressure P. The similitude relations generated by a dimensional analysis of this problem, involving the above parameters, can be written as:

$$\frac{S_r T_r^2}{\rho_r L_r^2} = 1 \tag{2.1}$$

$$\frac{A_r T_r^2}{Lr} = 1 \tag{2.2}$$

$$A_r = G_r \tag{2.3}$$

$$\epsilon_r = 1 \tag{2.4}$$

where

$$S_r = \frac{P_p}{P_m} = \frac{E_{dp}}{E_{dm}} = \frac{E_{fp}}{E_{fm}} = \frac{\sigma_{up}^t}{\sigma_{um}^t} = \frac{\sigma_{up}^c}{\sigma_{um}^c} = \frac{P_{fp}}{P_{fm}} \tag{2.5}$$

$$\rho_r = \frac{\rho_{dp}}{\rho_{dm}} = \frac{\rho_{fp}}{\rho_{fm}} \tag{2.6}$$

$$T_r = \frac{T_p}{T_m} \tag{2.7}$$

$$L_r = \frac{L_p}{L_m} \tag{2.8}$$

$$A_r = \frac{A_p}{A_m} \tag{2.9}$$

$$G_r = \frac{g_p}{g_m} \tag{2.10}$$

$$\epsilon_r = \frac{\epsilon^t_{up}}{\epsilon^t_{um}} = \frac{\epsilon^c_{up}}{\epsilon^c_{um}} \tag{2.11}$$

and where p denotes prototype and m denotes model. Response parameters scale as follows: L_r for dam displacement, A_r for dam acceleration, and S_r for dam stress and fluid pressure. In the experiments carried out here, $G_r = 1$ and equation 2.3 becomes

$$A_r = 1 \tag{2.12}$$

which, from equation 2.2, leads to

$$T_r = \sqrt{L_r}. \tag{2.13}$$

From equations 2.1 and 2.13,

$$S_r = \rho_r L_r. \tag{2.14}$$

Equation 2.5 indicates that the standard atmospheric pressure should be reduced by the pressure scale S_r in the model environment. This requirement also applies to the bulk modulus and vapor pressure of water, the prototype reservoir fluid. Because the density of most 'heavy' fluids is no more than a factor of two greater than that of water, S_r can be significant for small-scale models. Consequently, the requirements of equation 2.14 for the vapor pressure and bulk modulus of the model fluid and for the atmospheric pressure in the model environment cannot be met. This results in a model fluid that represents an incompressible fluid

that cannot cavitate. Such is the case in these experiments, in which water is the model reservoir fluid. The use of water as the reservoir fluid also establishes the density scale ρ_r as one, which requires that the material used to construct the model dam have a density equivalent to that of concrete. Regarding the absence of cavitation in the model fluid, the use of a membrane in the model between the dam and the water (as discussed later) allows separation along the dam-membrane interface whenever the water pressure reduces to atmospheric pressure. This phenomenon should be a reasonable representation of prototype cavitation (12).

The selection of a length scale L_r is typically based on the size of the prototype structure and the capabilities of the testing facility. The length scale for the present experiments is 115 which, when substituted into equation 2.14 with $\rho_r = 1$, results in a value of 115 for S_r. From equation 2.5, the model dam material must possess a modulus of elasticity, compressive strength, and tensile strength which are a factor of 115 less than the prototype concrete. Equations 2.4 and 2.11 state that the compressive and tensile failure strains of the prototype and model materials must be equal. Table 2.1 lists typical values for properties of mass concrete, the associated scale factor, and the target values for the model material.

A significant amount of work on the development of a plaster-based material with properties similar to those desired has been done at the University of California, Berkeley (UCB) (12). The result of that research was a mixture of plaster, water, sand, lead powder, and celite with the constituent ratios given in Table 2.2 and the final properties shown in Table 2.3. For comparison, a typical plaster of paris has an initial water:plaster ratio (w:p) of 0.5:1 by weight, a modulus of elasticity near 1,000,000 p.s.i., a density of 75 p.c.f., a compressive strength of 2,000 p.s.i., and a tensile strength of 400 p.s.i. The initial w:p governs the final strength and stiffness of the material, with an increased w:p decreasing the tensile and

compressive strengths as well as the elastic modulus. Sand is believed to increase the modulus of elasticity without affecting the strength of the mix. The addition of lead powder not only augments the density of the material, but also establishes a lower bound for its Young's modulus. Celite is used to control workability by absorbing excess water and decreasing the fluidity of the material.

Comparison of the model material target values and the properties attained by the UCB material indicates that the latter are close to the values required here. Thus, initially, a series of tests was conducted on plaster-based materials with the same components as the UCB mixture and similar component ratios. Test specimens were typically mixed for ten minutes and cast in aluminum or steel cylindrical molds which had been treated with silicone spray in order to facilitate the release of the specimen from the mold. Specimens were dried for 24 hours at 110 F and were released from their cylinders after the first five hours. The diameter of the test specimens varied from 1.5 to 2.0 inches, while the length:diameter ratio varied from 2.0 to 3.0. Uniaxial compression tests were used to determine the Young's modulus and compressive strength of the material, while split cylinder tests were used to measure its tensile strength. Tensile failure strains were not measured during these tests, and recorded compressive failure strains were considered unreliable due to crushing at the point of load application. Loads were applied slowly and so did not include strain-rate effects.

Four specimens were cast with constituent ratios identical to those of the UCB mix. The binding agent employed was a twenty-minute casting plaster manufactured by U.S. Gypsum and the sand used was Nevada 120, with a grain diameter of less than 0.15 millimeters. Testing indicated that the cylinders were substantially stronger than desired with a compressive strength of over 110 p.s.i. and a tensile strength of over 28 p.s.i., values which represent the limit of the testing

equipment's capabilities. Further investigation attributed the large strength to the lead powder (Pb), which apparently possesses binding properties in the presence of water. Subsequently, it was found that this binding did not occur with lead oxide powder (Pb_3O_4), and an extensive cylinder testing program was initiated with the same constituents as before but with Pb_3O_4 replacing Pb. Concern over the segregation of the lead resulted in a small grain size being chosen (99% of the powder had a grain size less than 0.044 mm). Also of concern were the consistency of the mix, and the time of set. Bleeding proved not to be a problem, so celite was eliminated. A great number of tests arrived at the constituent ratios displayed in Table 2.2 producing the material properties in Table 2.3 (Caltech 1). The material consistently achieved these properties over many cylinders. Comparison of these properties to the target values (Table 2.1) reveals that the modulus of elasticity and compressive strength are less than required, while the tensile strength is greater than required. These differences were considered acceptable. The consistency of the material after mixing was excellent and little segregation of the lead oxide powder occurred.

The above discussion has included the tensile strength of the dam material, which is the major material property affecting crack initiation, but has omitted other material properties which govern crack propagation, such as the critical mode I stress intensity factor K_{IC}. Linearly elastic fracture mechanics, which is believed to be valid for fracture processes in concrete dams (9, 24, 25, 26), holds that when the amplitude of the stress singularity at a sharp crack tip (the stress intensity factor, say, K_I for mode I) reaches a critical value (say, K_{IC} for mode I), crack extension occurs. Thus, material parameters such as K_{IC} should be properly scaled between prototype and model; otherwise, incorrect extents of cracks in the model may result. Units of K_{IC} are force per unit length to the 1.5, so the scaling

factor, denoted by K_r, is

$$K_r = L_r^{1.5} \tag{2.15}$$

following the previous analysis with $G_r = 1$. With $L_r = 115$ as for the present experiments, $K_r = 1{,}233$, a large value. No mention of this parameter in previous work on concrete dam modeling has been made, and, consequently, nothing is known about the fracture mechanics of plaster-based materials. In fact, an appropriate value for K_{IC} for dam concrete is not even available (24, 25, 26). No fracture tests have yet been conducted on the plaster-based model material described previously.

The plaster-lead oxide powder mixture does possess some undesirable characteristics. Lead oxide powder (and lead powder as well), when ingested in large enough quantities, attacks the human nervous system and can prove fatal. Consequently, respirators must be used when working with this substance. Saturation of the sand and lead oxide powder is difficult, making thorough mixing an arduous procedure. The fineness of the dry constituents decreases the void size of the mixture, which increases the amount of time required for the model to dry. Releasing the set material from a mold can be difficult; vaseline seems to be the most effective release agent for both wood and metal molds, but some bonding and loss of material from the model surface inevitably occurs. Wood molds must also be treated with a waterproofing agent such as form oil. Even after such treatment, wood molds are generally not reusable because water absorption causes warping of the wood. Finally, shrinkage on the order of 3% occurs as a result of water evaporation. This shrinkage is the single most undesirable characteristic of the mixture.

Because of the hazard associated with the fine lead oxide powder, a second

material with the model target properties was developed. This material combined lead (Pb) pellets (diameter of 1.6 millimeters) with plaster, water, sand, and celite. Contact between the lead pellets was slight and no effects of the undesirable binding were noted. The water:plaster ratio required was reduced to 6.5:1 from the 8.5:1 ratio for the lead oxide powder mixture, with the benefit that the amount of water lost during drying through evaporation and the resultant shrinkage was reduced. The shrinkage of this material is less than 2%, a substantial reduction of the 3% value associated with the plaster/lead oxide powder mixture. Surprisingly, no significant segregation of the lead pellets occurred. Tables 2.2 and 2.3 display the component ratios and final properties of this material (Caltech 2), respectively.

2.3 Model Geometry and Construction

The dam chosen as the prototype structure is Pine Flat Dam, a concrete gravity structure located on King's River near Fresno, California. Figure 2.1 shows the downstream elevation view of Pine Flat and a cross section of the highest non-overflow section. This dam was selected because its dimensions are typical of large gravity dams and because it has been the subject of several numerical studies as well as two sets of field tests performed in 1971. Pine Flat Dam is separated into vertical monoliths by vertical contraction joints running the height of the dam and placed at approximately 50 foot intervals along its length. The joints do not contain mortar, nor are they shear keyed, and experimental evidence indicates that some independent vibration of the monoliths occurs when they are subjected to low levels of excitation in the upstream-downstream direction (27). Consequently, it is assumed that they will respond individually to moderate and severe ground motion in this direction. This assumption provides some justification for testing

of a single monolith rather than the entire dam. The taller, nonoverflow monolith was chosen because it would be the most highly stressed during an earthquake and because the region of the neck has a high potential for cracking. The cross section shown in Figure 2.1 gives the dimensions of the monolith to be modeled. The model was to be placed on a 36- by 44 in. vibration table, which would apply the excitation motions to its base. A length scale of 115 was chosen to ensure that the table could accommodate the size and weight of the model, and resulted in a base dimension of $33\frac{1}{8}$" for the model dam. The model dimensions are shown in parentheses in Figure 2.1.

The model was made by mixing 2.25 cubic feet of the plaster/lead oxide material and pouring it into the wooden mold shown in Figure 2.2. The pouring and mold-removal processes governed the design of the mold. Originally, the pouring, setting, and drying stages were carried out with the mold in the horizontal position. However, cracking occurred on the bottom face of the model during drying and necessitated the development of an alternate technique. In the new process, the material was poured into the horizontal mold, which was then covered and sealed, rotated to its vertical position, and placed on the table. Thus, the setting and drying stages occurred while the model was on the table in the vertical position. The compressive stresses generated by the weight of the material reduced the possibility of horizontal shrinkage cracks, although such cracks could still form if the material stuck to the mold. The prevention of this sticking is particularly important for the upper third of the model, because the cracking induced by the dynamic loading is expected to occur in this area. The only sure way to prevent shrinkage cracks in this region is to reduce the contact with the mold. This was possible because the upper portion of the model set reasonably quickly, much faster than the lower two thirds, due to the large amount of material at the base of the

model. Thus, the mold was constructed so that the top part could be removed or pealed back, while still providing support to the lower portion of the model. This design also facilitates the drying process by allowing more contact with the air.

Due to the large water:plaster ratio, the setting and drying processes required a large amount of time. At room temperature, three to four weeks were needed for a complete set; i.e., for the model to gain enough strength to maintain its own shape. During this period, the sides of the mold remained in place to provide stability to the model. A thin wire was passed between the model and these sideboards in order to prevent the material from hanging up. Unfortunately, this procedure did not prevent the occurrence of shrinkage cracks, which originated at the base and propagated upward. Such cracks were revealed after the model had set and the sideboards had been removed, and, during the subsequent drying process, they grew to a width of $\frac{1}{8}$" and extended up to 18" vertically from the base. Figure 2.3 shows the extent of cracking in one of the earlier models. The cracks were caused by the friction developed between the wooden base of the mold and the model. This friction prohibited shrinkage from occurring along the base, and the resulting tensile stresses caused cracking. While the upper portion of the dam remained crack free, the vertical shrinkage cracks were too large to ignore, and several modifications were implemented.

In order to provide more freedom for movement over the base of the mold, an aluminum plate was placed over this base and covered with a 0.004 in. thick sheet of teflon. If the material bonded to the teflon sheet, the sheet would wrinkle and slide over the aluminum plate as shrinkage occurred. If bonding did not take place, the material would slip over the teflon sheet as the model shrank. Although this technique still restrained shrinkage enough to initiate vertical cracks during the setting stage, they were smaller than before. These cracks were filled

with Duco cement, and, to prevent further opening during the drying process, aluminum plates were placed on the upstream and downstream faces of the model and tightened against the model with threaded rods (Figure 2.4), putting the dam in a state of horizontal compression. The drying process required about three weeks, during which time the model was wrapped in plastic sheeting and kept at a temperature of 95 F. The plates needed tightening periodically during the drying, but caution was necessary to prevent overstressing of the model in the contact regions.

Using the above technique, the time between the pouring stage and testing was 6-7 weeks. This fact, coupled with the shrinkage crack problem at the base, led to the development of a composite model. Because the cracking caused by the dynamic loading was expected to occur within the upper half of the model(8), the material strength did not have to be represented in the lower half, which could be made of a material that satisfied the modulus and density requirements only. This lower half would effectively transmit the table motion to the top half of the model, which would be made of a plaster-based material. The plaster portion was cast in the same manner as the complete model, with the horizontal mold being covered, sealed and rotated into a vertical position after pouring. However, due to its reduced size, the setting and drying stages required much less time. Shrinkage was less of a problem, and the smaller plaster portion fit into an available oven. After drying, the top half of the model was epoxied to an aluminum plate and bolted to a second aluminum plate that had been fixed to the top of the bottom half (Figure 2.5).

The material developed for use in the lower half of the model was an epoxy-based compound. The polymer, Epoxylite Corporation's 8181-42, derives its strength from a chemical reaction between its two components, which are orig-

inally in liquid form and are mixed in a 1:1 ratio by volume. One constituent is an epoxidized oil containing aluminum oxide and barium, the other a polymerized fatty acid containing aluminum oxide and barium sulphate. In its liquid state, the epoxy is easily poured into a mold, and a chemical releasing agent simplifies mold removal. The material has a modulus of elasticity of approximately 5,000 p.s.i., a weight of nearly 150 p.c.f., and strengths well above the model target values. In order to increase the modulus of this material, glass beads 3 millimeters in diameter were added in a ratio of 20:1 by volume to the epoxy. The same lead pellets used in the plaster mixture were added to the polymer in a ratio of 2:1 by volume to compensate for the reduction of density caused by the inclusion of the glass beads. At room temperature, this compound cures in three to four days with minimal shrinkage. One objection to the epoxy base is its viscoelastic nature, which results in a material damping higher than that of concrete.

The model reservoir was a 72" by 46" by 5.25" wooden tank supported by eight posts placed off the vibration table on a concrete slab. The reservoir was also supported by a steel wire rope running from the top of the tank to the stationary base of the vibration table. This rope offset the horizontal force on the reservoir created by the reaction of the model to the hydrostatic pressure. The open end of the reservoir was placed several inches from the model's upstream face to allow for movement of the model. Plates were attached to the outsides of the reservoir and projected from this end past the upstream face of the model, creating a reservoir width of 6.75" in this area. These plates were made of aluminum over the lower half of the reservoir but of Plexiglas above so as not to obstruct filming of the model's response. To prevent water seepage from the wooden tank, flow out the open end of the tank around the model, and water damage to the plaster-based model material, the wooden tank was lined with a 0.004 in. thick polyethylene

membrane. Near the dam, this membrane was supported on the sides by the aluminum and Plexiglas plates and below by a rubber belt mounted beneath the reservoir. Enough slack was present in the membrane off to the sides at the upstream face of the dam so that the dam could retreat well over an inch from the reservoir without any loss of contact between the membrane and the dam face. Figure 2.6 shows a complete model dam-reservoir system, and Figure 2.7 is a plan sketch near the upstream face of the dam. It is important to note that the presence of the membrane prevents water from entering cracks during the times they are open at the upstream face, and that little is known about the extent to which water could penetrate such cracks. The presence of uplift pressure in the cracks would have a destabilizing effect on the portion of the dam above.

Property	Prototype Value	Scale Factor	Target Value
E	4,000,000 p.s.i.	115	35,000 p.s.i.
σ_u^c	4,000 p.s.i.	115	35 p.s.i.
σ_u^t	400 p.s.i.	115	3.5 p.s.i.
ρ	150 p.c.f.	1	150 p.c.f.
ϵ_u^c	0.0025	1	0.0025
ϵ_u^t	0.00012	1	0.00012

Table 2.1: Assumed concrete properties, the associated scale factors, and the model material target values.

	Parts by weight to one part of plaster		
Component	UCB	Caltech 1	Caltech 2
Water	10	8.5	6.5
Sand	12	20	12
Lead	24.12	-	17
Lead Oxide	-	25	-
Celite	2.2	-	2.25

Table 2.2: Constituent ratios of model materials.

Property	UCB	Caltech 1	Caltech 2
E (p.s.i.)	46,000	28,500	31,000
ρ (p.c.f.)	146	155	156
σ_u^c (p.s.i.)	27.3	28.0	18.6
σ_u^t (p.s.i.)	3.3	5.0	3.4

Table 2.3: Properties of model materials.

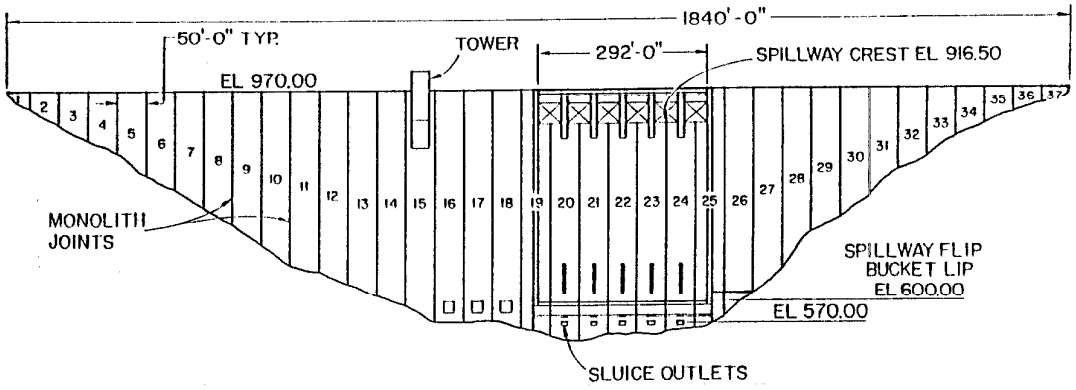

Figure 2.1: (a) Downstream elevation of Pine Flat Dam (from reference 27).

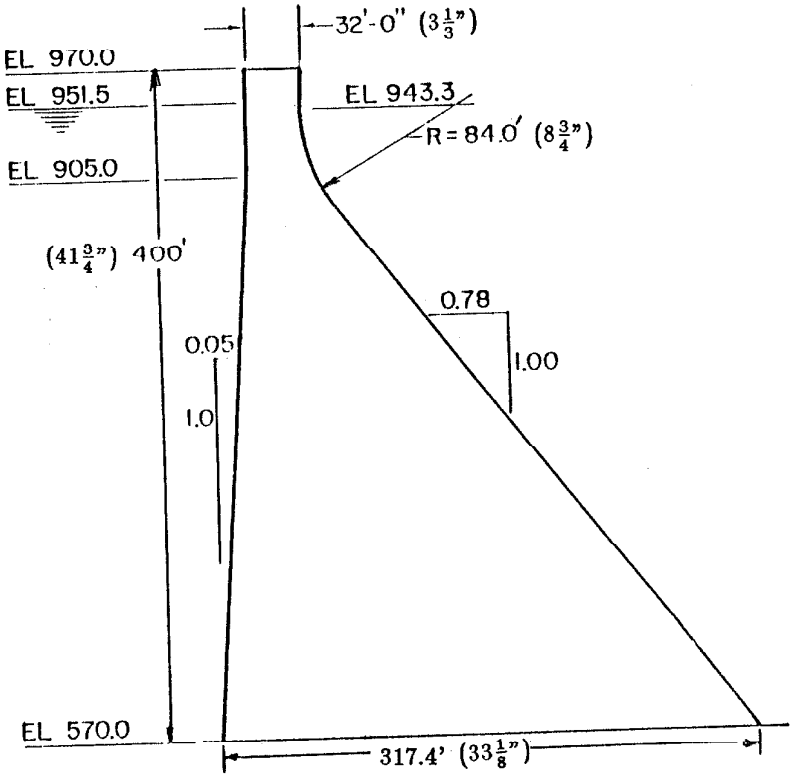

Figure 2.1 :(b) Cross-section of Pine Flat Dam, monolith 18 (from reference 29).

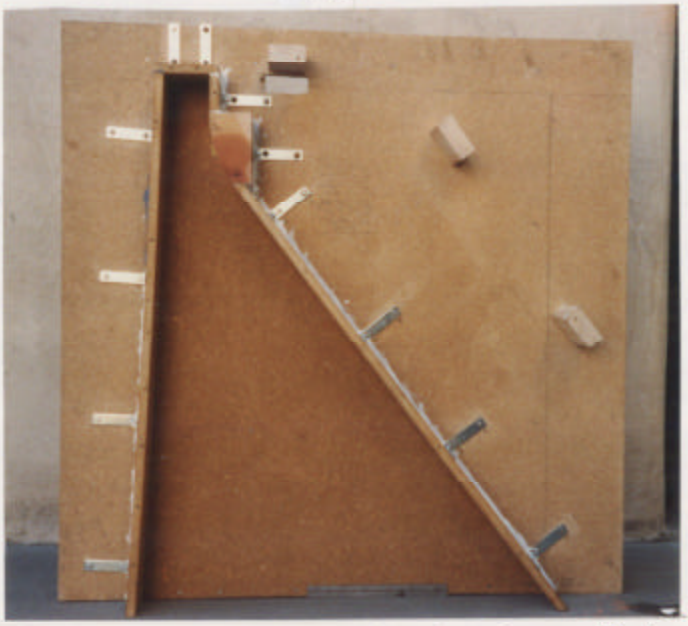

Figure 2.2: Wood mold used as form for model dam.

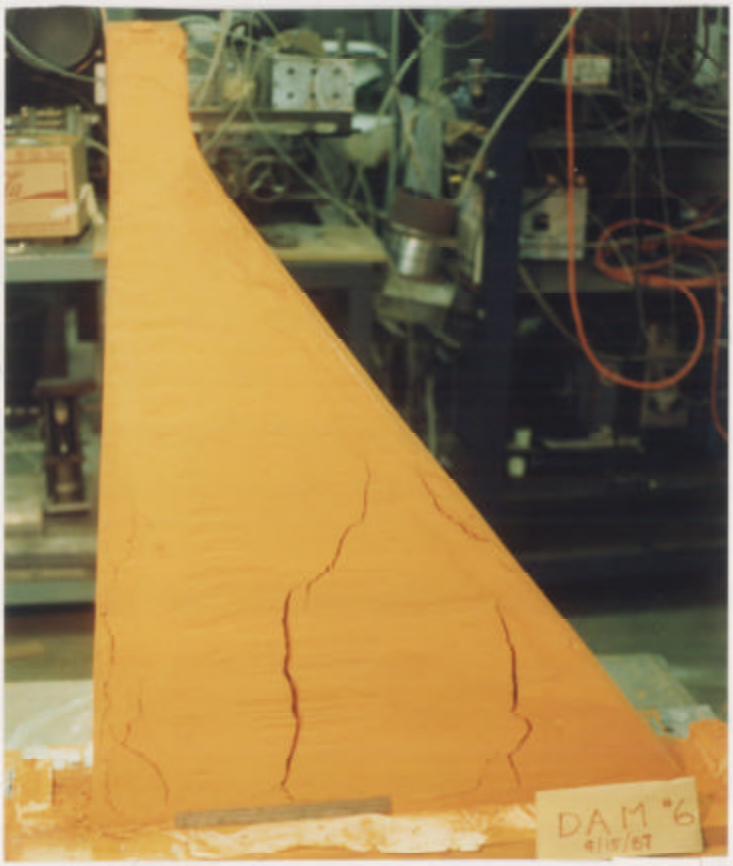

Figure 2.3: Shrinkage cracks on earlier model.

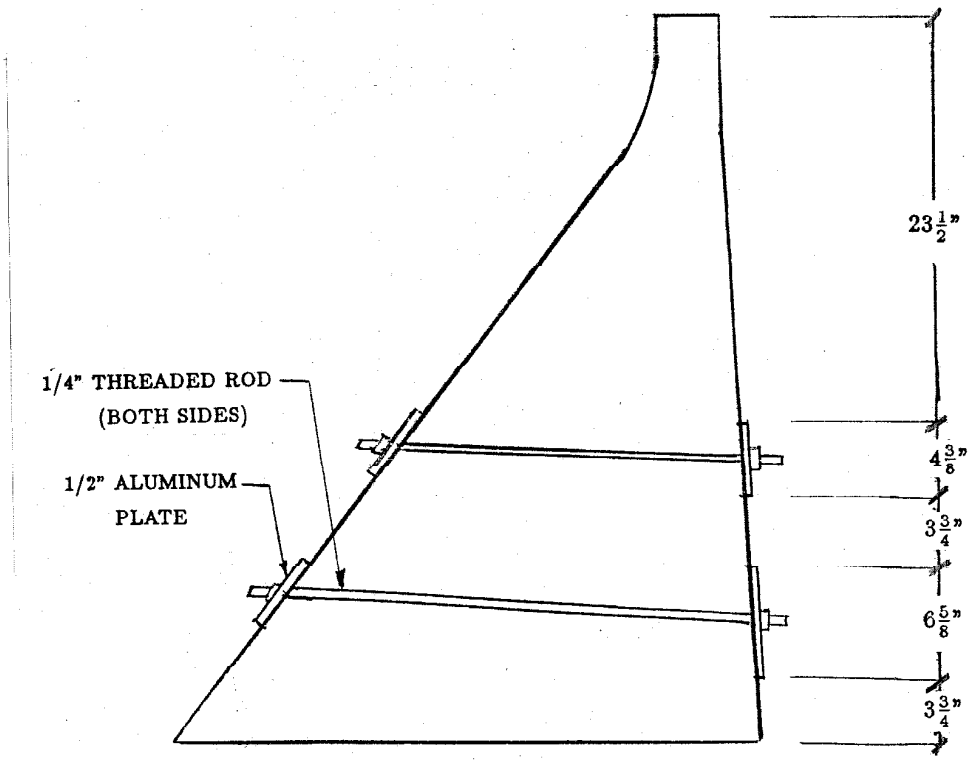

Figure 2.4: Placement of compression plates to restrict shrinkage crack growth.

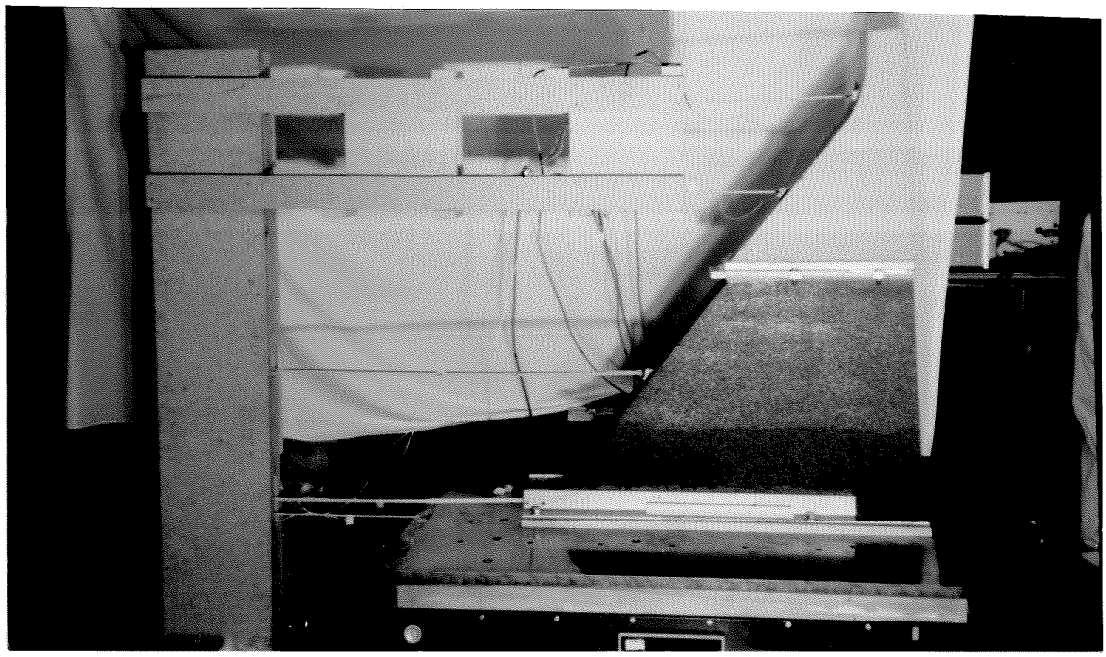

Figure 2.5: Composite model jointed at mid-height.

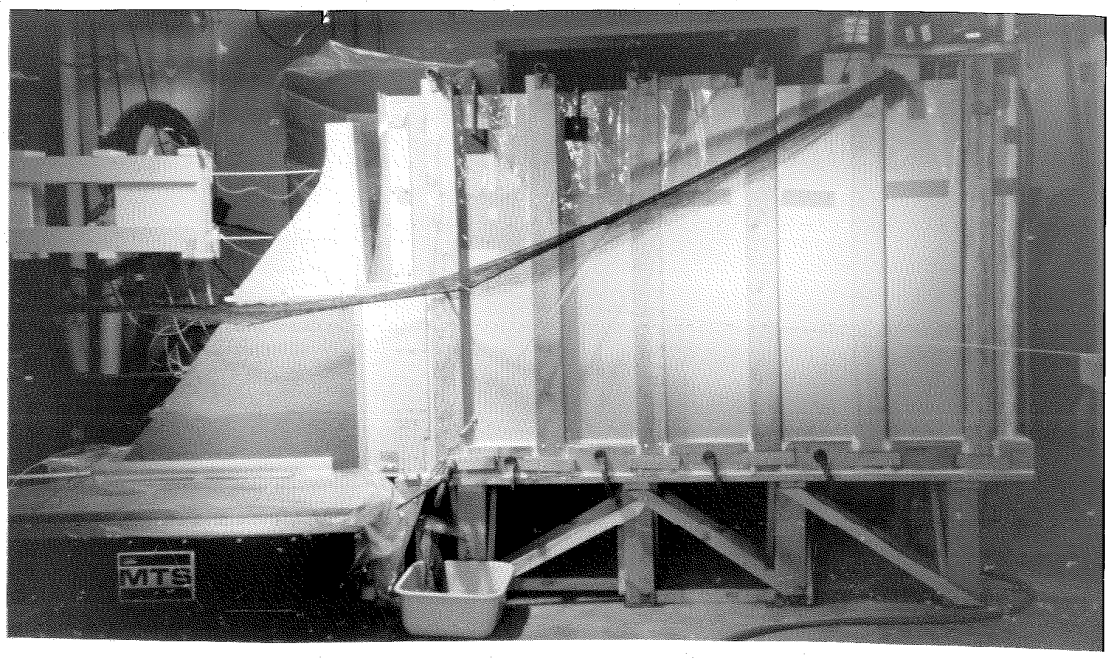

Figure 2.6: Model dam-reservoir system.

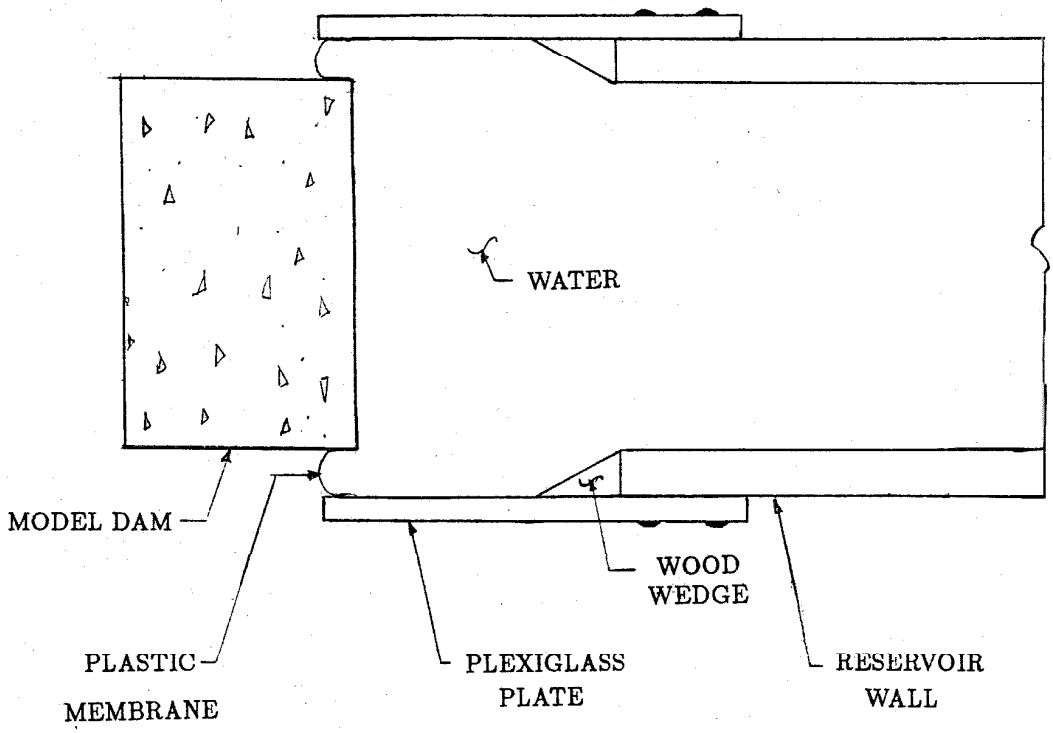

Figure 2.7: Plan view of dam-reservoir interface at top of model.

Chapter 3

Experimental Procedure

3.1 Introduction

Dynamic field tests of full-scale structures typically employ two types of excitation. In resonance testing, also known as frequency sweeps, harmonic loads from vibration generators are used to determine dynamic properties. Ambient tests employ naturally occurring random excitations such as wind or wave loadings. In both cases, the amplitude of excitation is low and the response of the system is linear.

Model testing allows a larger variety of excitations, and shaking tables can be used to simulate earthquake loadings. Amplitudes of the excitation can be selected to elicit linear or nonlinear responses. The shaking table used for the present investigation has a high-frequency capability, which is necessary for testing models that, for reasons of economy, must be tested at a very small scale, such as concrete dams.

3.2 Apparatus

An MTS unidirectional servohydraulic vibration table delivered one horizontal component of ground motion to the model. The table consists of a 36" by 44"

steel plate supported by two granite blocks, each of which is enclosed in a steel case. A thin layer of hydraulic fluid between the granite and steel provides a surface of minimum friction to facilitate table motion. The table is driven by a 3" diameter piston mounted directly beneath it. The piston is capable of producing 3300 pounds of dynamic force over a frequency range of 0-150 Hz with a 3" peak displacement amplitude. Movement of the piston results from the porting of hydraulic fluid pressurized to 3000 p.s.i. Porting (and, consequently, table motion) is controlled by circuitry in the dynamic response controller, which can be operated in acceleration or displacement control modes. Under acceleration control, excitation waveforms are maintained by comparison of the rms value of the input signal to the rms value of the table motion, which is monitored by system accelerometers. The error signal generated by this comparison is applied to a servovalve, which attempts to compensate for discrepancies by modifying the flow of hydraulic fluid to the piston. Results in Chapter 4 will illustrate how well an input waveform is reproduced. Two sources provided the signals used to drive the table, depending on the type of test being carried out. A Hewlett-Packard function generator produced sinusoidal signals for the frequency sweeps, while a computer controlled digital-to-analog converter (DAC) was used for the earthquake excitations. This DAC, designed and built at Caltech, can convert digitized signals to their analog form at a maximum rate of 200,000 samples per second. The function generators were controlled manually, while a Zenith 120 personal computer initiated the earthquake tests through interactive software and output signals to the DAC.

Acceleration and displacement transducers were used to record the model's dynamic response. Entran accelerometers were selected because of their size and frequency response characteristics. They possess a flat frequency response to 250 Hz, measure 0.27" x 0.14" x 0.14", and weigh 0.5 grams. The particular accelerom-

eters employed had full scale ranges varying from 10 to 500g and outputs varying from 0.5 to 12 millivolts per g. Schaevitz linear variable differential transformers (LVDT) were utilized as displacement transducers. The frequency range of these devices is 0 - 1 kHz, and, for a full scale range of +/- 0.5", the output averages 6.10 volts per inch. An LVDT with a range of +/- 1.0" and an output of 4.56 volts per inch was also used.

The accelerometer signals initially passed through an 8 channel amplifier with selectable gains ranging from 1 to 1500. They were then transferred to a high pass filter to eliminate any DC voltage component. The conditioned signals are sent through a second amplification stage and another high pass filter before entering an analog-to-digital converter (ADC). The displacement signals passed through a single, independent conditioning stage, which included amplification and high pass filtering, prior to entering the ADC. The ADC is a 16 channel, 12 bit integrated circuit design with a maximum sampling rate of 28,570 samples per second. Full scale output of the ADC is selectable and corresponds either to +/- 2.5 volts or +/- 5.0 volts. The output of the ADC is stored in computer memory and written to a 5.25" floppy disk. The data sampling and storage are accomplished simultaneously with the output of the excitation on the same Zenith 120.

Two methods were tried for recording crack initiation and propagation in the model. The first used strips of nickel print, a conductive paint that was applied to the surface of the model dam perpendicular to the probable path of crack propagation. The Zenith computer was set to monitor a small current flowing through each strip and to record the time when the current stopped, which, hopefully, would be due to breakage of the strip caused by the propagating crack. However, tests of an early model (not one reported on here) showed that the nickel

strips could span a crack of enough width so that the propagation information was not captured. Thinning of the nickel by a solvent (toluene) was also tried, but current stoppages were then detected under tensile strains not associated with cracking, probably due to microcracking in the strips. Consequently, the method was abandoned.

The second method was high-speed photography and employed two 16 millimeter cameras. The primary camera was a Photosonics 1P placed approximately seven feet from the model, photographing the region of the neck of the dam on a flat side which represents a joint plane. At this distance the field of vision includes 8.5 vertical inches, and the intent of this close positioning was to capture details of the crack initiation and growth. The second camera, a Redlake Locam, was located 8 ft. behind the primary camera. Cracking would be more difficult to discern from this distance, but the relative motion of the portions of the model separated by the crack would be more clearly visible. The frame rate of the primary camera was 180 frames per second (f.p.s.), that of the secondary camera 500 f.p.s. Filming was initiated manually prior to excitation, but computer control of the cameras is available. The resulting 16mm films are believed to be the first high-speed visual records of the cracking and post cracking behavior of a dam model.

3.3 Testing Procedures

Tests were performed on three separate models. The first was made entirely of the plaster/lead oxide material (the monolithic model). Frequency sweeps and earthquake tests were carried out on this model without a reservoir. The remaining two models were composites with the bottom half made of the polymer, glass,

and lead-pellet compound previously described. The upper half of one of the composites was also made of the plaster/lead oxide mixture, while the upper half of the other was made of the plaster/lead-pellet material. Frequency sweeps were carried out on these models with an empty and a full reservoir; most of the earthquake tests used a full reservoir. In the "full" reservoir, the water level was maintained two inches from the top of the model dam. All excitations were applied in the upstream-downstream direction. All of the tests were carried out with the base of the model dam fixed to the table. Although some sliding and opening along the base could occur during a strong earthquake, numerical studies indicate that nonlinear behavior in the upper part of the dam, especially in the region of the neck, is more important regarding potential instability of the structure (8).

The first stage in the dynamic testing of each of these models was the determination of the model's natural frequencies and damping by means of a frequency sweep. These sweeps were conducted with the table under acceleration control; i.e., the controller maintained a selected table acceleration amplitude while the frequency was varied over the range of interest. A sine wave was fit to the model's digitized response data by a least-squares algorithm developed at Caltech (28). The algorithm outputs the exact frequency of excitation, acceleration and displacement response amplitudes, and phase differences between responses and the excitation. With this information, frequency response curves and mode shapes can be constructed.

In the test on the monolithic model, four accelerometers were placed on the upstream face at distances of 5.625", 13.812", 30", and 41.5" from the top of the model (points 1, 2, 3, 4 in Figure 3.1). The time history recorded by the last of these was considered to be the base motion of the model. Displacement transducers were also placed on the upstream face at the same levels as the accelerometers.

A fifth LVDT monitored the displacement of the table directly. For the tests on the composites, where the reservoir structure was present, the transducers were placed on the downstream face at the same elevations with the exception of the accelerometer at point three, which was omitted. For the monolithic model, the excitation amplitude was 0.015g and the frequency range was 15-110 Hz. All tests on the composite models were carried out at a base acceleration of 0.04g with a similar frequency range. The response of each of the models during the frequency sweeps should have been well within the linear range.

The second stage of testing, which used the same instrumentation as the frequency sweeps, subjected the model to earthquake-like time histories. A low-level excitation was followed by a high-level one sufficient to cause cracking. Further tests on the cracked model were then carried out to investigate its stability. The ground motion chosen was the N00E component of the 1940 Imperial Valley, California, earthquake, since its frequency content is representative of California earthquakes and since it has been used as the excitation in several numerical studies of concrete gravity dams. The digitized acceleration time history contained 2688 acceleration points at an interval of 0.02 seconds, resulting in a duration of 53.74 seconds. The time scale was compressed by a factor of 10.72 before application to the model. Linear interpolation between existing data points resulted in 8192 acceleration values used in the digital to analog conversion process. The ADC sampled 65,520 total points, with a D to A conversion (excitation output) occurring every eight samples. A total of 9 channels (4 accelerometers and 5 LVDTs) were sampled during the tests on the monolithic model, resulting in 7,280 points per channel and a Nyquist frequency of 728 Hz. Tests on the composites used only eight channels, resulting in 8,190 data points and a Nyquist frequency of 819 Hz. All 60 Hz electrical noise contained in the recorded signals was filtered in the

postprocessing by zeroing this component in the signal's Fourier transform. The inverse transform then provided a time history free of the 60 Hz noise.

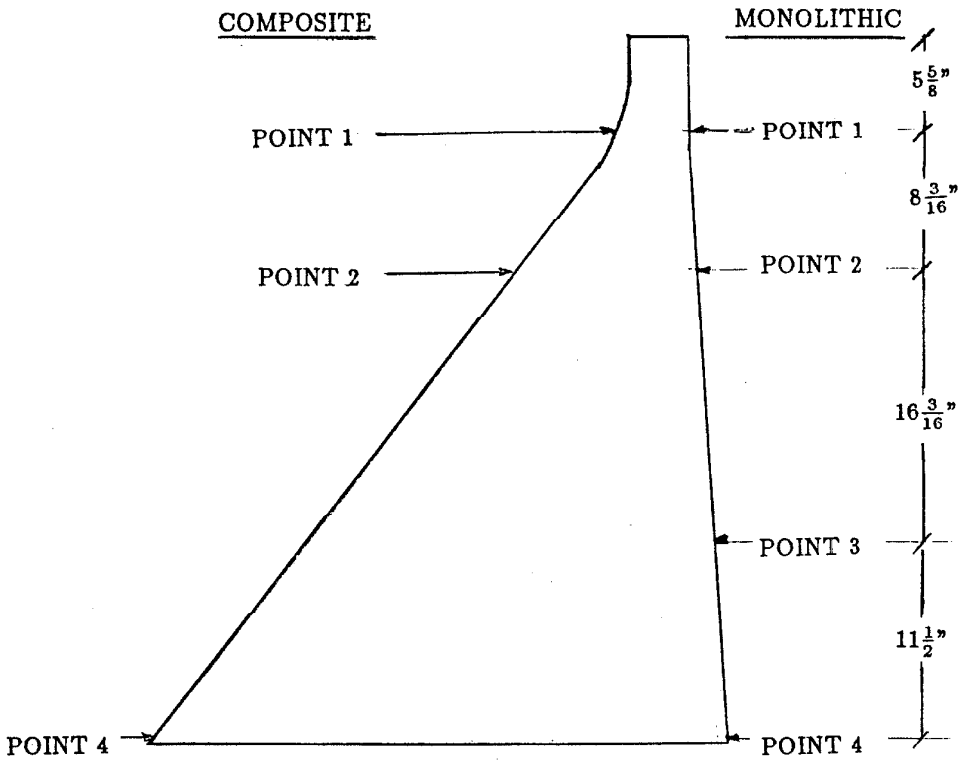

Figure 3.1: Sketch detailing positions at which the model dam's response was monitored for the monolithic (right-hand side) and composite (left -hand side) models.

Chapter 4

Test Results

4.1 Introduction

This chapter presents the results of the shaking table tests on three models of a single nonoverflow monolith of Pine Flat Dam. Included are results from the frequency sweeps and the earthquake tests; the latter typically include time histories of the actual base acceleration, the response acceleration at point 1 and the relative displacement between point 1 and the base, as well as Fourier transforms of the base and point 1 accelerations, photos of the posttest crack state, and prints of some of the film frames at specific instants of time. Recall that model displacements scale as $\frac{1}{115}$ those of the prototype, model and prototype accelerations are the same, and the model time scale is compressed by a factor of 10.7. All recorded displacements and accelerations are horizontal components (upstream direction positive).

It is important that the frequency and damping of the fundamental mode of the model approximate those of the prototype. Data on Pine Flat Dam is available from previous forced vibration tests (27). With a water level 90 feet below the crest, the fundamental resonance occurred at about 3.47 Hz with damping around 3% of critical. Results of a two-dimensional mathematical model (30) indicate that this frequency is less than the fundamental frequency with empty reservoir

by about 5%, which puts the latter at 3.65 Hz. An estimate for the full reservoir case (water level 20 feet below the crest, which corresponds to the full model condition) from the results of (30) comes to about 2.92 Hz (3.04 Hz if water compressibility is neglected). Thus, reasonable target frequencies for the model would be 39 Hz with empty reservoir and 33 Hz with full reservoir; the latter uses the incompressible water value since water compressibility does not scale, and is 15% below the empty reservoir frequency. It should be noted that higher modes of the model will not correspond to those observed during the forced vibration tests on Pine Flat Dam because of the large effect of three-dimensional action on the higher modes of the prototype.

4.2 Monolithic Model

This model was constructed entirely of the plaster-based model material (lead oxide powder) and was subjected to a frequency sweep and several earthquake tests, the last two of which involved nonlinear behavior. The reservoir was omitted in all cases. In order to maintain the integrity of the lower part of the dam where some vertical shrinkage cracks had been repaired, the compression plates (Figure 2.4) were left on during the tests.

4.2.1 Frequency sweep (Figure 4.1)

Frequency response curves for the model (Figures 4.1(a) and 4.1(b) for points 1 and 2, respectively) indicate a fundamental frequency of 37.7 Hz (3.51 Hz prototype) and a second natural frequency of 96.4 Hz (9.01 Hz). Damping coefficients were determined by the half-power method as 3.8% of critical and 2.8% of critical, respectively. The frequency and damping of the fundamental mode are close to

the field measured values mentioned above. The absence of a second resonance for point 2 (Figure 4.1(b)) is due to the proximity of a node in the mode shape at the transducer location.

4.2.2 Low-level earthquake tests (Figures 4.2 through 4.7)

As previously mentioned, the acceleration input to the table was the N00E component of the 1940 Imperial Valley earthquake with its time scale compressed by a factor of 10.7 and its amplitude adjusted variously. The first three seconds of this time history, together with its Fourier transform, appear in Figure 4.2 (amplitude scale of one). An initial test at a low enough level to produce only linear behavior resulted in the actual table motion shown in Figure 4.3. The Fourier transform, also shown in the figure, is depressed in the vicinity of the fundamental frequency of the model dam (31 to 48 Hz). This undesirable behavior was attributed to inadequacy in the table control capability and was remedied by increasing the frequency content in this frequency interval. The Fourier transform of the original input was multiplied by the function shown in Figure 4.4 which, after an inverse Fourier transform, yielded the modified table input time history shown in Figure 4.5. This time history was used to drive the table in subsequent tests, including a second low-level one, results of which appear in Figures 4.6 and 4.7. Considerable amplification of the motion at point 1 in the vicinity of the fundamental frequency of the dam is evident in Fig. 4.7.

4.2.3 Initial cracking earthquake test (Figures 4.8 through 4.11)

The amplitude level of the table input was increased significantly in order to ensure crack formation. The table acceleration reached 1.7g, although this peak was preceded by the cracking. Initiation and propagation of the cracks are well

documented by the film of the model's response. Frame by frame analysis of the film reveals that the first crack originates on the upstream face 13.7 in. (131.3 ft.) below the crest (Figure 4.10(a)) directly after a 1.01g upstream base acceleration pulse (peak A at 0.404 sec. in Figure 4.8(a)). This crack initially propagated horizontally but then dipped down as it neared the downstream face (Fig. 4.10(b)), stopping approximately 2.75 in. (26.4 ft.) from this face. It is expected that a crack path along the plane of principal tension would look similar to the obtained profile. Presumably, the crack stopped because the stress intensity factor dropped below the critical value. The maximum downstream relative displacement of point 1 associated with the opening of the crack immediately after it formed was 0.044 in. (5.1 in.) at 0.421 sec. (peak B in Fig. 4.8(c)). After a 1.1g base pulse in the downstream direction (peak C at 0.419 sec. in Fig.4.8(a)), the dam swung upstream, closing the crack to the upstream face and creating tensile stresses on the downstream side parallel to this face. In the frame of Fig. 4.10(c), the crack has extended to the downstream face in a direction perpendicular to it. The direction of propagation is thought to be from the old crack tip to the downstream face. Presumably, when the tensile zone spread inward to the old tip and reached sufficient amplitude to satisfy the propagation criteria (at which time initiation criteria were not satisfied on the downstream face), the crack restarted, but in a new direction since the plane of principal tension was now perpendicular to the downstream face. The maximum upstream relative displacement of point 1 associated with the opening of this segment immediately after it was formed was 0.063 in. (7.3 in.) at 0.450 sec. (peak D in Fig. 4.8(c)).

Two other cracks formed off the initial crack later in the time history as seen in Fig. 4.11, and probably resulted from impacts and high shear stresses along the plane of the initial crack. The first started 1.75 in. (16.8 ft.) from the upstream

face and propagated downward and the second started 3.0 in. (28.8 ft.) from the downstream face and propagated upward. Figures 4.10 (d) and (e) show the first frames in which the two cracks were visible and correspond to times of 0.97 sec. and 1.15 sec., respectively.

The response of the top block of the dam exhibited a strong 12 Hz motion, which is seen in the time histories of Figs. 4.8 (b) and (c) and in the spectrum of Fig. 4.9(b). It would be wrong to conclude that this is solely a rocking frequency, because an examination of the film showed a complicated rocking-sliding motion with significant impacts on the steeper downstream segment of the initial crack. These impacts could produce large upstream accelerations, which could explain the sharp upstream spikes in the acceleration record at point 1 (Fig. 4.8(b)). The sequence shown in Figs. 4.10 (f) through (n) is representative of the complicated motion of the cracked dam. Of particular note are the impact on the downstream segment of the initial crack in Fig. 4.10(j) and the impact near the upstream face in Fig. 4.10(m). Peak relative displacements during the test at point 1 reached 0.069 in. (7.9 in.) upstream at 2.349 sec. and 0.053 in. (6.1 in.) downstream at 1.1 sec. (peaks F and E in Fig. 4.8(c)). The residual displacement at point 1 is only 0.005 in. (0.6 in.), probably a result of the resistance to sliding provided by the V shape of the initial crack.

4.2.4 Second high-level earthquake test (Figures 4.12 through 4.15)

Since the dam did not fail in the previous test, another test was conducted to further observe the stability of the dam in the presence of cracks. The amplitude level was increased and resulted in a peak base acceleration of over 3.75g in both the upstream and downstream directions. Because 3.75g represents the maximum possible voltage input (5 volts) to the ADC, precise measurement of the peak

value was not possible. A spurious voltage from the DAC delivered a pulse to the table at the beginning of the excitation which created upstream displacements exceeding the range of the LVDTs during most of the first 0.6 s. During this period, the top block impacted the wedge of material formed by the vertical crack (Fig. 4.14(a)) near the upstream face and dislodged it (Figure 4.15). Interestingly, the resulting loss of bearing to the top block did not cause failure of the structure, even though subsequent shaking was strong. Fig. 4.14(b) shows an example of the rocking displacement exhibited by the top block subsequent to loss of the supporting wedge. Note from Figure 4.15 that little permanent displacement of the top block occurred.

4.3 First Composite Model

This model employed the polymer-based lower portion and the plaster- based top (lead oxide powder). Frequency sweeps were carried out with and without water and were followed by four high-level earthquake tests with various reservoir conditions. When water was included, the level was placed 2 in. (19.2 ft. prototype) below the crest of the dam.

4.3.1 Frequency sweeps (Figure 4.16)

A frequency response curve for the dam with empty reservoir appears in Figure 4.16(a) and shows resonances at 48.5 Hz (4.5 Hz) and 100 Hz (9.3 Hz). These values exceed those of the monolithic model; however, the frequencies are still in a reasonable range. Possible reasons for this increase could include a more intact model (recall the shrinkage cracks in the base of the monolithic model) and a high dynamic modulus of the polymer material. Larger than desired damping

values (9.9% of critical in the fundamental mode and 8.4% in the second mode) for the composite model can be attributed to the viscous nature of the epoxy and represent a disadvantage of that material. In spite of this large damping, it was felt that much could still be learned from earthquake tests, and four were carried out. The table accelerations used in some of these tests, much stronger than those measured during actual earthquakes, should be viewed with these damping values in mind.

The addition of water in the reservoir decreased the resonant frequencies of the two modes to 40 Hz (3.7 Hz) and 94 Hz (8.8 Hz); damping values were 11% and 8% of critical, respectively (Figure 4.16(b)). The reduction in the resonant frequency of the fundamental mode is approximately 18%, somewhat larger than the 15% predicted by the two-dimensional mathematical model. Actually, a smaller decrease would be more logical considering the existence of some lateral flexibility in the sides of the reservoir structure and the flexibility of the membrane in the slack area off to the sides of the upstream face of the model (Fig. 2.7). In addition, the table control system had difficulty in holding the fundamental resonance, as is evident from Fig. 4.16(b). Explanations for this and the larger than expected reduction in the resonant frequency of the fundamental mode, which were possibly connected, were not found.

4.3.2 Initial cracking earthquake test (Figures 4.17 through 4.20)

The earthquake testing was begun with water in the reservoir. The table motion which cracked the model had a peak acceleration of 0.64g at 2.352 sec. (peak A in Fig.4.17(a)). During the 0.025 in. (2.83 in.) downstream relative displacement at 2.364 sec. (peak B in Fig 4.17(c)) which followed this peak acceleration, a trace of a crack opened on the upstream face $13\frac{3}{4}$ in. (131.8 ft.) below the crest appeared.

The next motion of the dam, which followed the 0.33g downstream acceleration of the base at 2.368 sec. (peak C in Fig. 4.17(a)), displayed the inclined crack shown in Figure 4.19 open from the downstream face $8\frac{5}{8}$ in. (82.6 ft.) below the crest, whose occurrence coincided with the upstream relative peak displacement labeled D at 2.384 sec. in Fig. 4.17(c). No other cracking or opening was evident.

Following the test, the dam was examined closely for visible cracks (Fig 4.20). The cracks mentioned above on the filmed side are c-d-e and a-b; segment b-c was not visible in the film. The crack profile on the opposite side differed from that on the filmed side, consisting of a circular arc which intersected the downstream face $1\frac{1}{8}$ in. (146 ft.) below the intersection on the filmed side (Fig. 4.20). Thus, the cracking was three-dimensional, which could have resulted from a number of sources, including the presence of inhomogeneity in the dam. The extent to which such 3-D cracking could occur in an actual dam monolith is unknown.

The observed crack openings in the film may not have coincided with actual crack initiations because it seems unlikely, considering the geometry of the crack a-b-c-d-e, that initiation from point e could have occurred first. A logical scenario is that the crack a-b-c-d occurred first, and then d-e followed, propagating from d to e during a downstream displacement, but this cannot be concluded from the evidence.

4.3.3 Second earthquake test (Figures 4.21 through 4.24)

A major concern about the previous test was the possibility that the plastic membrane restrained the opening of the crack at the upstream face of the dam. The in-plane stiffness of this membrane was quite high, and the water pressed it firmly against the dam. To reduce any resistance to crack opening provided by the membrane for the second earthquake test, a lubricant was placed between the dam and

the membrane, and a fold was inserted in the membrane at a level slightly below the crack on the upstream face.

With an increased amplitude level, the table responded with the strongest series of acceleration pulses early in the excitation (Fig 4.21(a)): peak A downstream (1.56g, 0.195 sec.), peak C upstream (2.32g, 0.207 sec.), peak E downstream (2.13g, 0.221 sec.), and peak G upstream (1.22g, 0.232 sec.). This part of the acceleration produced the largest relative displacements (Fig 4.21(c)): peak B upstream (0.042 in., 0.200 sec.) and peak H downstream (0.089 in., 0.250 sec.); the maximum displacement of 0.089 in. corresponds to 10.2 in. prototype. The film frames of Fig 4.23 illustrate this response; Fig. 4.23(a) corresponds to displacement peak B and Figs. 4.23(b) and (c) are taken from the series D, F, and H. During the latter, a new lower crack trace formed on the filmed side (see also Fig 4.24(a)). The mechanism of formation of this crack is unclear. Of course, by this point, the cracked state of the dam is very complicated (Fig. 4.24). One feature of the response evident from the film was that the larger crack openings occurred on the upstream face, a logical effect of the static water pressure. Significant upstream openings occurred at downstream relative displacement peaks I, J, and K in Fig. 4.21(c); frames in Figs. 4.23(d) and (e) are taken from peak I. Also, note that the permanent horizontal displacement was small (Fig. 4.21(c)).

Amplification of the acceleration response at point 1 in the present test was much smaller than for the first test, which was linear for most of its duration. The average of the Fourier transform in Fig. 4.18(b) between 20 and 50 Hz divided by a similar quantity for Fig. 4.18(a) gives an amplification of about three (first test); the same exercise for Fig. 4.22 (present test) gives essentially no amplification. This feature is the result of the strong nonlinear behavior. The acceleration time history at point 1 (Fig. 4.21(b)) shows a number of upstream and downstream

spikes resulting from impacts. These impacts could have occurred during crack closing and during collisions in sliding episodes.

4.3.4 Third earthquake test (Figures 4.25 through 4.27)

This test was another attempt to determine whether the plastic membrane, even with lubrication and fold, was restraining crack opening on the upstream dam face. The water and membrane were eliminated, and the important static water force was approximately applied by a nylon strap placed across the upstream face $9\frac{1}{2}$ in. below the crest. This location coincided with the resultant of the static water pressure above the crack on the upstream face. The strap was connected to a rubber rope and tightened to load the model with this resultant force which equaled 10 lbs. The rubber rope was flexible enough so that the expected displacement would not significantly alter the applied force. Of course, in this test the added mass effect of the water was not included.

The table excitation was similar to the one for the second test but scaled down in amplitude to a peak acceleration of 1.56g (Fig. 4.25(a)). Resulting displacements of the dam were roughly similar and proportionately smaller (compare Figs. 4.21(c) and 4.25(c)). This added confidence to the results of the second test. Fig. 4.26 shows that, like the second test, little amplification of the base acceleration occurred at point 1.

4.3.5 Fourth earthquake test (Figures 4.28 through 4.30)

The upstream dip of the main crack in Fig. 4.27 suggested that absence of the static water force might allow a significant sliding displacement in the upstream direction. Therefore, a final test was conducted with neither the reservoir nor the nylon strap present. The table motion was nearly identical to that from the third

test (1.42g peak acceleration, Fig 4.28(a)). Some noticeable sliding did occur in the upstream direction; the permanent displacement from Fig. 4.28(c) equaled 0.05 in. (5.75 in.). That this sliding was not greater reflects the three-dimensionality of the crack profile; i.e., the upstream dip of the main crack on the filmed side was absent on the opposite side (Fig. 4.30(b)). The downstream bias of the acceleration spikes in Fig. 4.28(b) could be due to collisions with a barrier on the crack plane which prevented further upstream sliding.

4.4 Second Composite Model

The top portion of the first composite was replaced with one constructed from the plaster-based material using lead beads. Frequency sweeps were again conducted with and without water, followed by three earthquake tests, all with water. Again, the water level stood 2 in. (19.2 ft.) below the crest.

4.4.1 Frequency sweeps (Figure 4.31)

Frequency response curves of the model are presented in Figure 4.31 as in Figure 4.16. Without water, the fundamental resonance occurred at 37.5 Hz (3.50 Hz) with 10% damping, and the second resonance was 120.5 Hz (11.26 Hz) with 10% damping. Compared to the first composite model, the frequency is significantly lower and the damping roughly the same at the fundamental resonance, while the frequency for the second resonance is substantially higher. This was disturbing, and no explanation was apparent. It is possible that some damage had occurred to the polymer base during the previous tests. Also note that the shaking table again had difficulty maintaining the fundamental resonance.

For the tests with water, it was decided that folds in the membrane were

necessary to eliminate resistance to crack opening on the upstream face of the dam. Since the locations of the crack intersections with the upstream face could not be predicted precisely, a series of 10 folds spaced one inch apart was placed over the general area where cracking was expected to occur. Each fold consumed 2 in. of material, and construction was possible only by circumventing the entire reservoir. No lubrication was employed. Results of the frequency sweep with water were 34 Hz (3.18 Hz) and 9.4% damping for the fundamental resonance and 103 Hz and 10.2% damping for the second resonance Fig. 4.31(b). Thus, the added mass effect was weak for the fundamental mode, in contrast to its strong effect for the first composite model. The probable cause of this result is the folding of the membrane, which could have contained trapped pockets of air or could have made the slack area off the sides of the upstream face of the model more flexible. In any case, eliminating restraint to crack opening at the upstream face took preference over the added mass of the water (the static water pressure was properly represented). Actually, the added mass for a prototype gravity dam during an earthquake may be less than that predicted by the 2-D mathematical model, say, if adjacent monoliths are not vibrating together.

Although the performance of the model was less than desired, the fundamental frequency was still in a reasonable range, and it was felt that earthquake tests could yield important information about cracking in concrete dams, so three tests were carried out.

4.4.2 Initial cracking earthquake test (Figures 4.32 through 4.35)

The acceleration pulses that cracked the second composite model contained the maximum acceleration and occurred early in the excitation (Figure 4.32(a)): peak A (-0.92g at 0.194 sec.) and peak C (1.52g at 0.204 sec.). Associated peak dis-

placements are labeled B (0.02 in. at 0.200 sec.) and D (-0.053 in. at 0.216 sec.) in Fig. 4.32(c); the maximum displacement of -0.053 in. corresponds to -6.13 in. prototype. The first cracking seen on the film occurred at displacement B and ran inward from the downstream face 6.9 in. (66.2 ft.) below the crest along a straight path at an angle 24 degrees below horizontal (Fig. 4.34(a)). An upstream segment of this crack, which completed the same straight path (Fig. 4.34(b)), became visible during the next swing of the dam downstream (displacement D).

One scenario of crack propagation is that the downstream segment formed during displacement B and the upstream segment formed during displacement D (propagation starting from the interior crack tip), but then the orientation of the upstream segment is puzzling because it would not be perpendicular to the principal tensile stress. Another scenario is that the entire crack propagated during displacement B but that only a portion at the downstream end was visible on the film. However, if this were the case, it is also not obvious that the crack would remain straight. Unfortunately, the film is unable to resolve this matter as the above mentioned cracking was visible only on the two frames shown in Figures 4.34(a) and 4.34(b).

The rest of the response was characterized by the opening and closing of the crack described above, mostly at the upstream end, with little sliding and no other cracks forming. Figures 4.34 (c), (d), and (e), which occur at displacement peaks E, F, and G respectively, show the frames that contain the largest crack openings. Little permanent displacement resulted (Figure 4.32(c)). The average amplification of the base acceleration at point 1 between 20 Hz and 50 Hz is approximately two (Fig. 4.33). Reasons for the downstream bias of the acceleration spikes (Fig. 4.32(b)) at point 1 are not apparent.

4.4.3 Second earthquake test (Figures 4.36 through 4.39)

In order to explore the upper limits of table motion that the cracked model could withstand, the table input was significantly increased and resulted in a maximum acceleration of 3.53g in the upstream direction at 0.205 sec. (peak E in Fig. 4.36(a)). The most significant feature of the response is a 0.225 in. (2.16 ft.) sliding displacement downstream which was initiated by acceleration E. Prior to this event, the maximum displacement had reached 0.035 in. downstream at 0.173 sec. (peak B in Fig 4.36(c)) and 0.063 in. upstream at 0.203 sec. (peak D in Fig. 4.36(c)), which followed base pulses of 1.09g upstream at 0.159 sec. (peak A in Fig. 4.36(a)) and 2.15g downstream at 0.194 sec. (peak C in Fig. 4.36(a)), respectively. The frames of Fig. 4.38 depict these responses, starting with the upstream crack opening occurring at displacement B (Fig. 4.38(a), 0.173 sec.). The crack closed previous to displacement D, but then began to open on the downstream side and began to experience sliding in the downstream direction (Fig. 4.38(b), 0.200 sec.). Further sliding over the rough surface was accompanied by regained contact, and even some grinding, at the downstream end and by opening at the upstream end (Fig. 4.38(c), 0.21 sec.). By 0.24 sec., the top block was firmly entrenched at its downstream corner and began to rock so as to further open the upstream end of the crack (Fig. 4.38(d)). The crack reached its maximum upstream opening at 0.25 sec. (Fig. 4.38(e)) and, because of its misalignment due to sliding, closed only at the interior contacts, leaving a significant residual opening at the upstream face (Fig. 4.38(f), 0.27 sec.). Such a residual opening in the prototype would greatly facilitate water penetration into the crack.

The rest of the response was characterized by further opening and closing of the crack, mostly at the upstream face, and small amounts of sliding back and

forth, which had a small net effect (Fig. 4.36(c)). No further cracks formed. Little amplification of the base acceleration at point 1 occurred between 20 and 50 Hz, although significant amplification is present at higher frequencies (Fig. 4.37). The acceleration spikes at point 1 are now evenly distributed between the upstream and downstream directions (Figure 4.36(b)).

4.4.4 Third earthquake test (Figures 4.40 through 4.42)

The main purpose of this test was to observe the response to an excitation with a longer duration than before. To accomplish this, the first 2.5 secs. of the table input used previously was repeated over the second 2.5 secs. of the excitation. The amplitude was reduced somewhat and resulted in a maximum acceleration of 2.51g at 2.605 sec. (peak L in Fig. 4.40(a)). Before the third test was carried out, the portion of the dam above the crack was placed back in its original position.

Two major episodes of sliding resulted from this test; the first produced about 0.1 in. (11.5 in.) of slip downstream and the second roughly 0.08 in. (9.2 in.) downstream (Fig. 4.40(c)). Interestingly, the resultant permanent slip was similar to that of the previous test. Acceleration and displacement peaks (Fig. 4.40) associated with the first episode were acceleration A (0.91g, 0.158 sec.), displacement B (-0.041 in., 0.175 sec.), acceleration C (-1.02g, 0.184 sec.), displacement D (0.018 in., 0.200 sec.), acceleration E (1.79g, 0.207 sec.), and displacement F (-0.096 in., 0.255 sec.). Preceding the sliding, a significant upstream opening occurred at displacement B (Fig 4.42(a)), which then closed during displacement D. Shortly thereafter, the sliding was initiated by the upstream acceleration E as shown in Fig 4.42(b) (0.21 sec.). The sliding was accompanied by opening of the crack at the upstream end which continued to displacement peak F (Fig. 4.42(c)). The only other significant opening to occur before the second sliding episode was

one on the upstream side which occurred at displacement peak G (Fig. 4.42(d), 1.12 sec.).

Acceleration and displacement peaks (Fig 4.40) associated with the second sliding episode are acceleration H (1.74g, 2.56 sec.), displacement I (-0.16 in., 2.578 sec.), acceleration J (-1.72g, 2.583 sec.), displacement K (-0.007 in., 2.604 sec.), acceleration L (2.51g, 2.605 sec.), and displacement M (-0.2 in., 2.650 sec.). The sliding was again preceeded by a significant upstream opening of the crack (peak I, Fig. 4.42(e)), which closed during displacement K. The upstream acceleration L initiated the sliding that is shown at an early stage in Fig. 4.42(f) (2.61 sec.) and later in Fig 4.42(g) (2.62 sec.). Sliding was accompanied by downstream crack opening and halted once contact was reestablished there (Fig. 4.42(h), 2.63 sec.). Then, rocking opened the upstream end of the crack to the position shown in Fig. 4.42(i) (2.67 sec.). Other large upstream openings occurred at displacement peaks N, O, P, and Q in Fig 4.40(c).

The resulting configuration of the dam was similar to that after the previous test and is not shown. Some amplification of acceleration at point 1 in the 20 Hz range is evident from Fig. 4.41, but this is hard to find in the time history response (Fig. 4.40(b)).

4.5 Comparison to Numerical Results

Although no numerical simulations of these experiments were carried out, some qualitative comparisons to other numerical results can be made. For this purpose, the study in (8) was selected. It used a 2-D finite element model of Pine Flat Dam including water and foundation and subjected it to the S00E and vertical components of the 1940 Imperial Valley ground motions, with actual amplitudes scaled

by a factor of 1.5. Cracks were represented by the smeared crack approach, and the criterion for crack propagation used an equivalent tensile strength determined from the critical stress intensity factor and the element size. No water intrusion into open cracks was permitted, similar to the present experiments.

Three analyses carried out in (8) employed an initial straight crack in the neck region. The crack sloped down toward upstream at 19 degrees in one case, was level in another, and sloped up toward upstream at 18 degrees in the third. With a coefficint of friction of 0.75, all three arrangements proved to be stable, and the top block slid downstream 0.9, 1.9, and 3.4 feet, respectively. The geometry of the first crack is closest to the one which developed during the test on the second composite model which experienced about 2.2 feet (prototype) downstream sliding, and the ground motions for the experiment were much stronger than for the numerical analysis. In the three analyses, high tensile stresses occurred near the ends of the cracks with orientations parallel to the cracks. This indicated the likely formation of branch cracks which could have been similar to the ones observed in the test on the monolithic model.

Another analysis in (8) employed an initially uncracked dam in order to model actual crack initiation and propagation. Crack initiation occurred in the neck region perpendicular to the dam face, and the crack turned down as it propagated into the interior of the dam (Figure 4.43). This behavior was noted for the inital crack in the monolithic model, although it propagated less far than did the one in the numerical model. This difference could be attributed to differences in the ground motions and in the critical stress intensity factor. In the numerical model, the cracking extended to the opposite side by reinitiation along the side of the initial sloping crack (Figure 4.43), rather than by extension from the tip of the initial crack as occurred in the experiment on the monlithic model. A crack

also formed along the base of the dam in the numerical model (Figure 4.43), but this crack had a much smaller effect on the response of the dam than did the neck cracking.

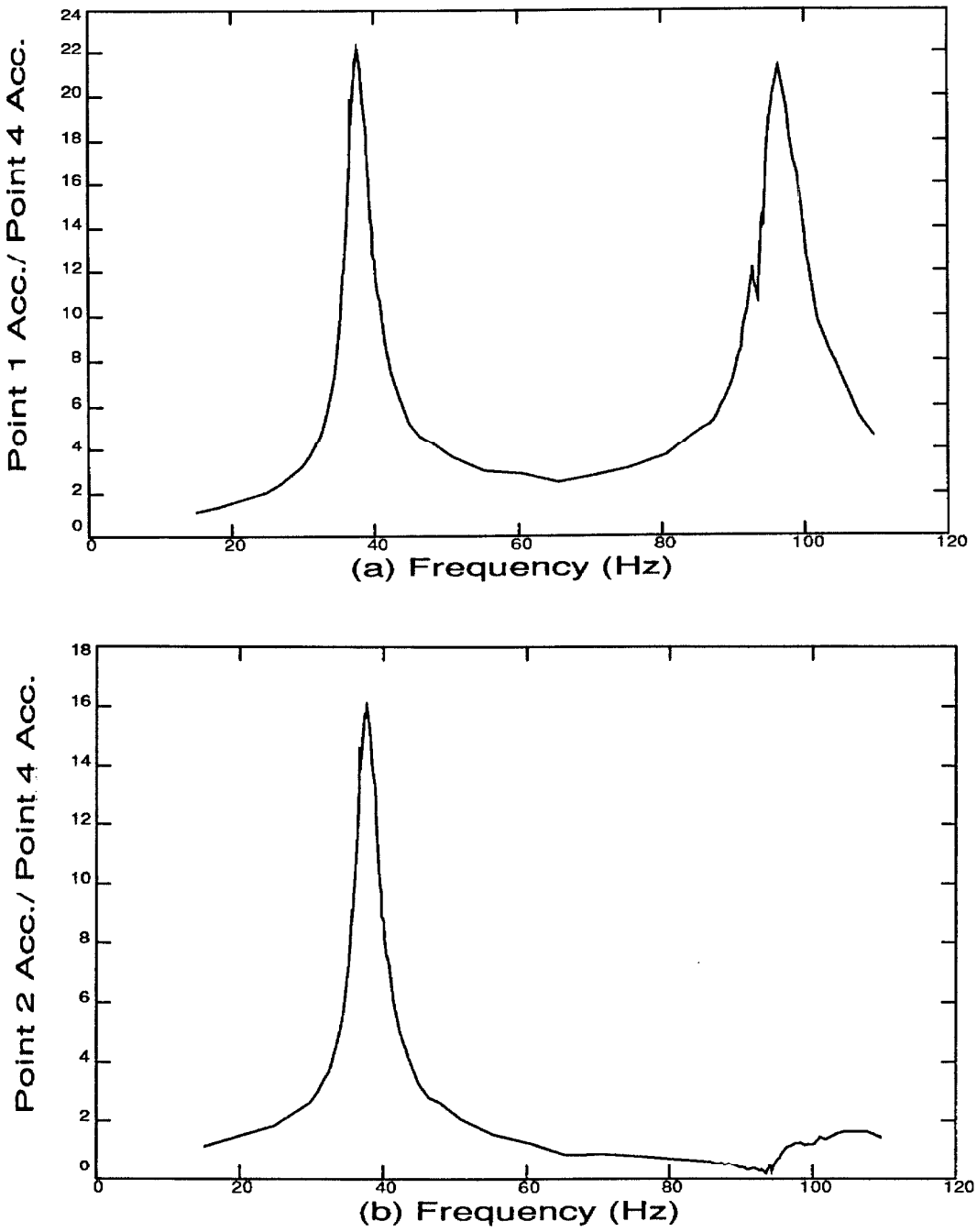

Figure 4.1: Acceleration frequency response curves (dam acceleration/base acceleration) resulting from the frequency sweep of the monolithic model for points 1 (a) and 2 (b).

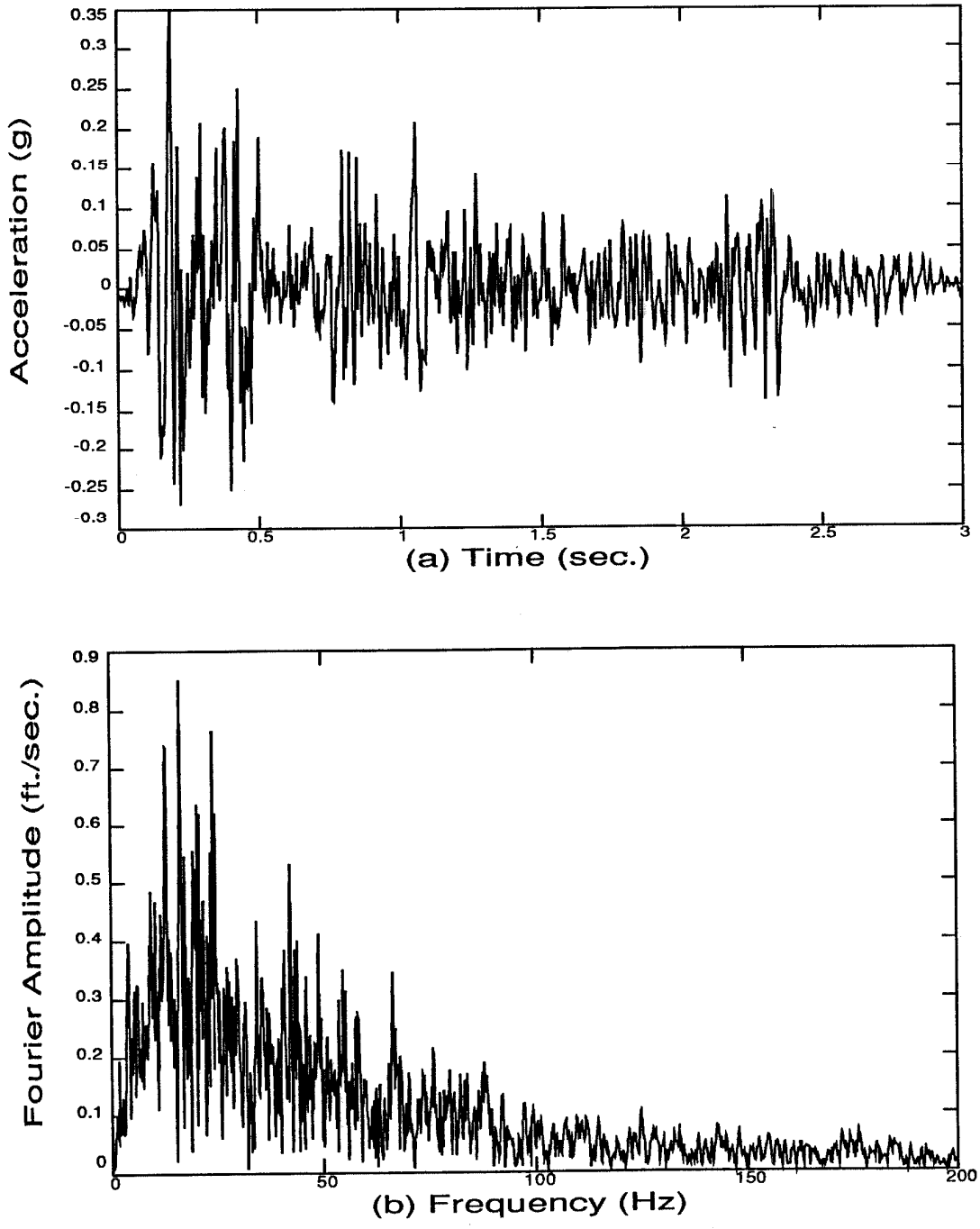

Figure 4.2: S00E component of the 1940 Imperial Valley accelerogram and its Fourier transform (time scale compressed by 10.7).

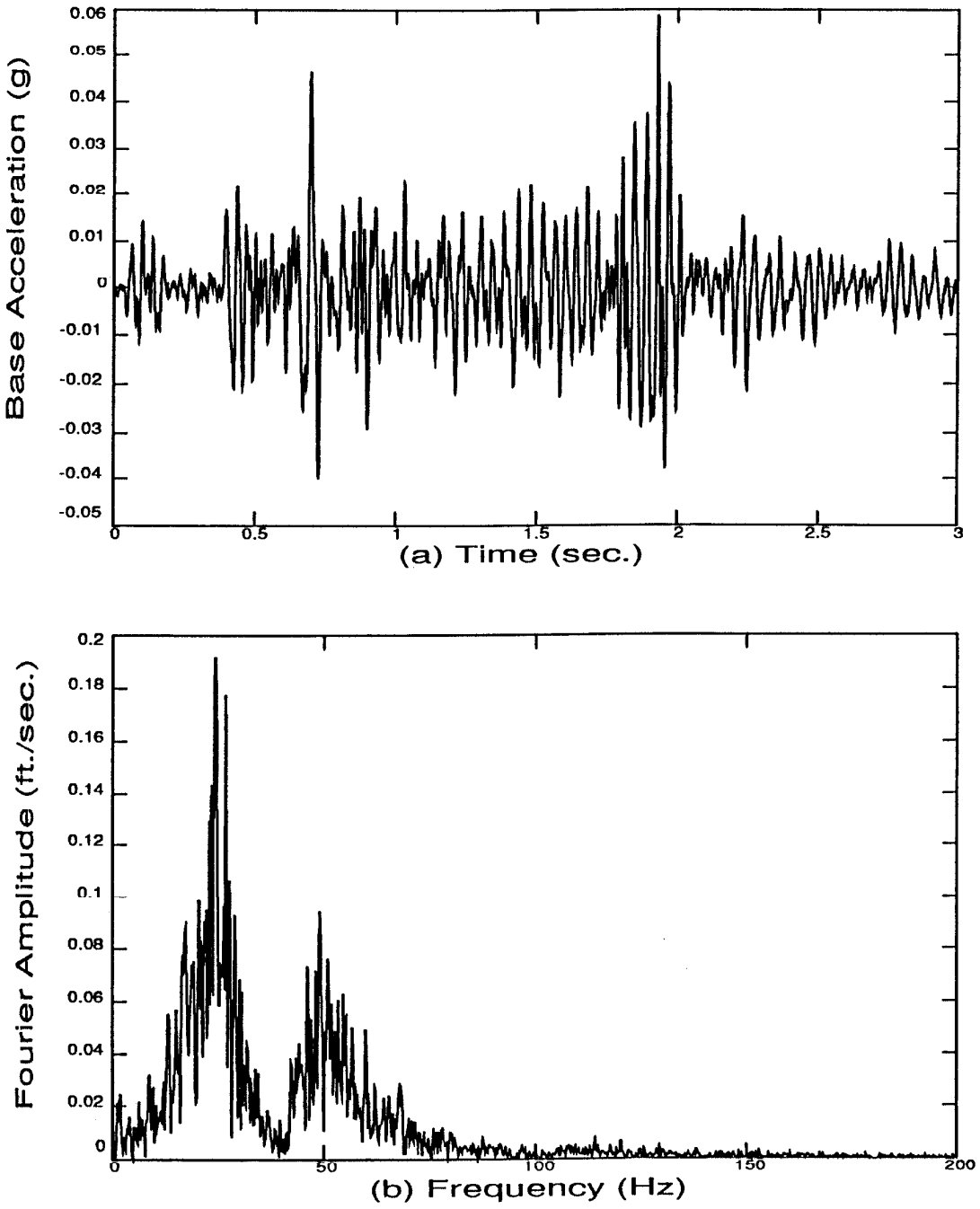

Figure 4.3: Actual base acceleration and its Fourier transform for the first low-level earthquake test on the monolithic model.

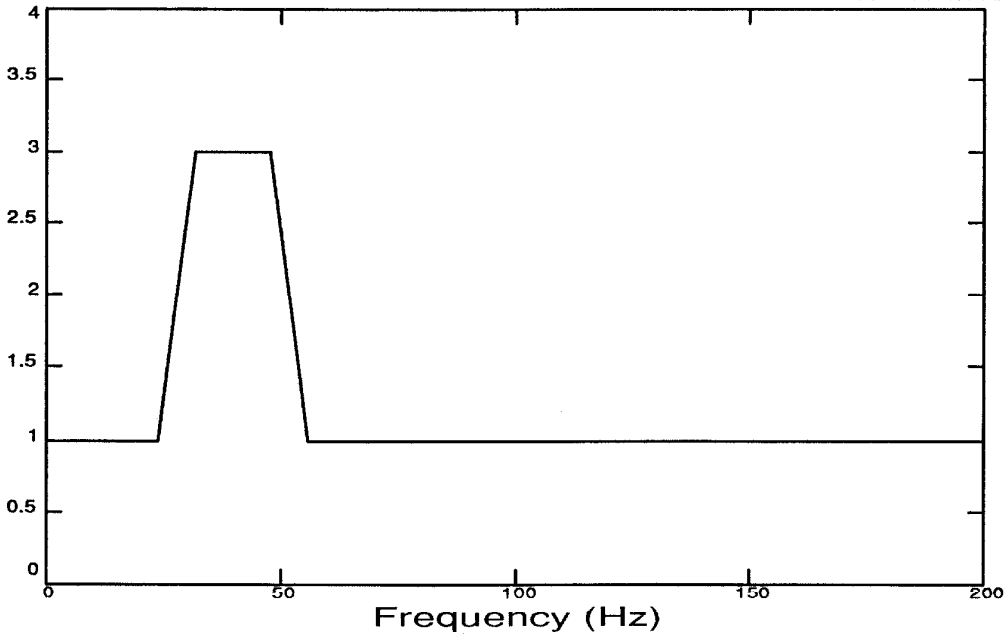

Figure 4.4: Function used to modify the frequency content of the input table acceleration.

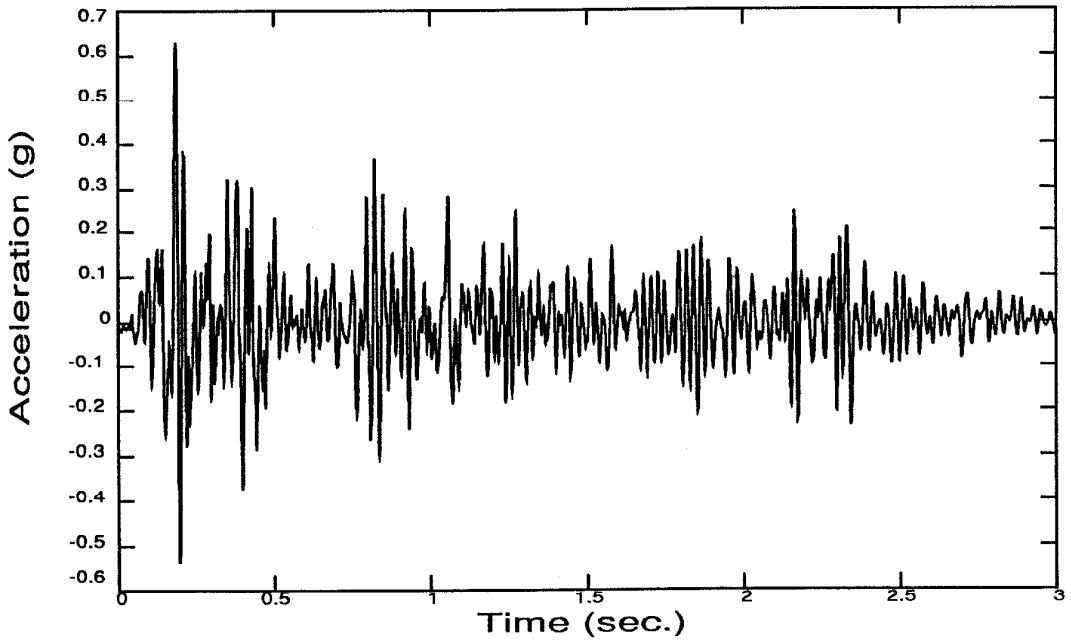

Figure 4.5: Modified table input acceleration.

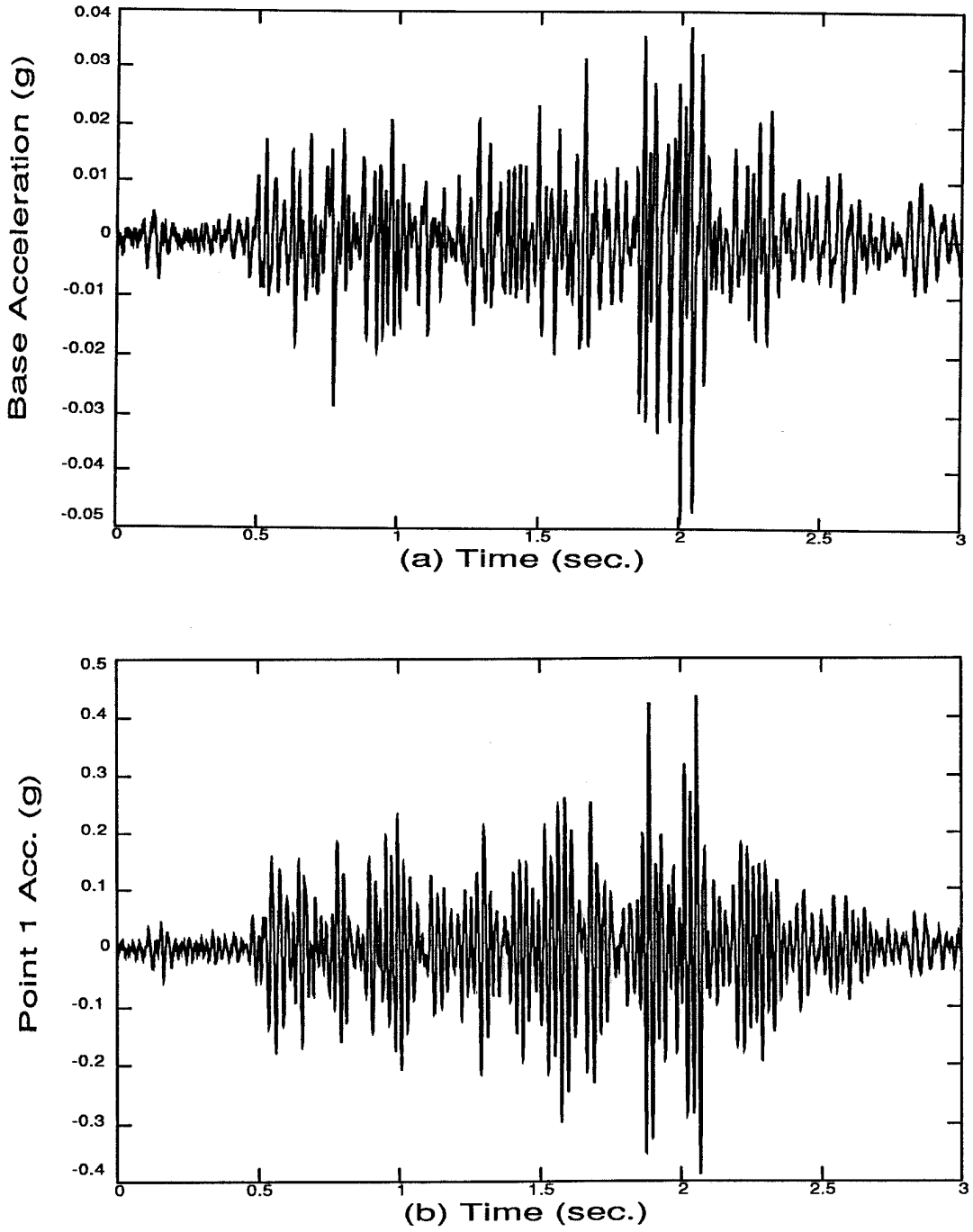

Figure 4.6: Base motion (a) and dam response at point 1 (b) for the second low-level earthquake test on the monolithic model.

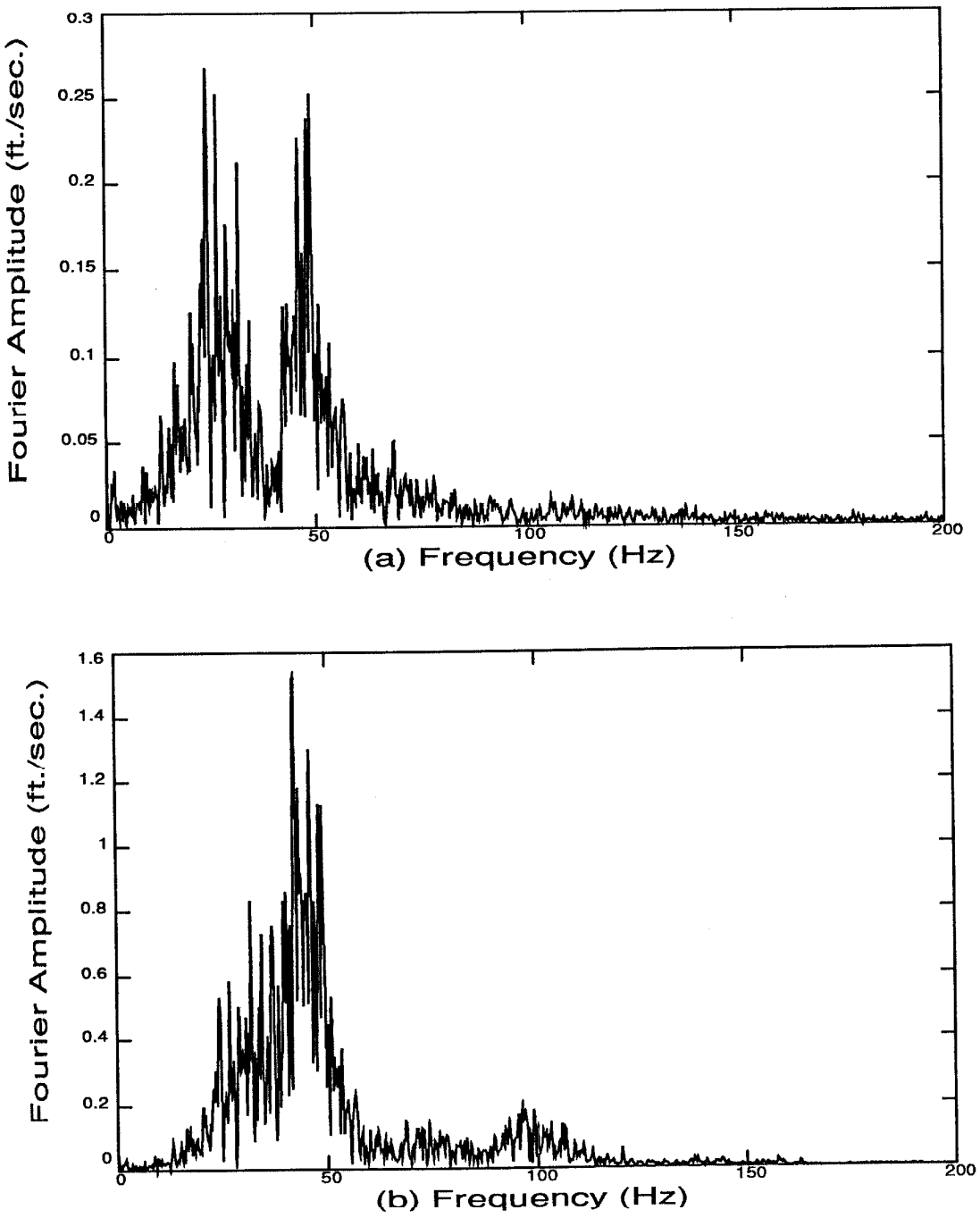

Figure 4.7: Fourier transforms of the base motion (a) and dam response at point 1 (b) for the second low-level earthquake test on the monolithic model.

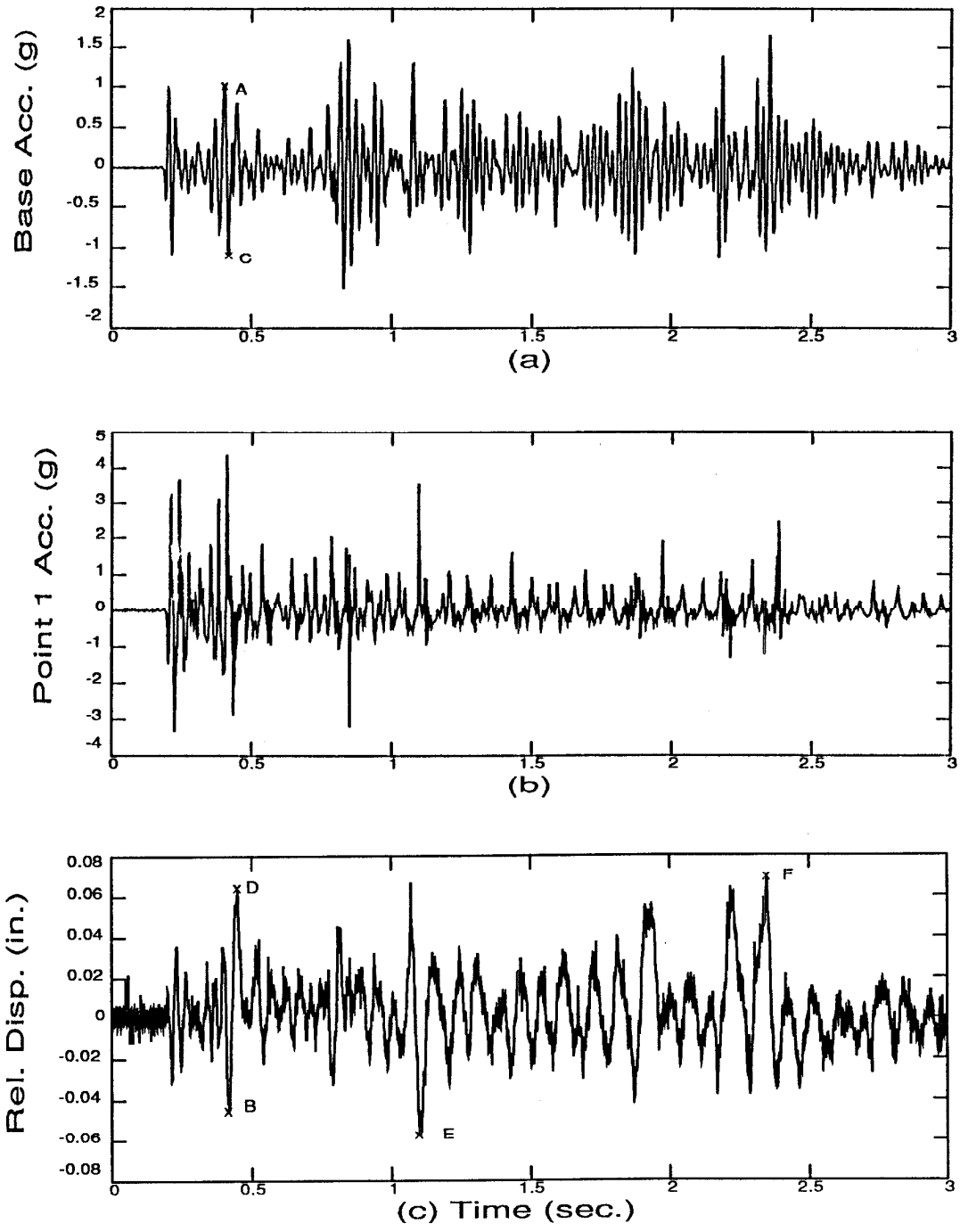

Figure 4.8: (a) Base acceleration, (b) acceleration response at point 1, and (c) displacement of point 1 relative to the base for the initial cracking earthquake test on the monolithic model.

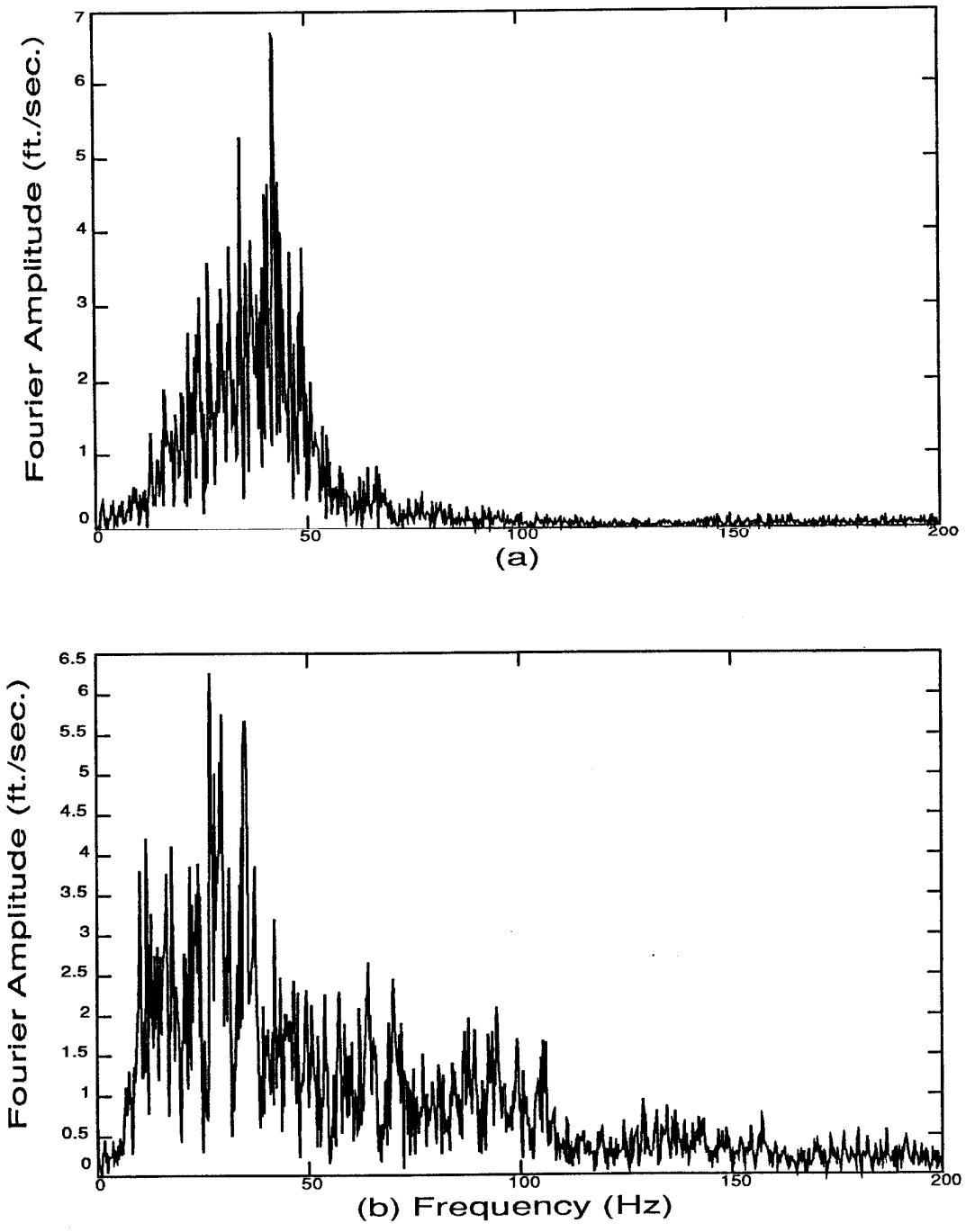

Figure 4.9: Fourier transforms of the base motion (a) and dam response at point 1 (b) for the initial cracking earthquake test on the monolithic model.

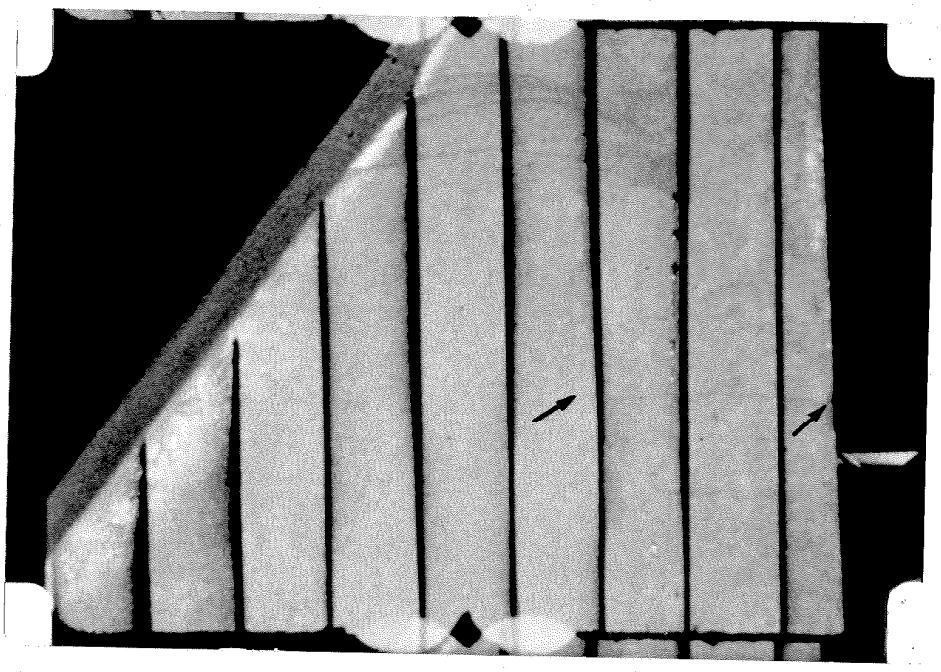

Figure 4.10: (a) t=0.412 sec.

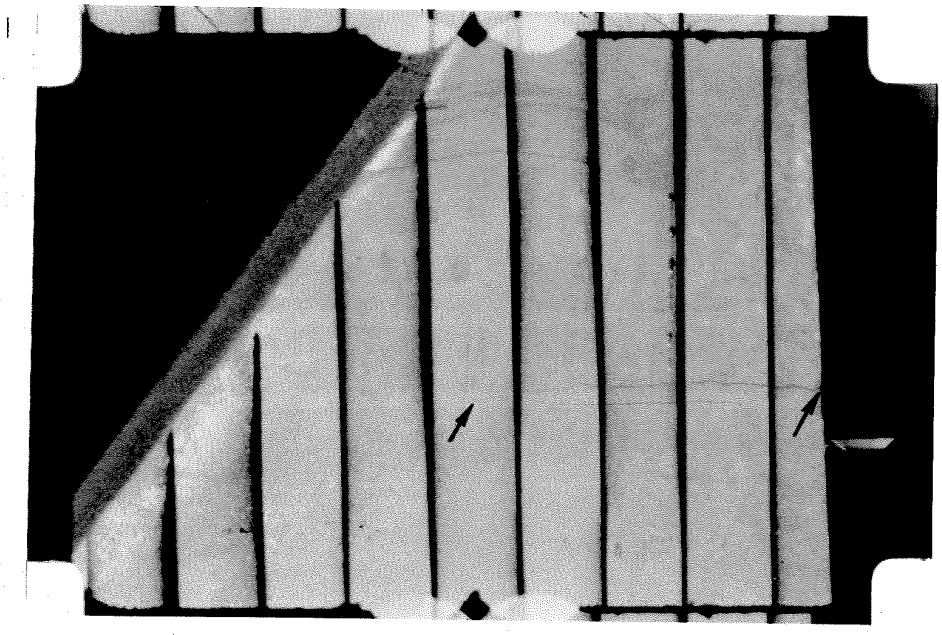

Figure 4.10: (b) t=0.418 sec.

Figure 4.10: Film frames at specific instants of time of the initial cracking earthquake test on the monolithic model.

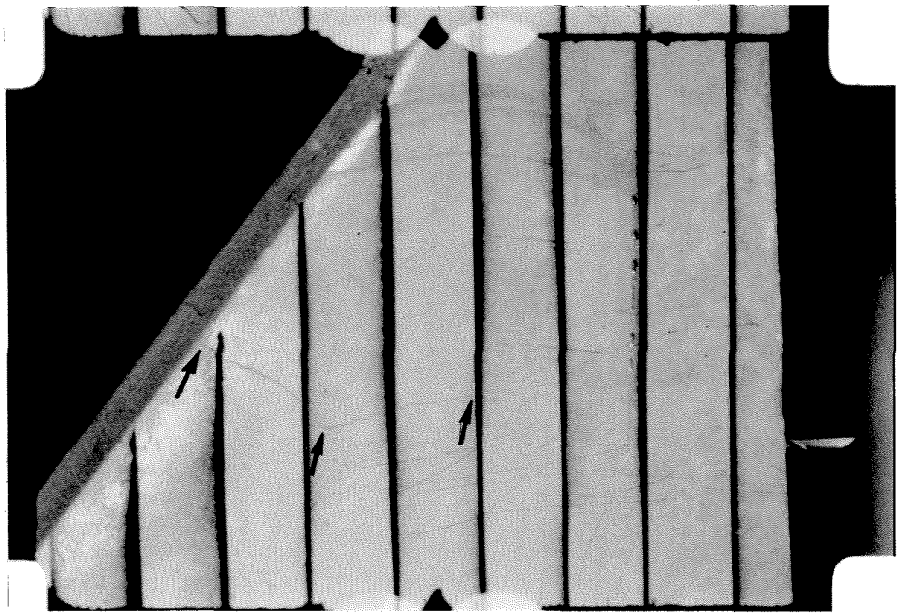

Figure 4.10: (c) t=0.430 sec.

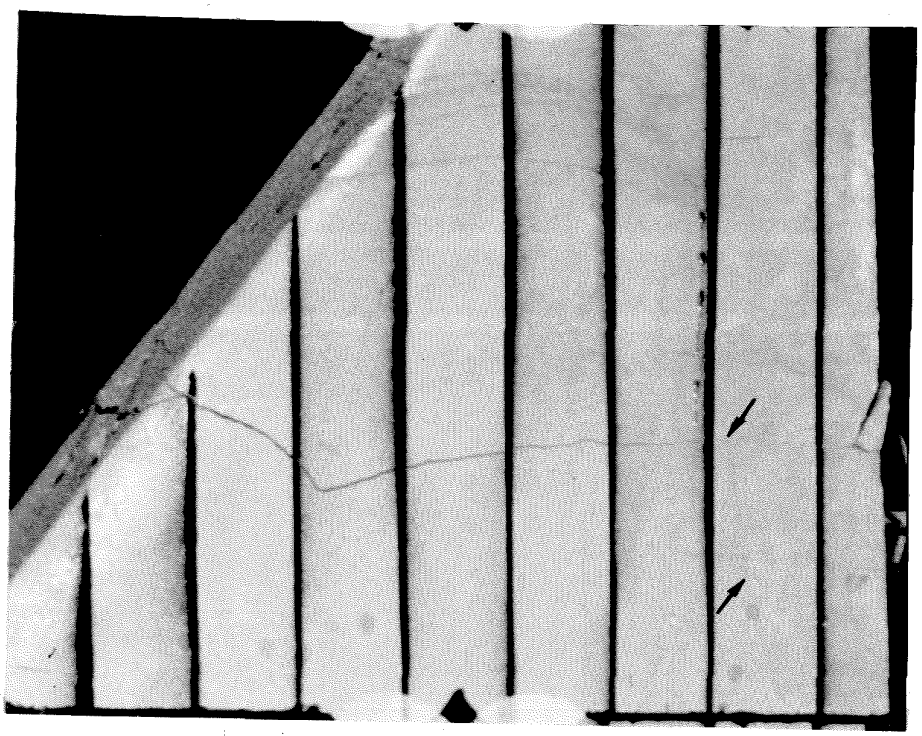

Figure 4.10: (d) t=0.97 sec.

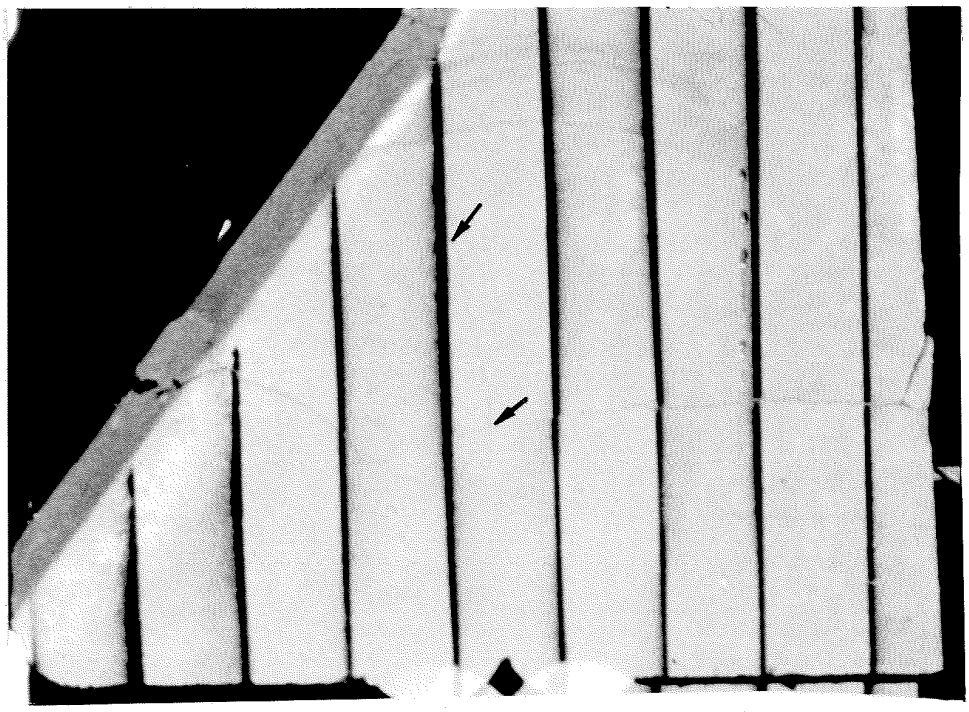

Figure 4.10: (e) t=0.1.15 sec.

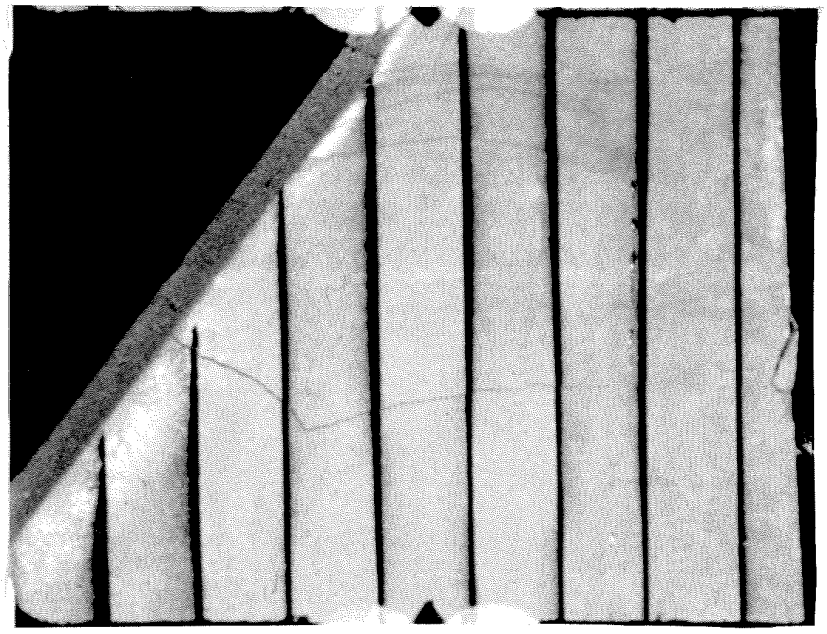

Figure 4.10: (f) t=0.80 sec.

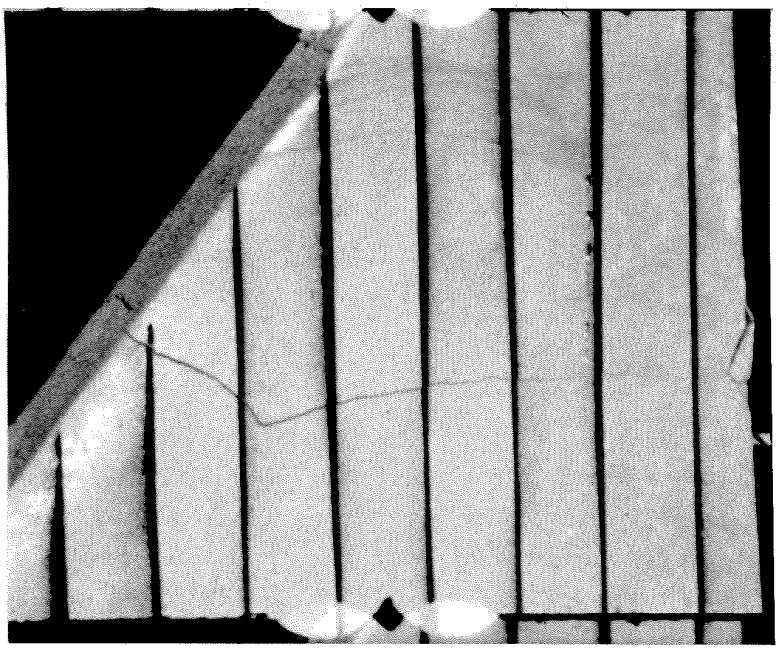

Figure 4.10: (g) t=0.806 sec.

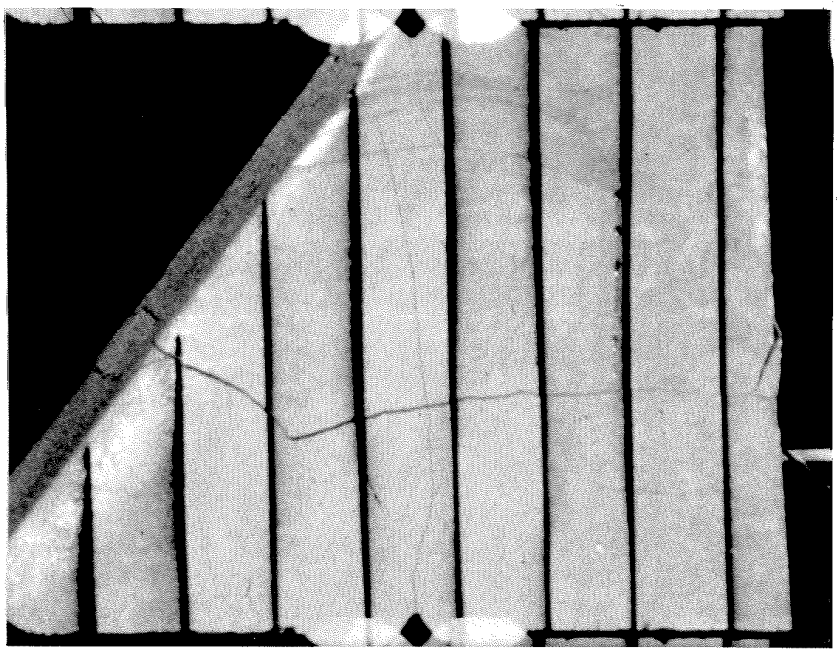

Figure 4.10: (h) t=0.812 sec.

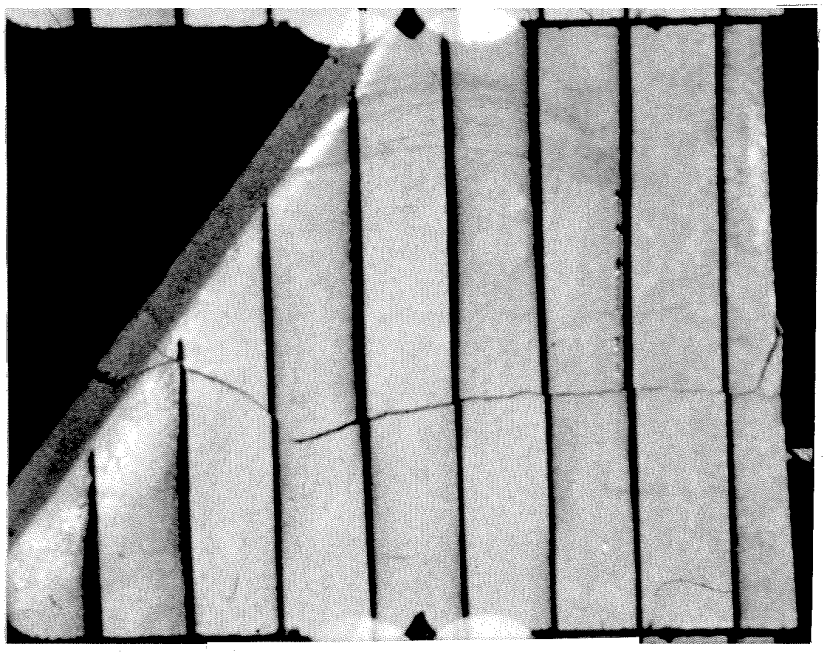

Figure 4.10: (i) t=0.818 sec.

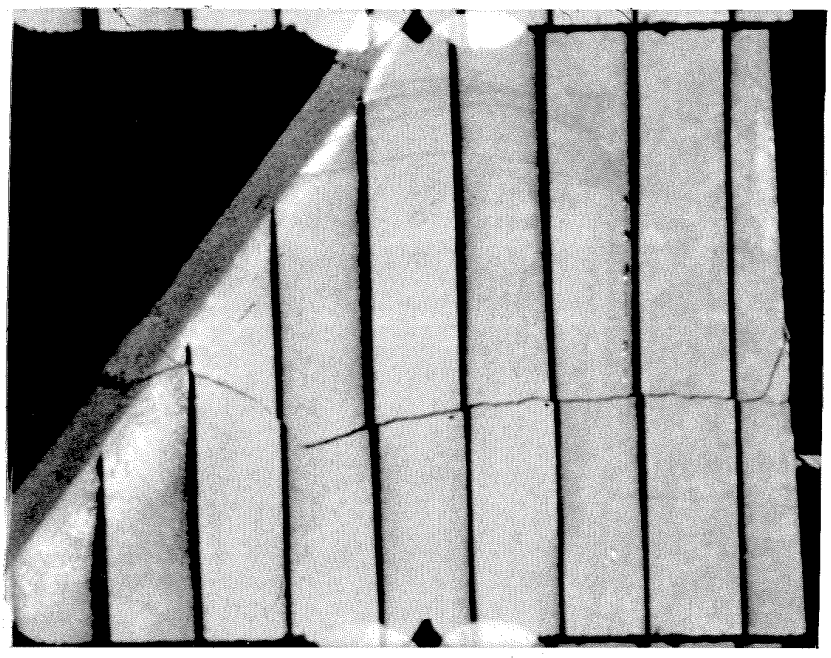

Figure 4.10: (j) t=0.824 sec.

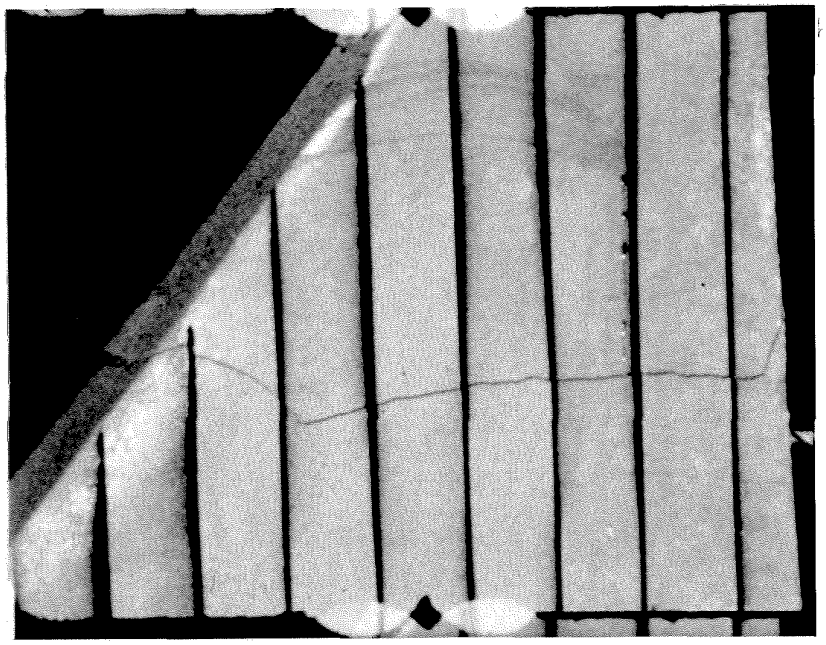

Figure 4.10: (k) t=0.830 sec.

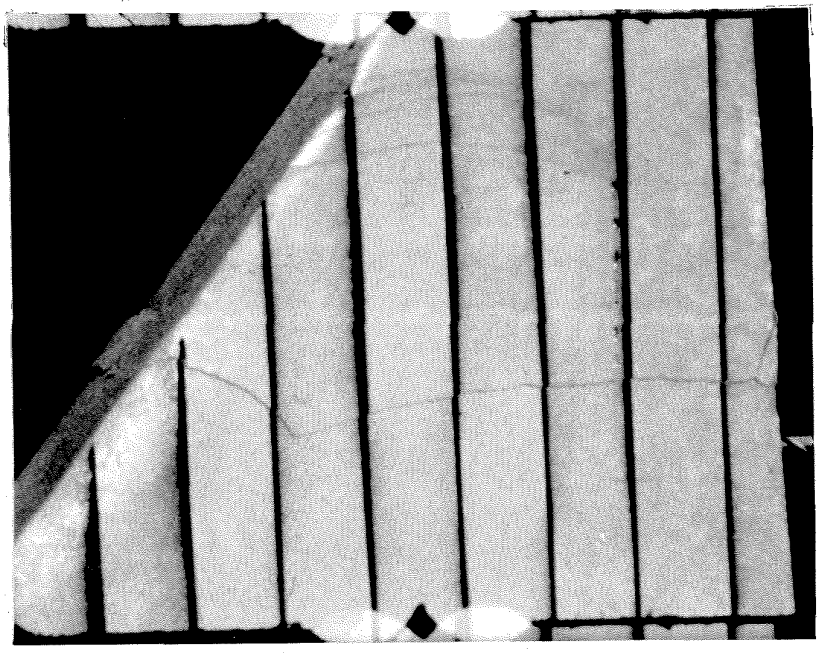

Figure 4.10: (l) t=0.836 sec.

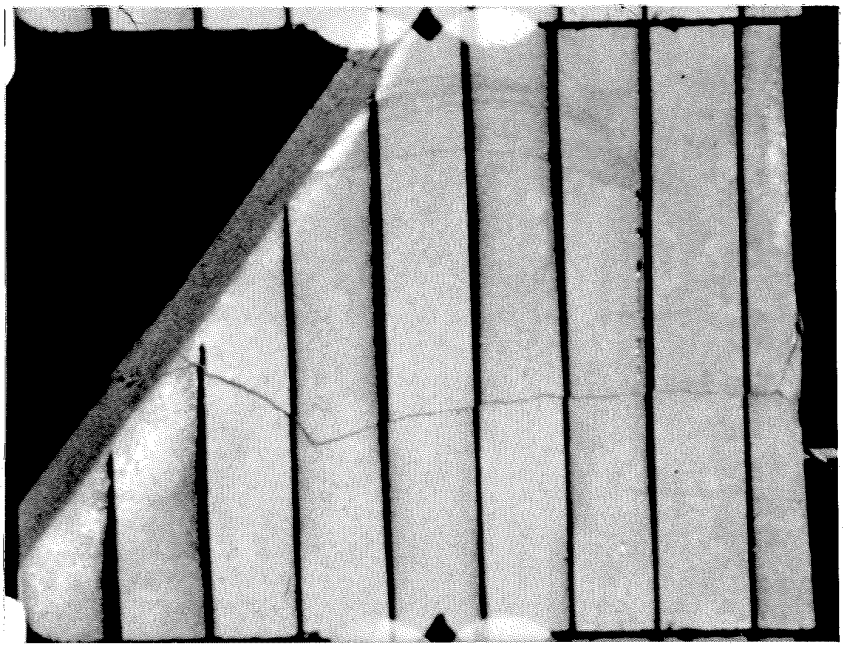

Figure 4.10: (m) t=0.842 sec.

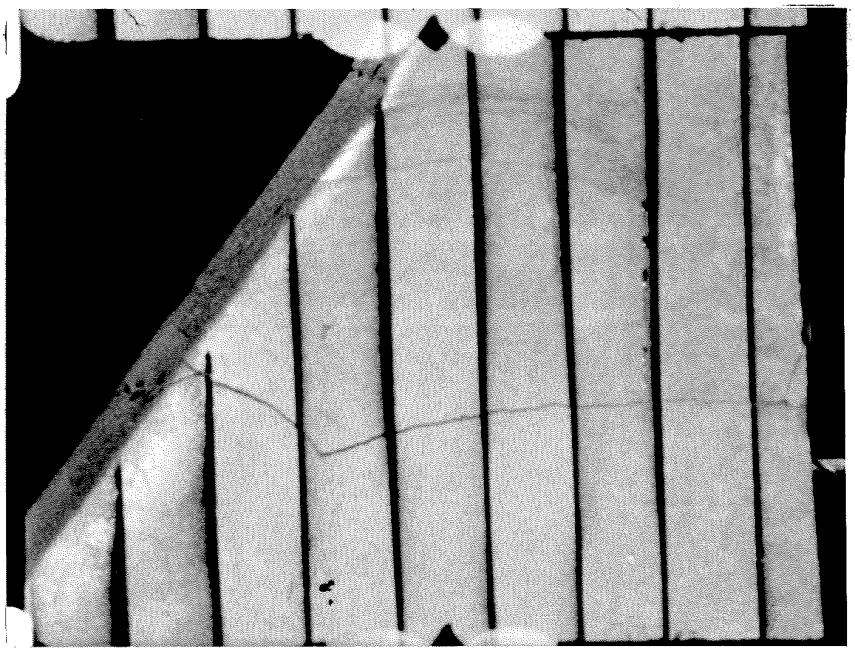

Figure 4.10: (n) t=0.848 sec.

Figure 4.11: (a) Filmed side of monolithic model after initial cracking earthquake test.

Figure 4.11: (b) Opposite side of monolithic model after initial cracking earthquake test.

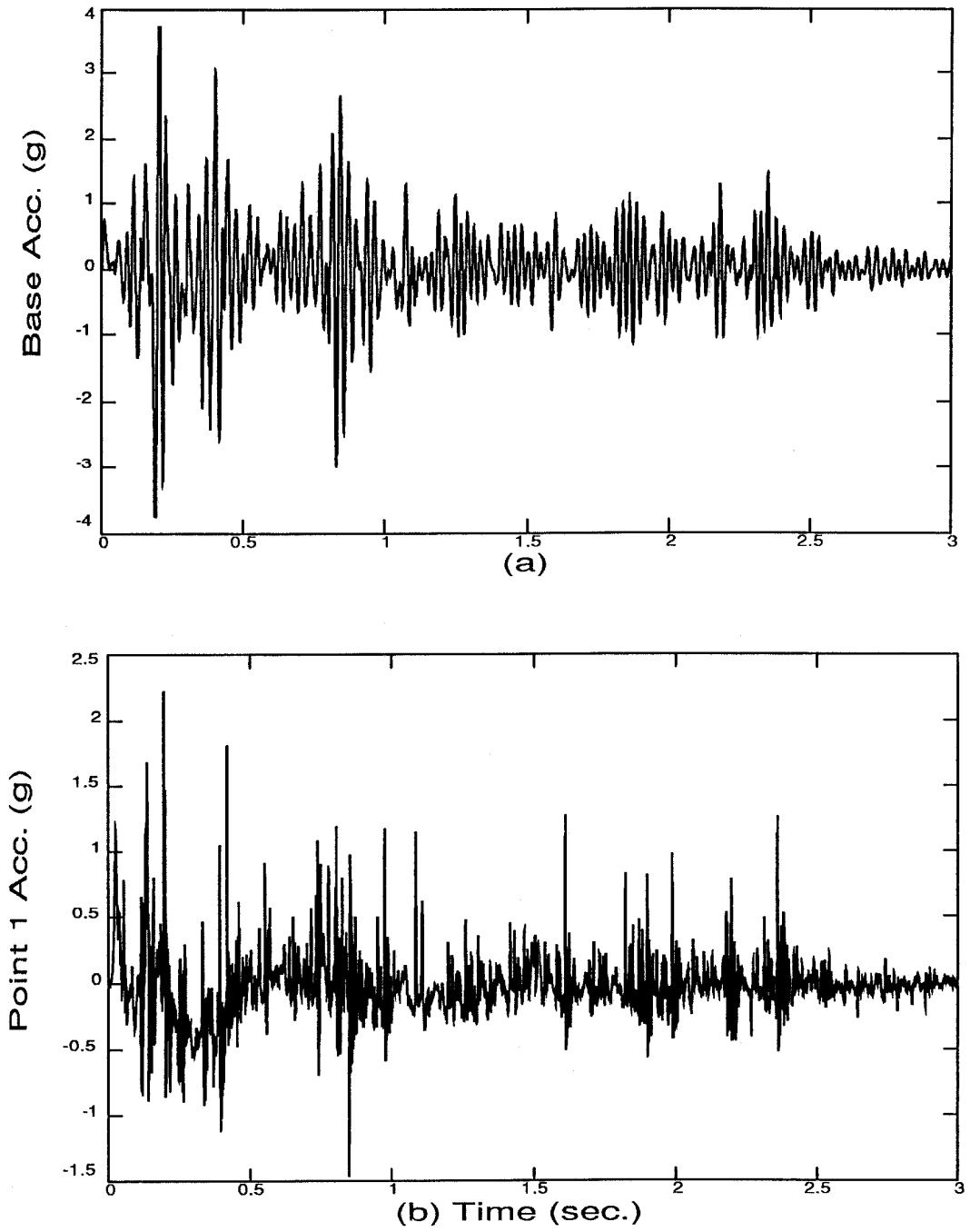

Figure 4.12: (a) Base acceleration and (b) dam acceleration response at point 1 for the second earthquake test on the monolithic model.

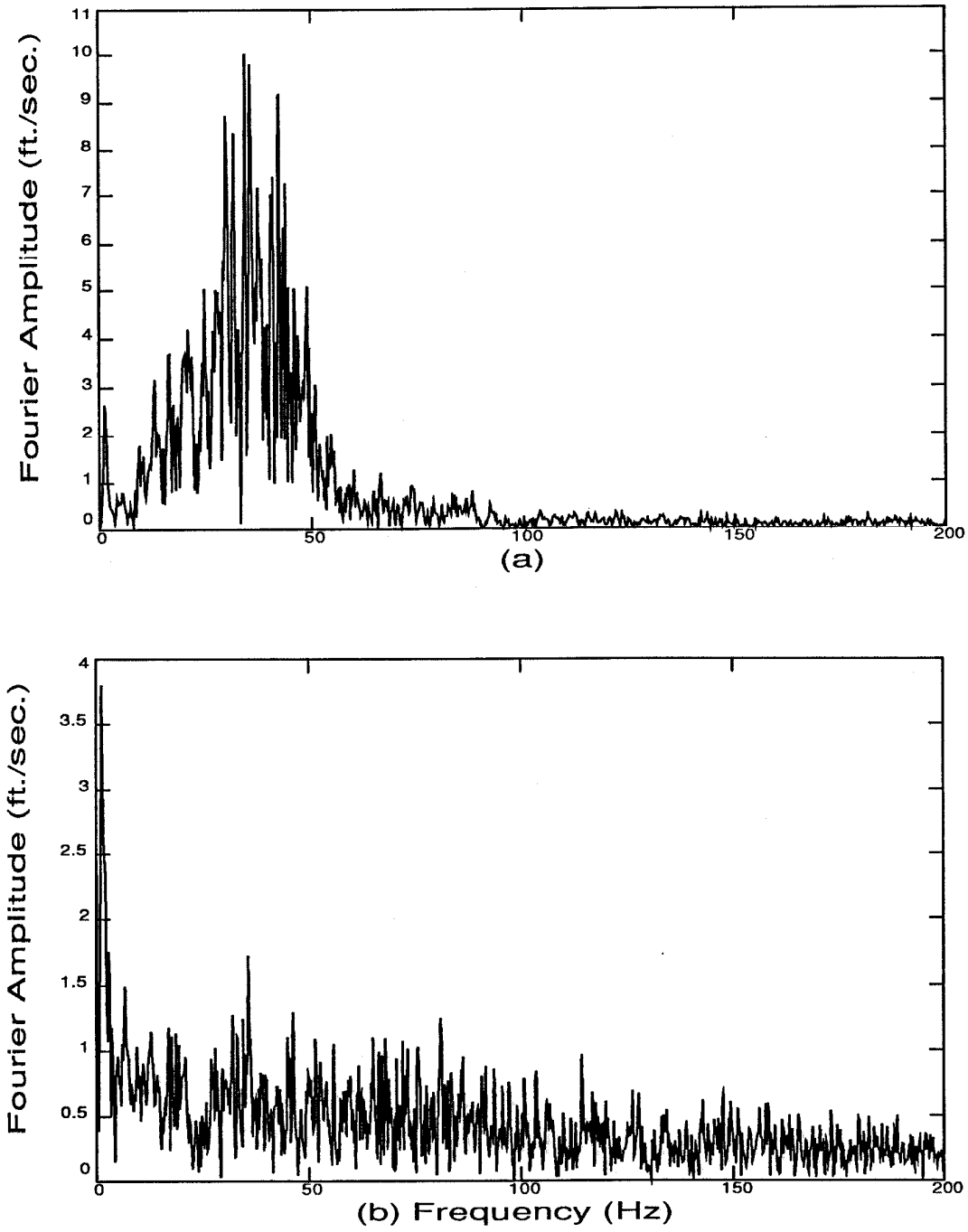

Figure 4.13: Fourier transforms of the base motion (a) and dam response at point 1 (b) for the second high-level earthquake test on the monolithic model.

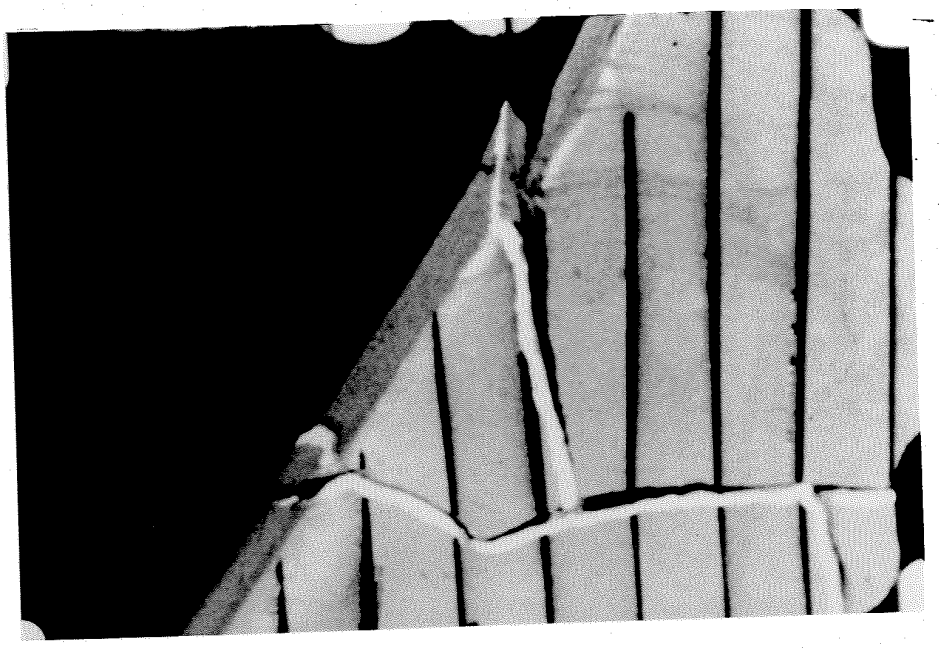

Figure 4.14: (a) t=0.26 sec.

Figure 4.14: (b) t=1.2 sec.

Figure 4.14: Film frames at specific instants of time of the second earthquake test on the monolithic model.

Figure 4.15: (a) Filmed side of monolithic model after second earthquake test.

Figure 4.15: (b) Opposite side of monolithic model after second earthquake test.

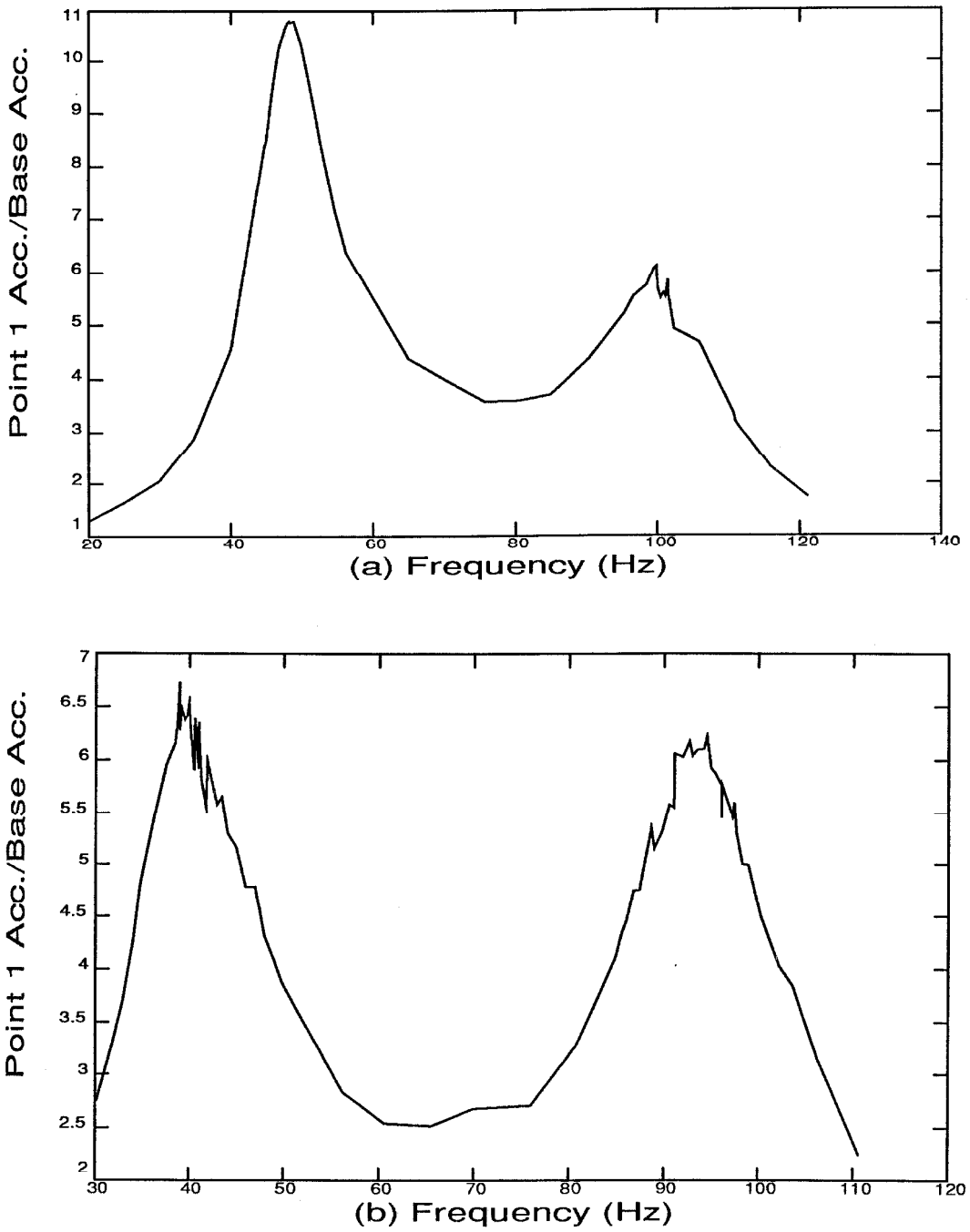

Figure 4.16: Amplification at point 1 (dam acceleration/base acceleration) resulting from the frequency sweeps of the first composite model (a) without water and (b) with water.

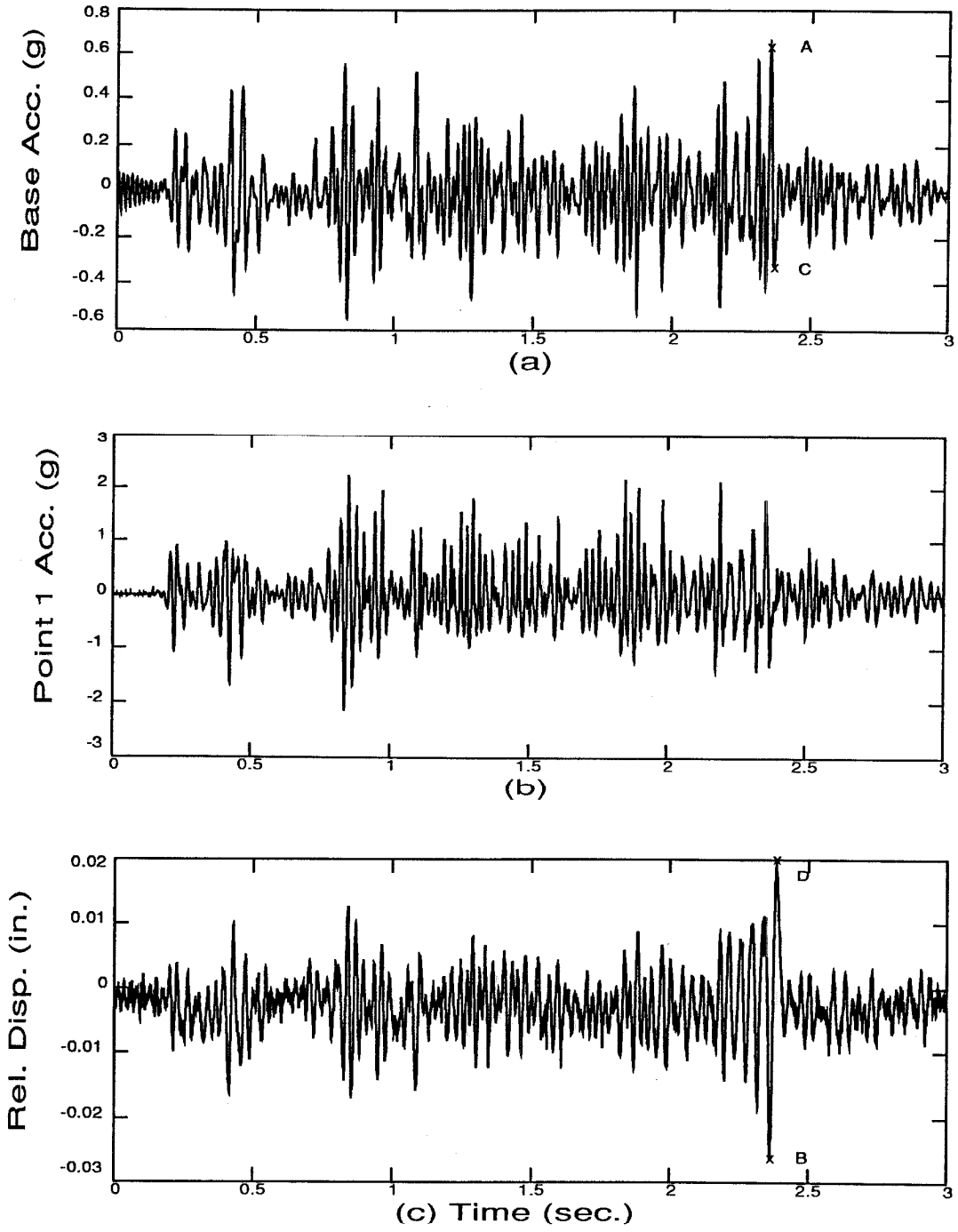

Figure 4.17: (a) Base acceleration, (b) acceleration response at point 1, and (c) displacement of point 1 relative to the base for the initial cracking earthquake test on the first composite model.

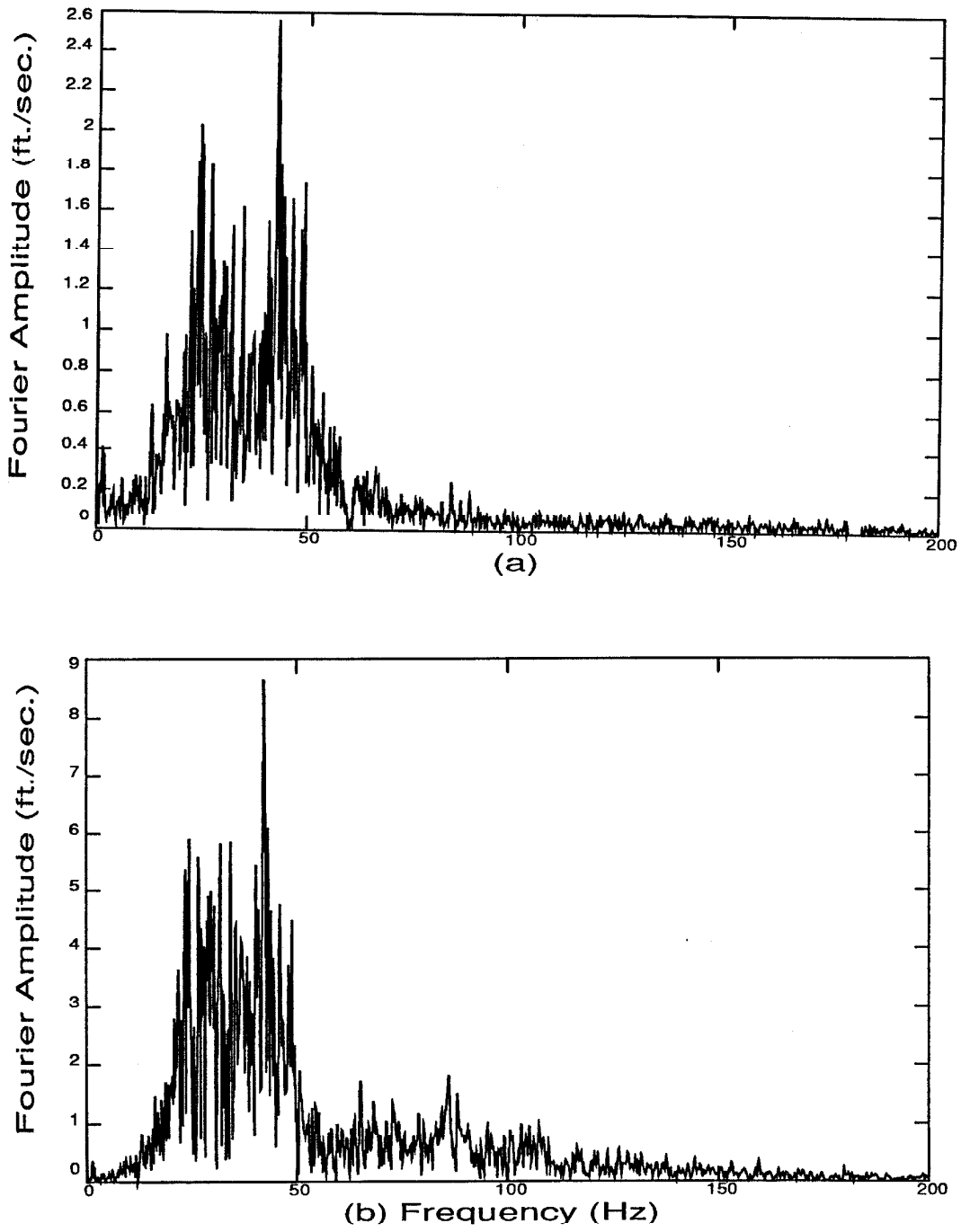

Figure 4.18: Fourier transforms of the base motion (a) and dam response at point 1 (b) for the initial cracking earthquake test on the first composite model.

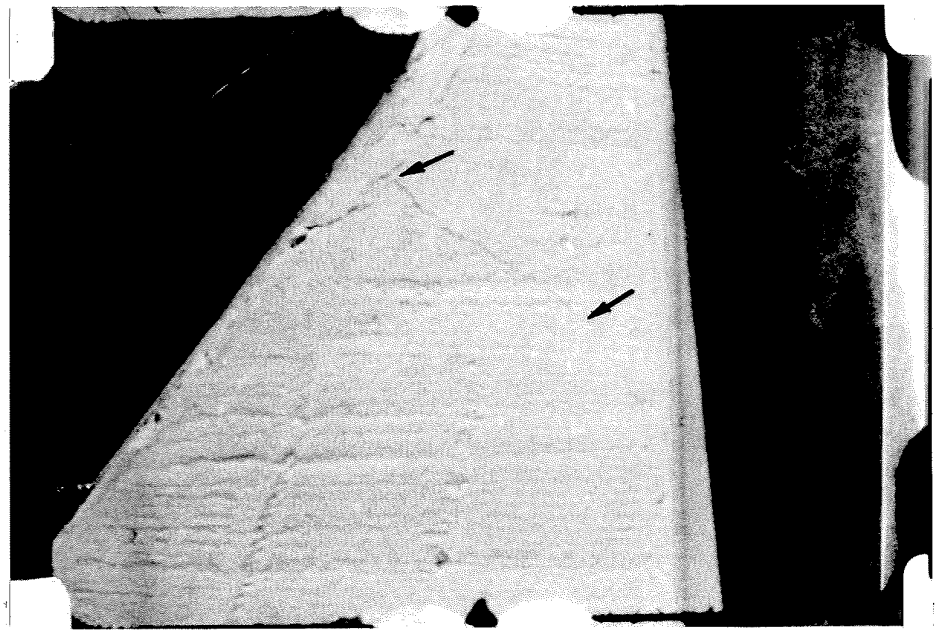

Figure 4.19: Downstream crack opening during first test on first composite model (t=2.384 sec.).

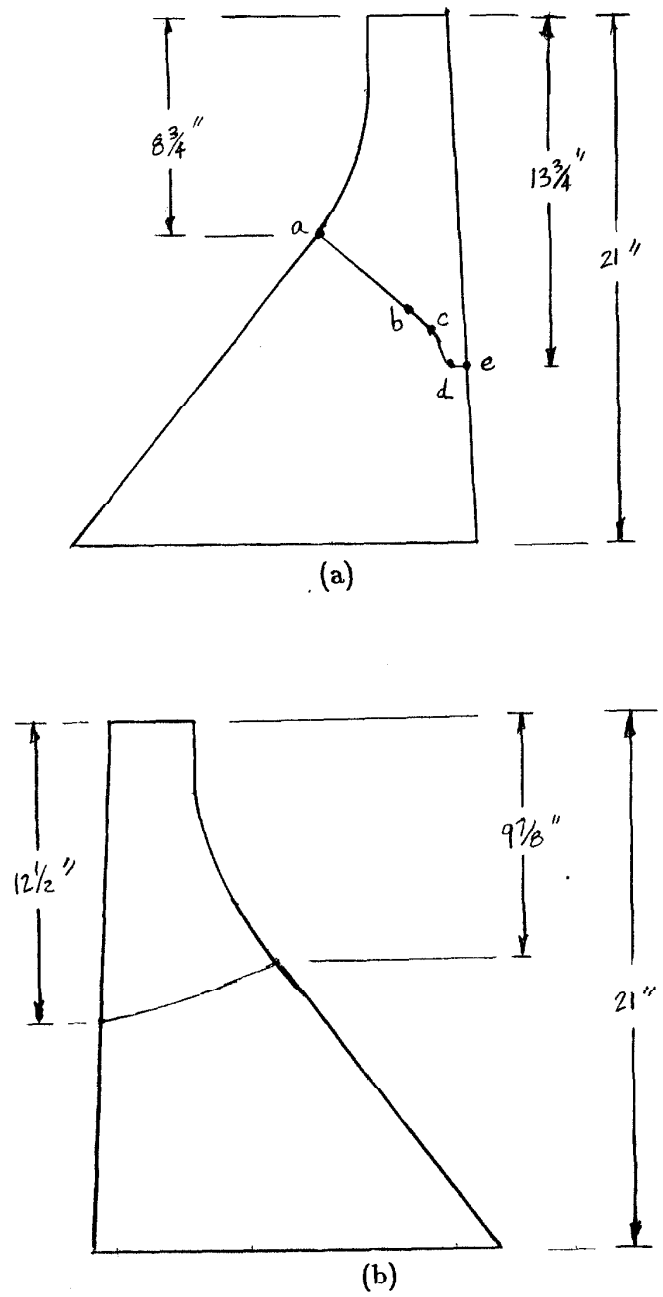

Figure 4.20: Sketch of the plaster portion of the first composite showing the extent of cracking after the initial earthquake test: (a) filmed side, (b) opposite side.

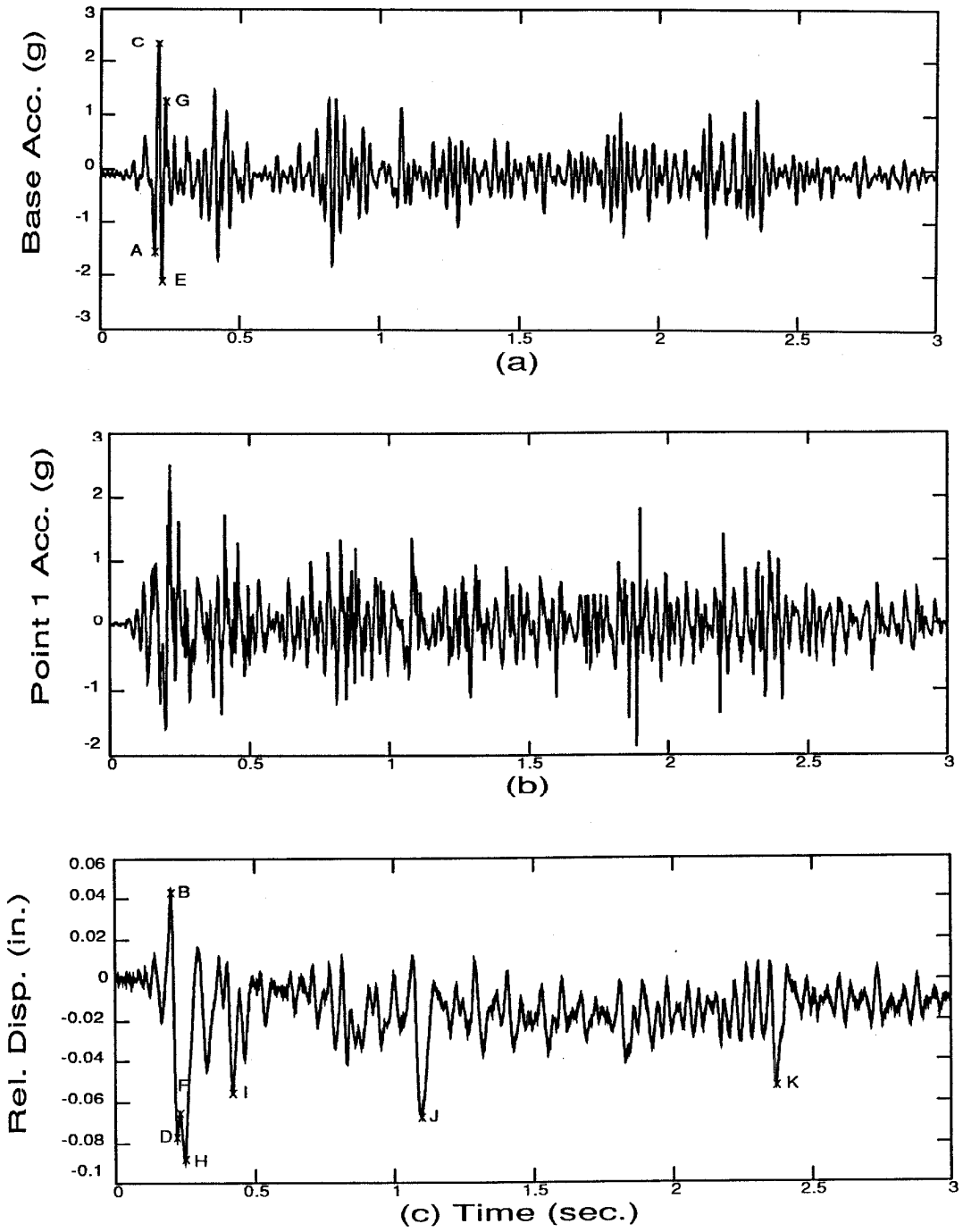

Figure 4.21: (a) Base acceleration, (b) acceleration response at point 1, and (c) displacement of point 1 relative to the base for the second earthquake test on the first composite model.

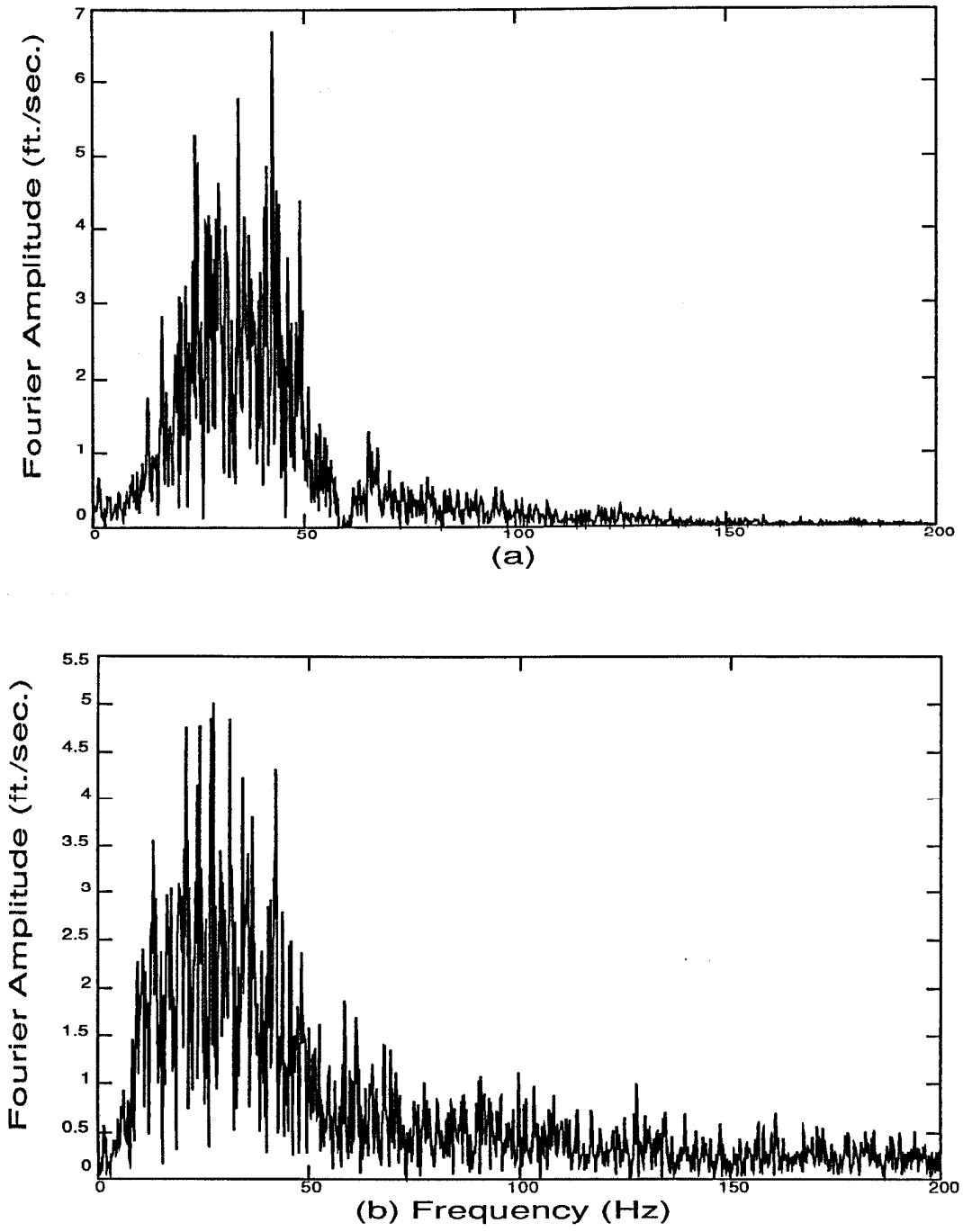

Figure 4.22: Fourier transforms of the base motion (a) and dam response at point 1 (b) for the second earthquake test on the first composite model.

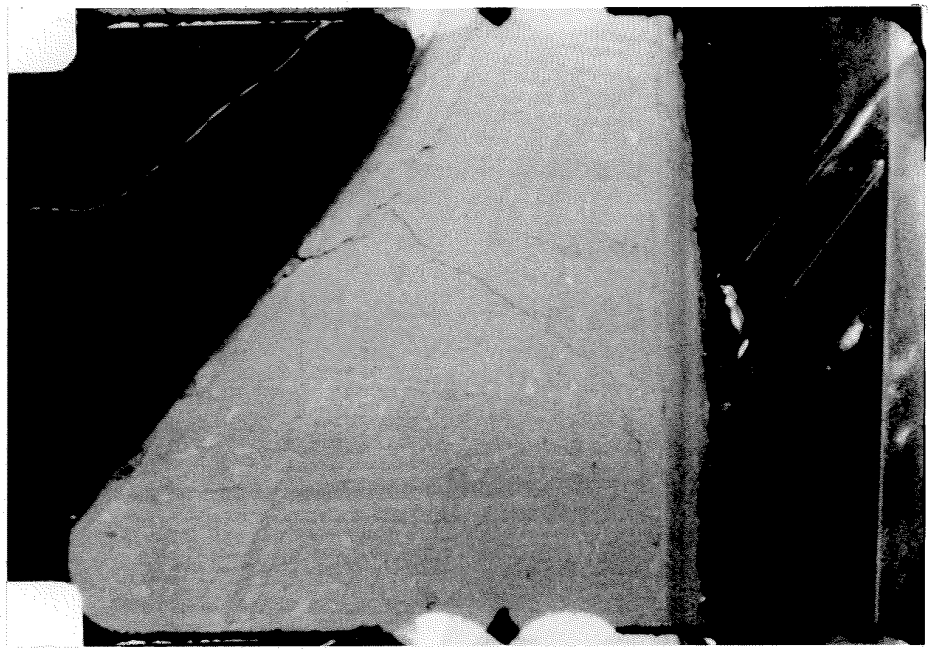

Figure 4.23: (a) t=0.2002 sec.

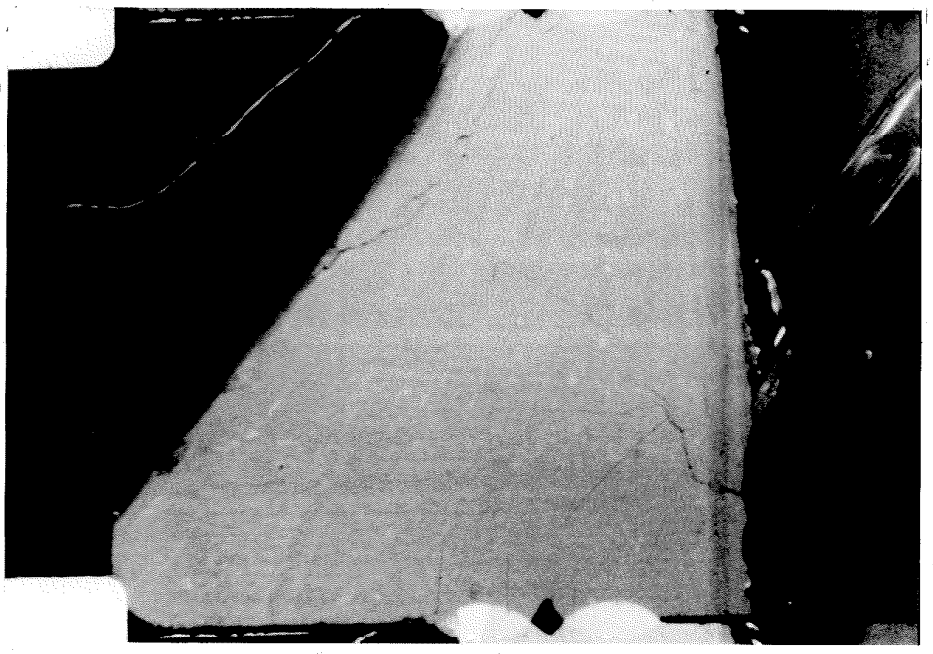

Figure 4.23: (b) t=0.2123 sec.

Figure 4.23: Film frames at specific instants of time of the second earthquake test on the first composite model.

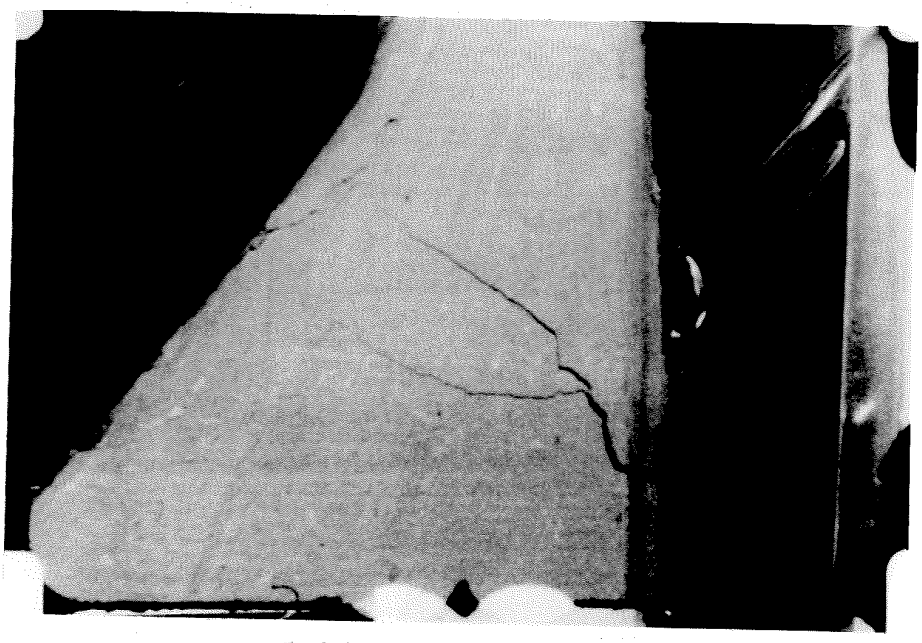

Figure 4.23: (c) t=0.2244 sec.

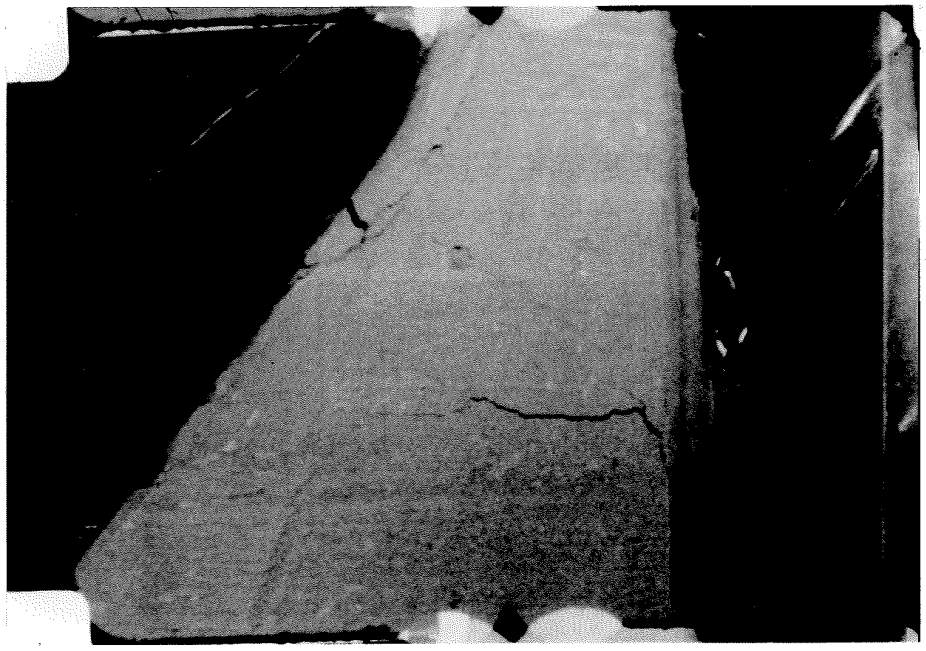

Figure 4.23: (d) t=0.4184 sec.

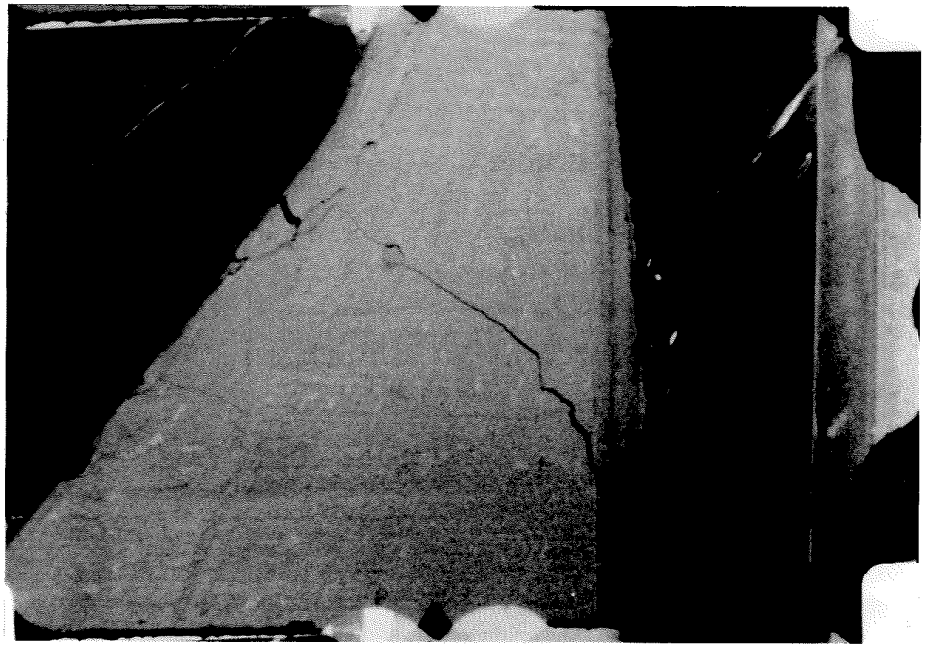

Figure 4.23: (e) t=0.4244 sec.

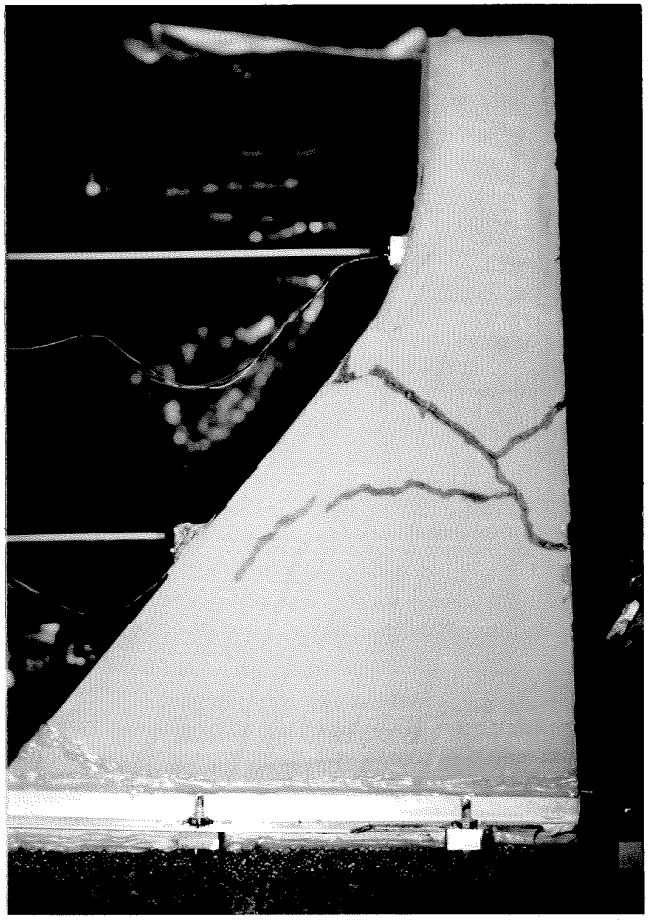

Figure 4.24: (a) Filmed side of first composite model after second earthquake test.

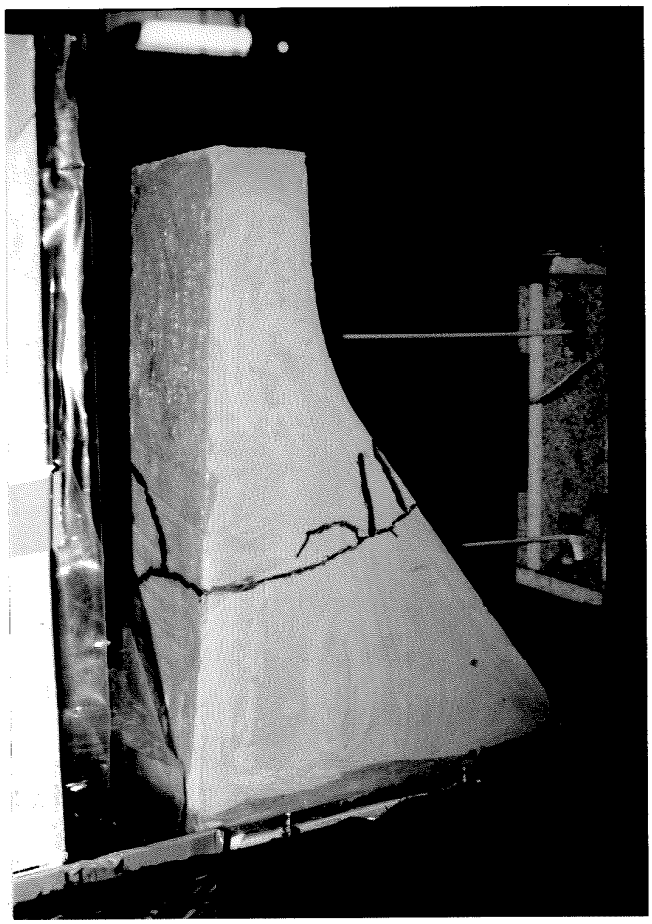

Figure 4.24: (b) Opposite side and upstream face of first composite after second earthquake test.

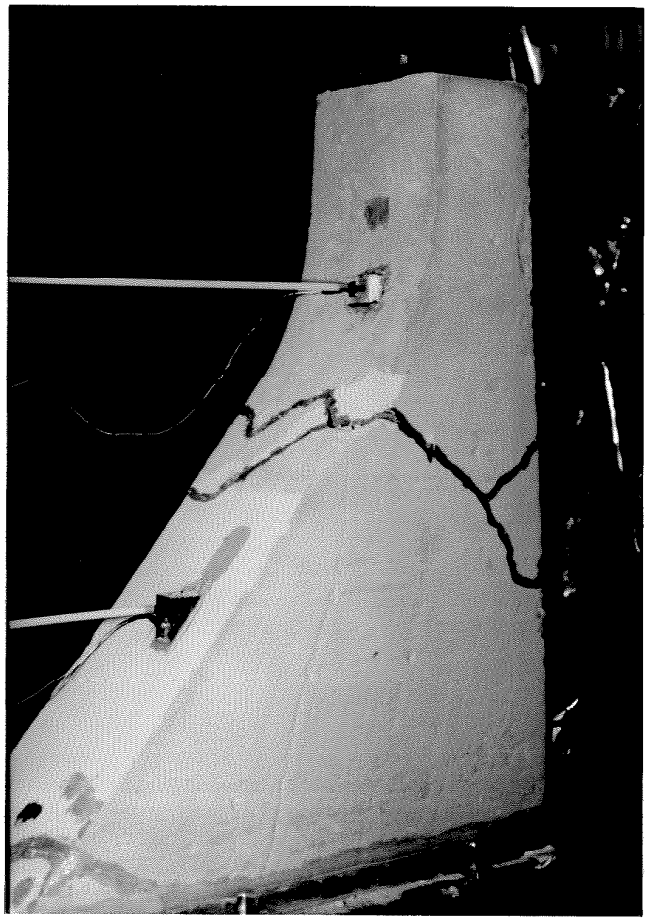

Figure 4.24: (c) Filmed side and downstream face of first composite after second earthquake test. The lower crack shown in part (a) had not been traced when this photo was taken.

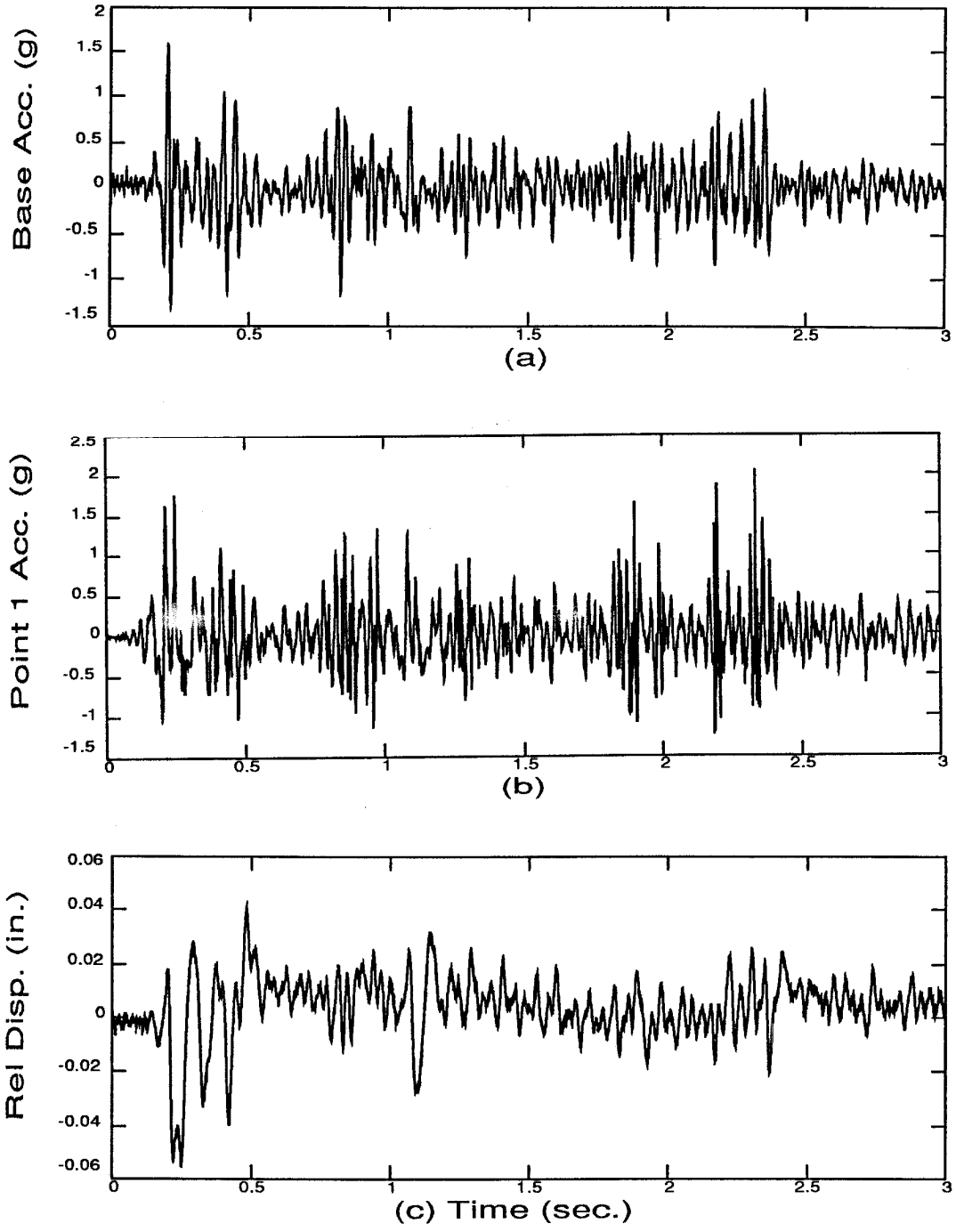

Figure 4.25: (a) Base acceleration, (b) acceleration response at point 1, and (c) displacement of point 1 relative to the base for the third earthquake test on the first composite model.

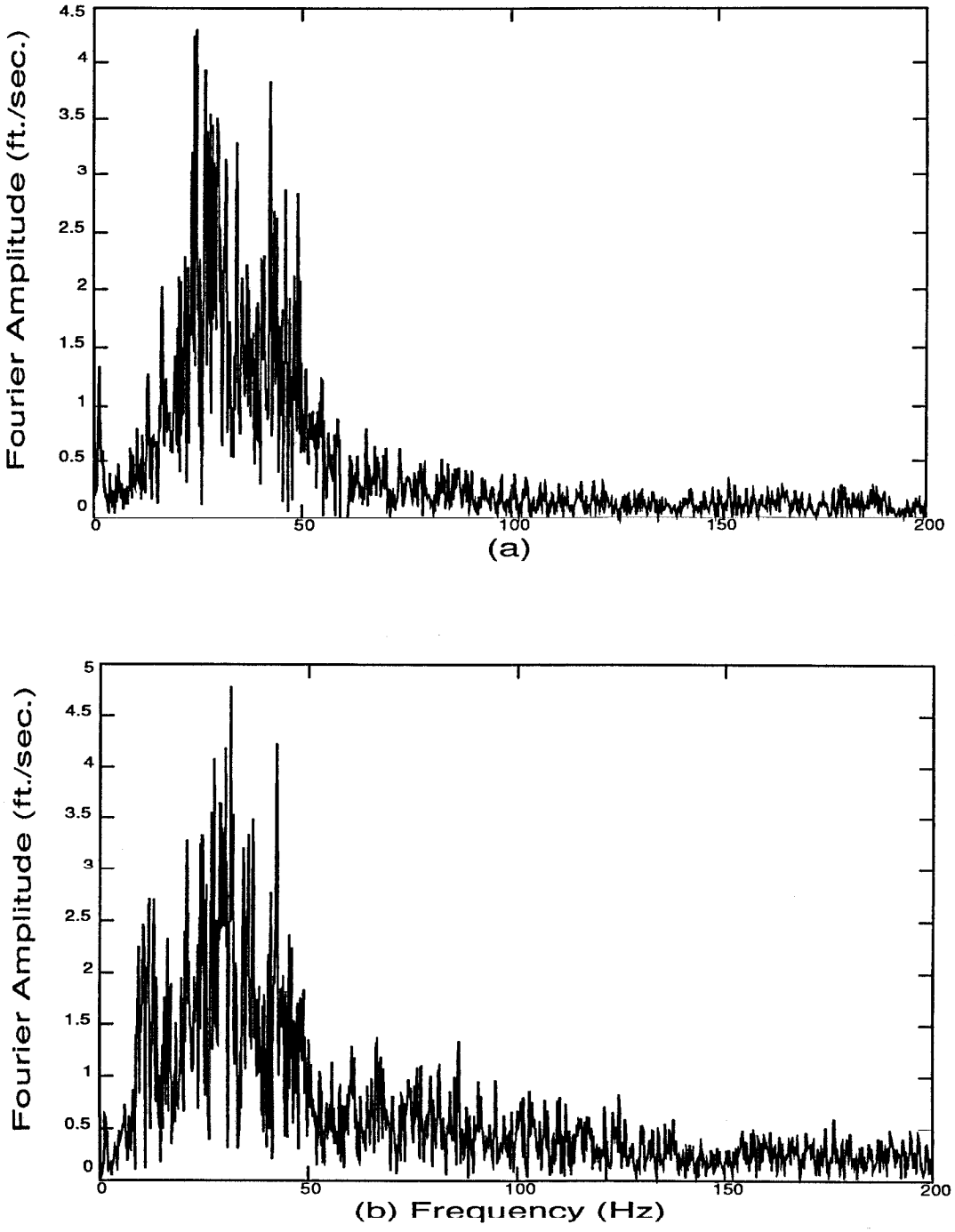

Figure 4.26: Fourier transforms of the base motion (a) and dam response at point 1 (b) for the third earthquake test on the first composite model.

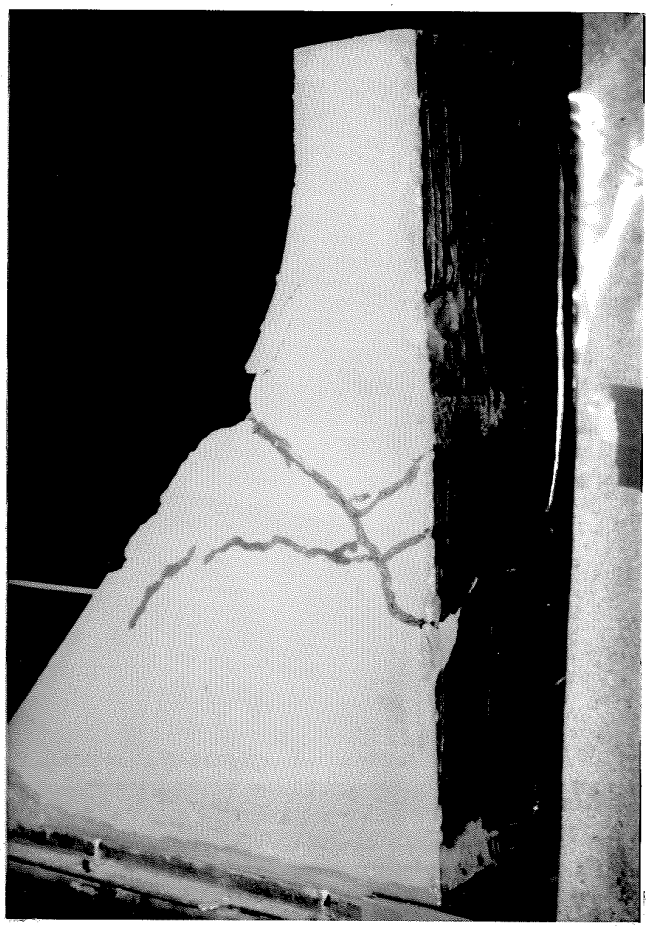

Figure 4.27: Filmed side and upstream face of first composite model after third earthquake test.

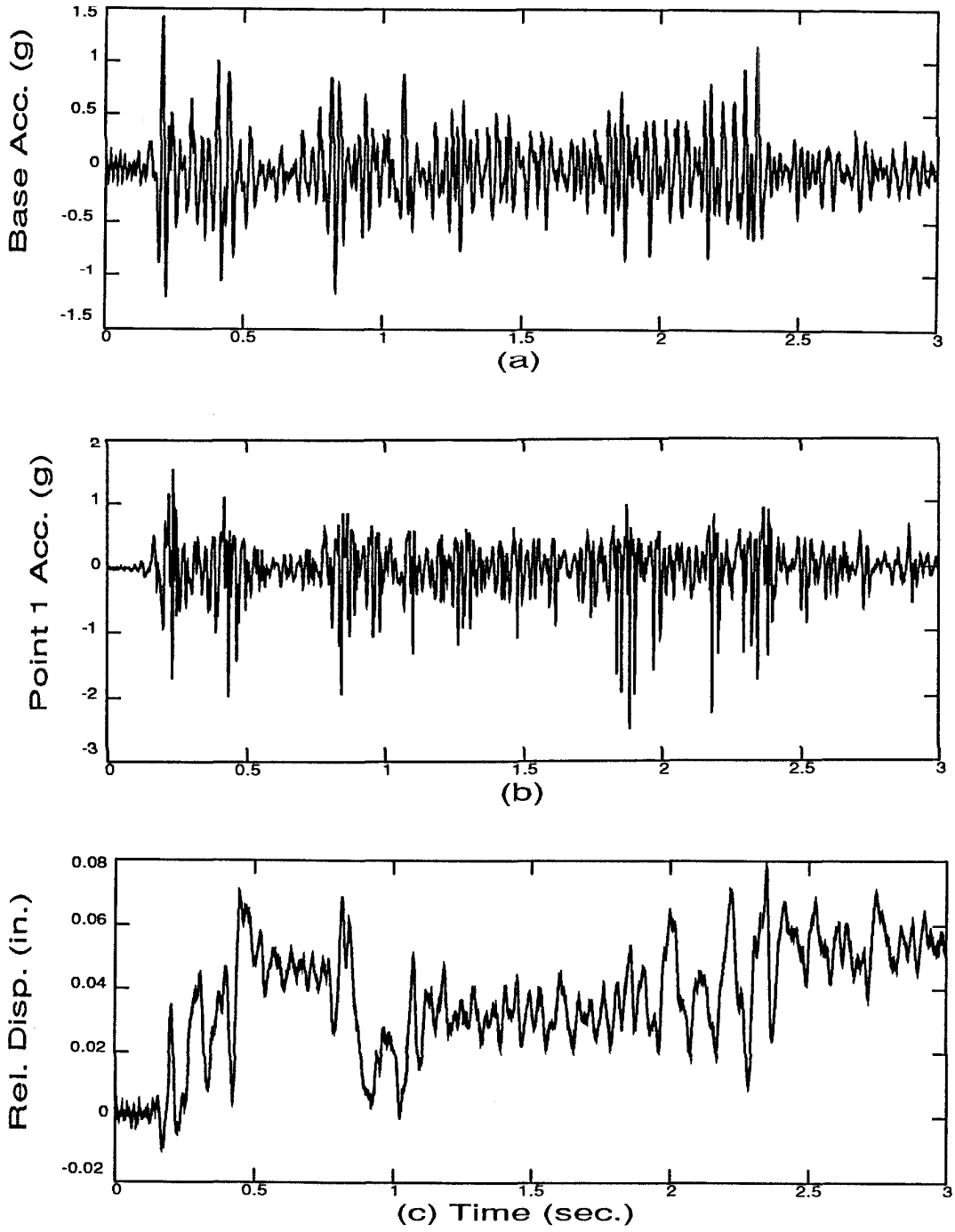

Figure 4.28: (a) Base acceleration, (b) acceleration response at point 1, and (c) displacement of point 1 relative to the base for the fourth earthquake test on the first composite model.

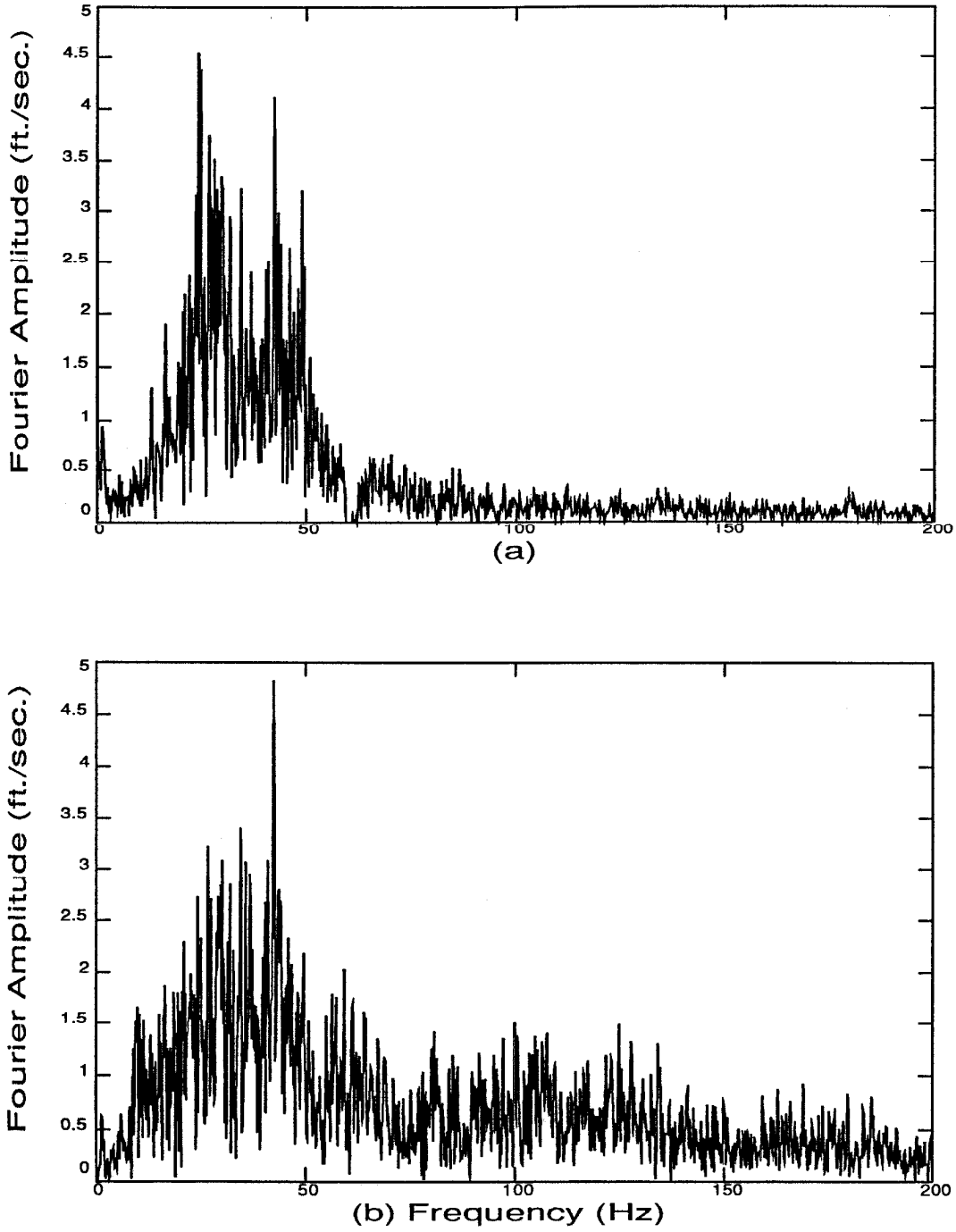

Figure 4.29: Fourier transforms of the base motion (a) and dam response at point 1 (b) for the fourth earthquake test on the first composite model.

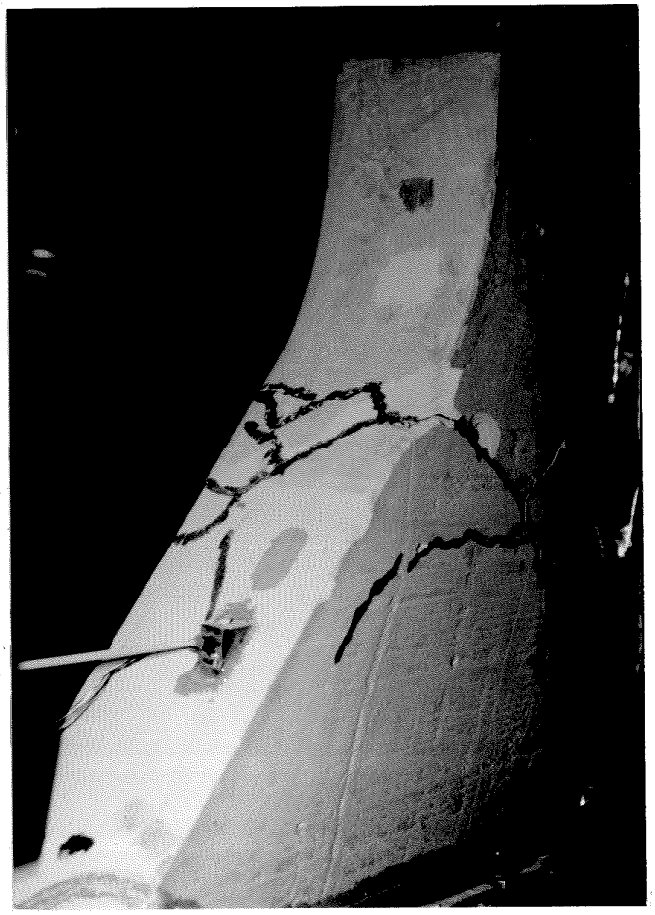

Figure 4.30: (a) Filmed side and downstream face of first composite after fourth earthquake test.

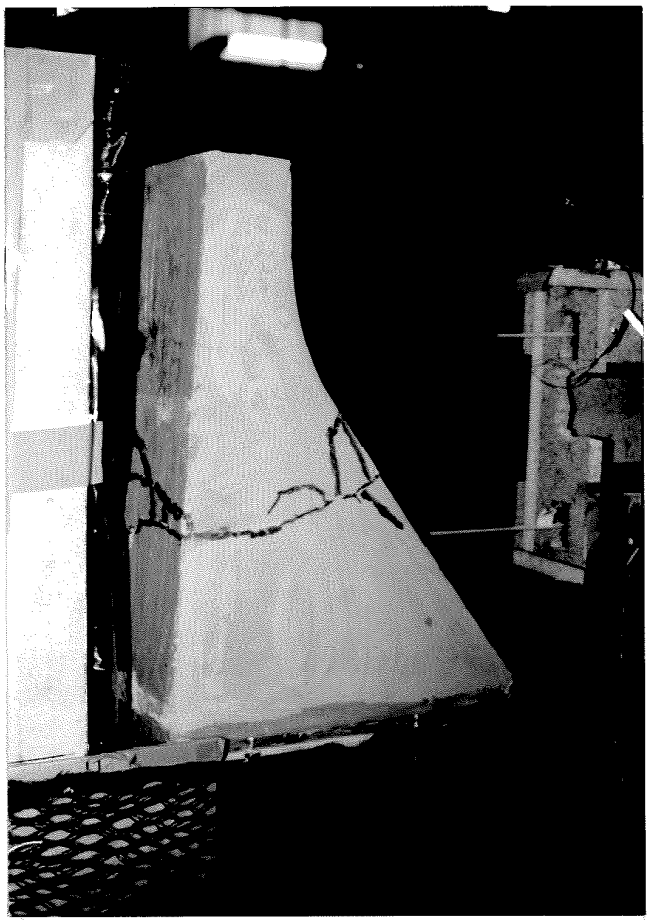

Figure 4.30: (b) Opposite side and upstream face of first composite after fourth earthquake test.

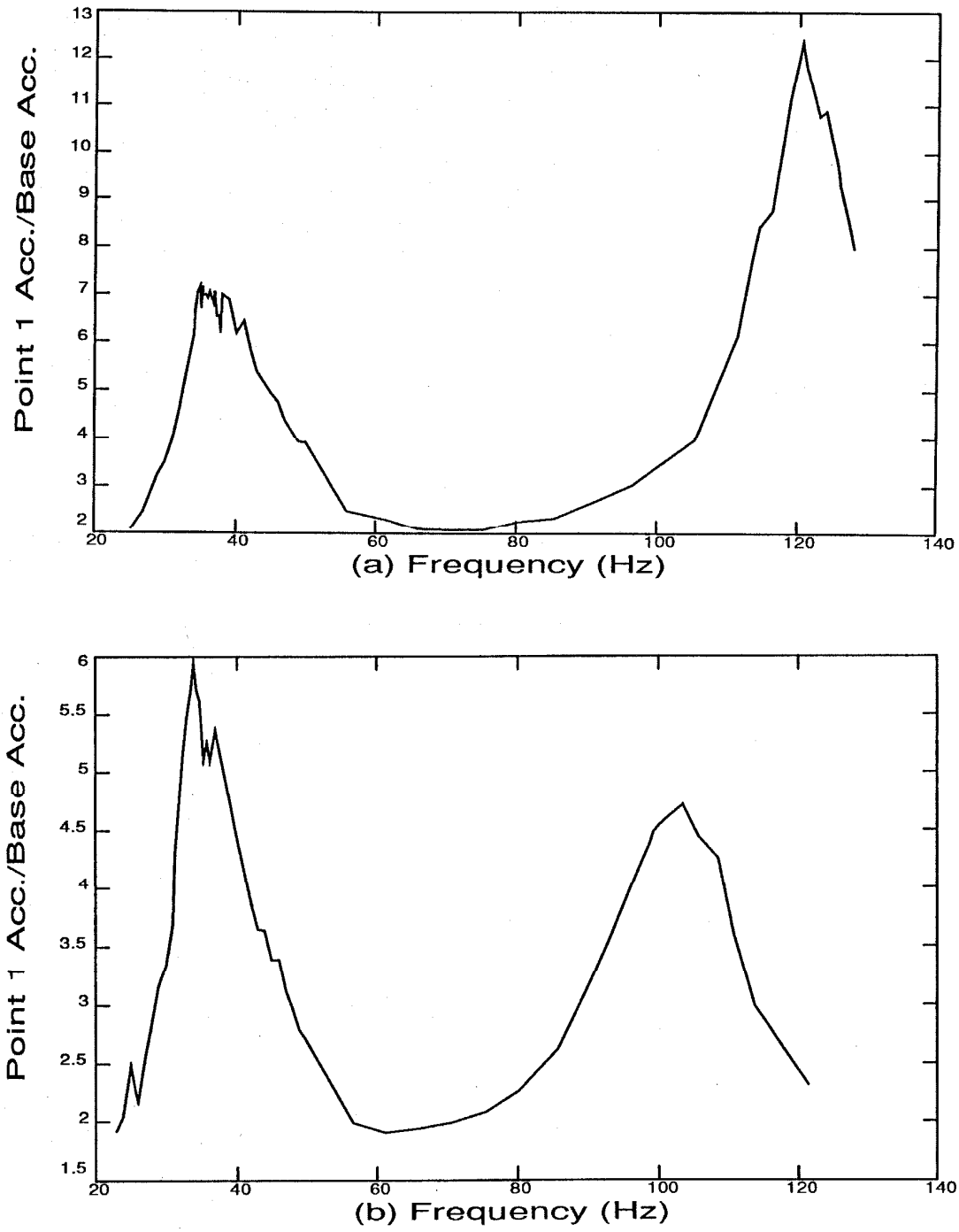

Figure 4.31: Amplification at point 1 (dam acceleration/base acceleration) resulting from the frequency sweeps of the second composite model (a) without water and (b) with water.

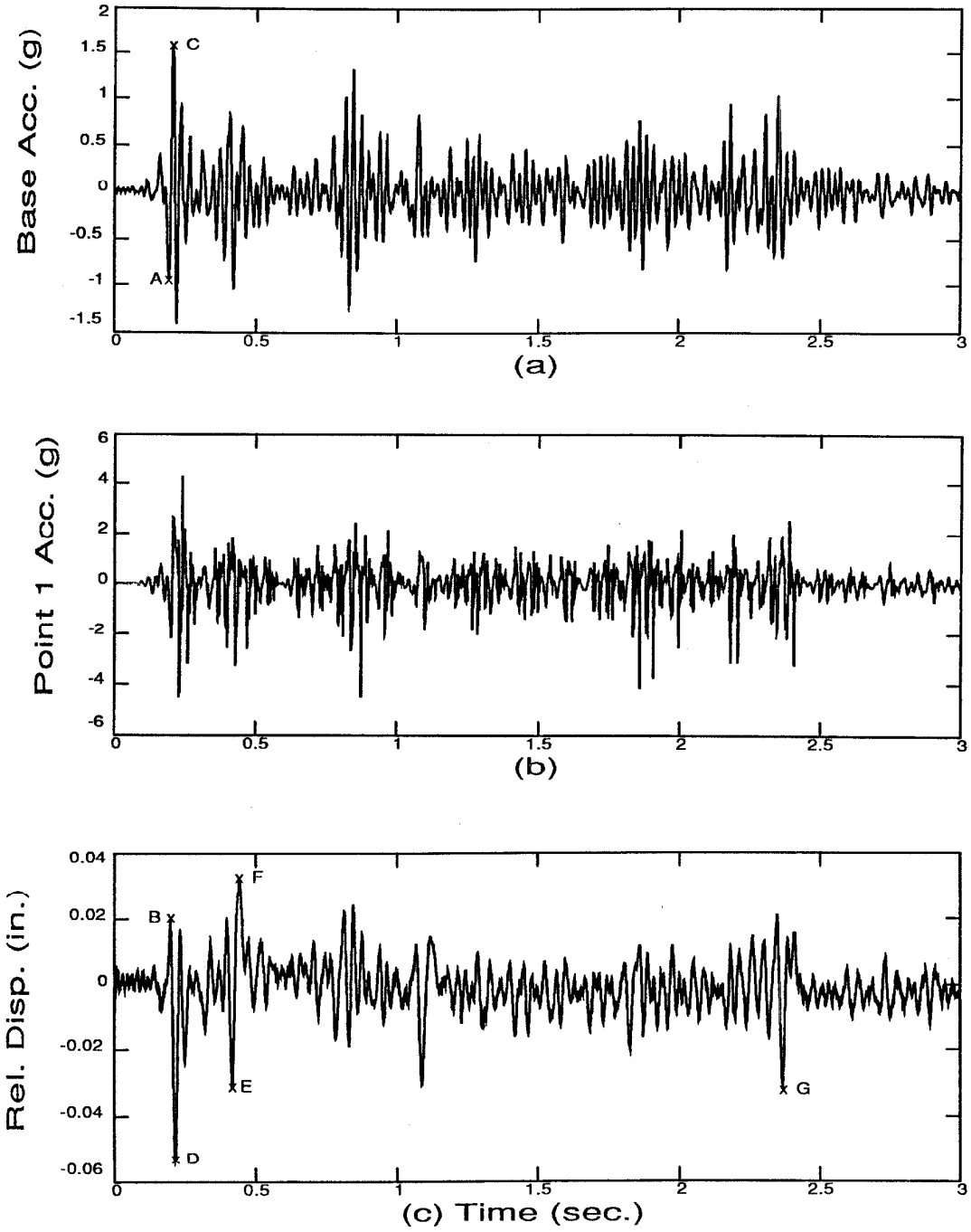

Figure 4.32: (a) Base acceleration, (b) acceleration response at point 1, and (c) displacement of point 1 relative to the base for the initial cracking earthquake test on the second composite model.

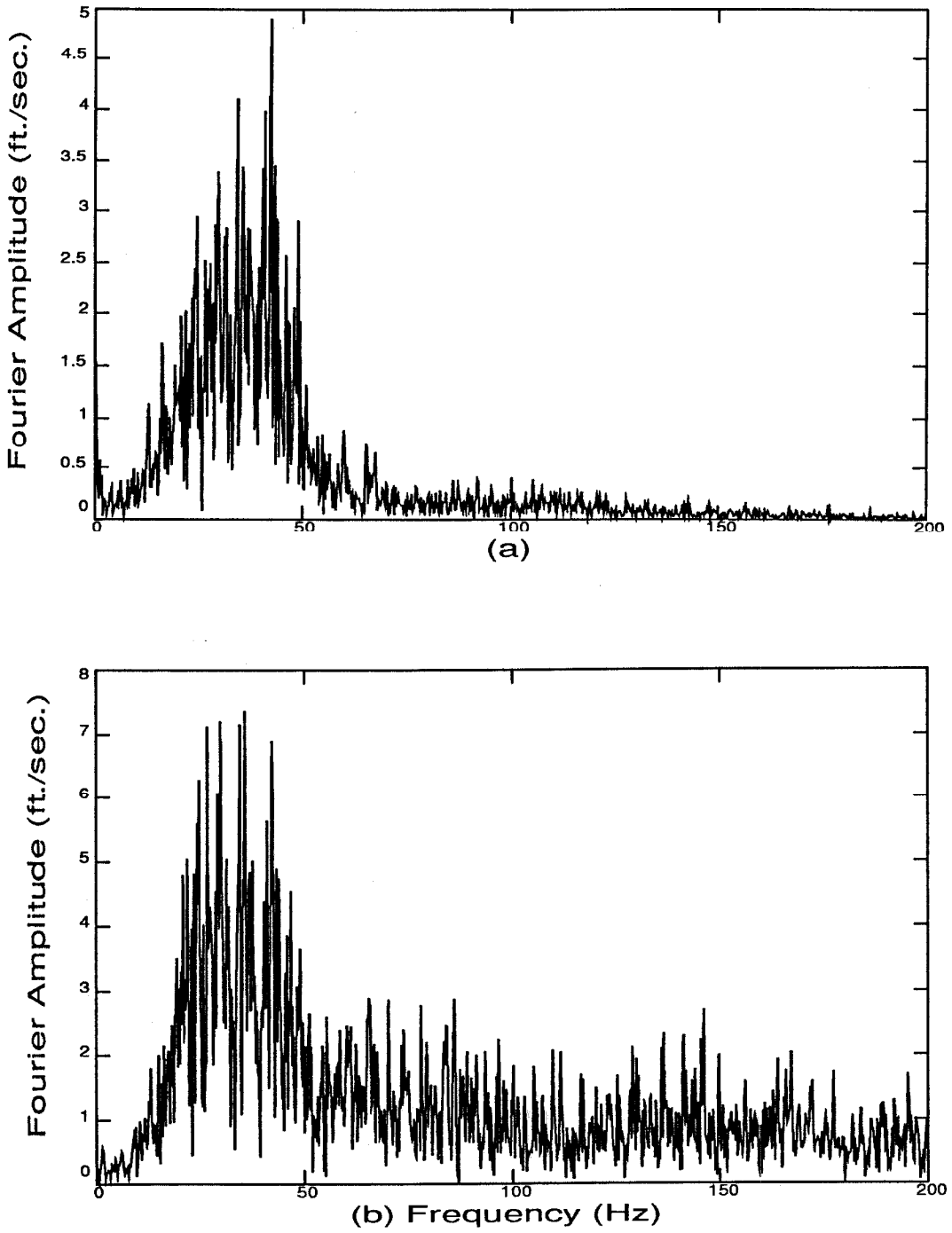

Figure 4.33: Fourier transforms of the base motion (a) and dam response at point 1 (b) for the initial cracking earthquake test on the second composite model.

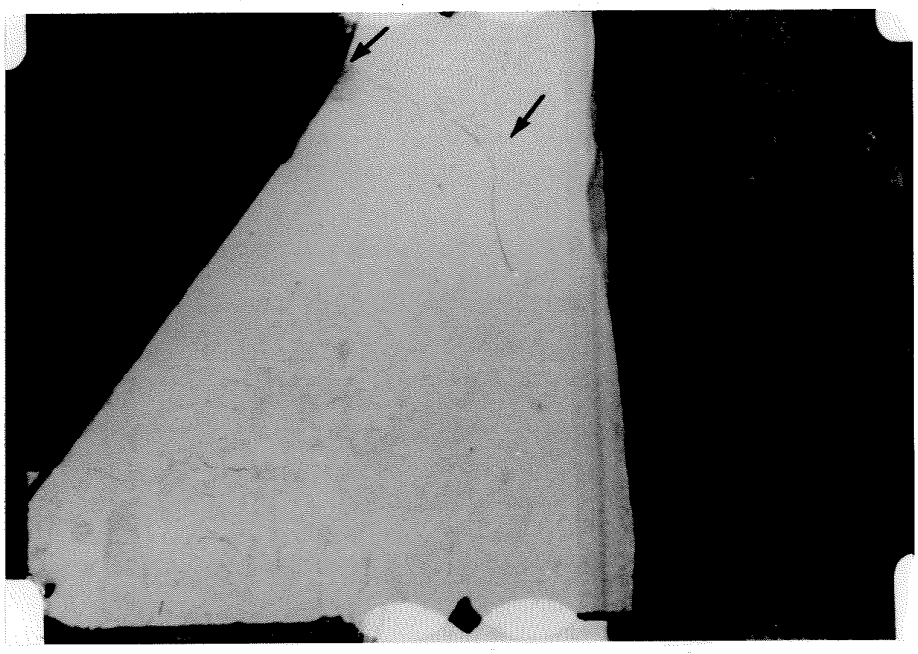

Figure 4.34: (a) t=0.200 sec.

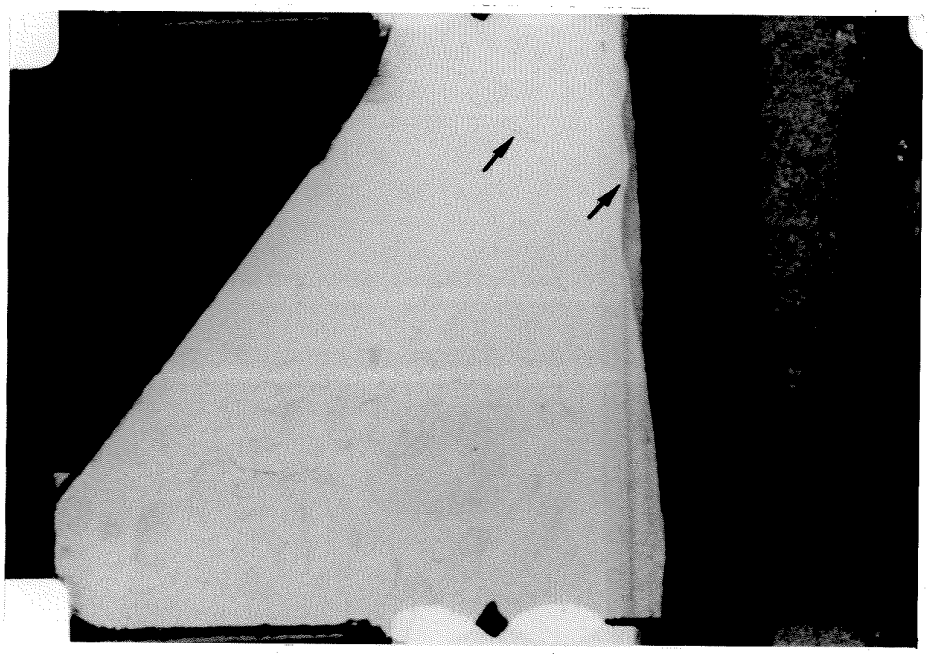

Figure 4.34: (b) t=0.216 sec.

Figure 4.34: Film frames at specific instants of time of the initial cracking earthquake test on the second composite model.

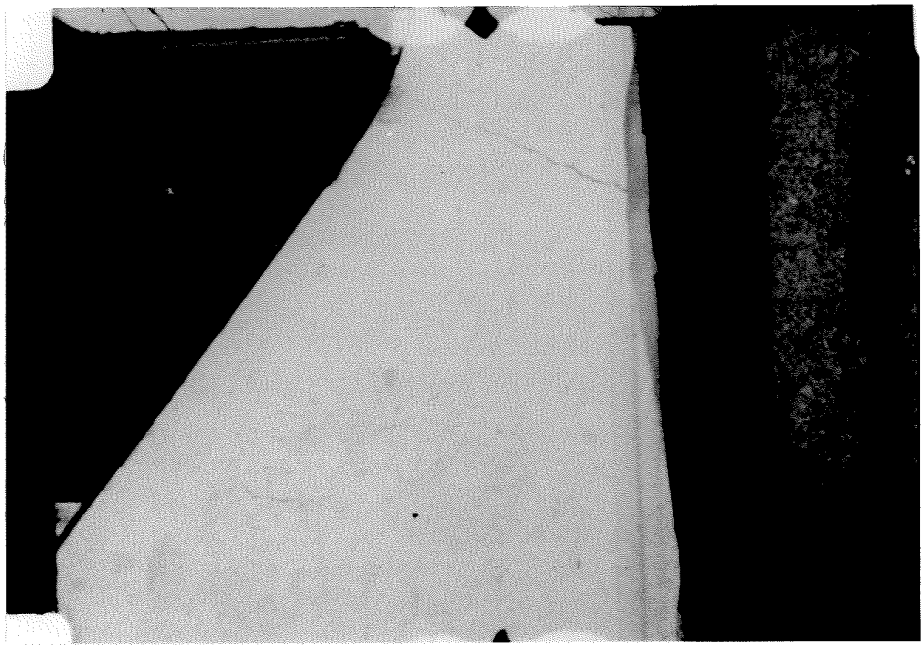

Figure 4.34: (c) t=0.4176 sec.

Figure 4.34: (d) t=0.4418 sec.

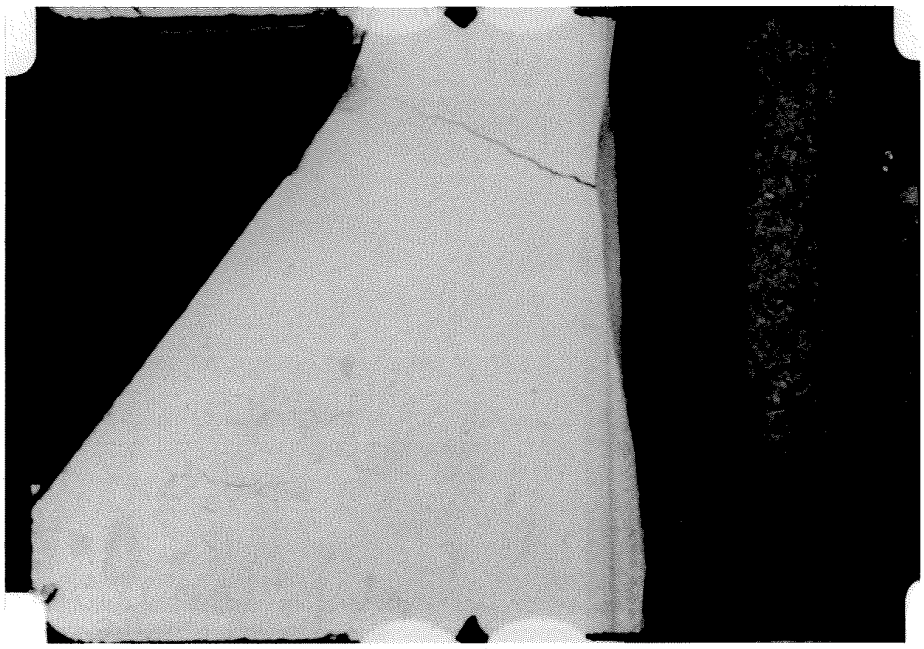

Figure 4.34: (e) t=2.368 sec.

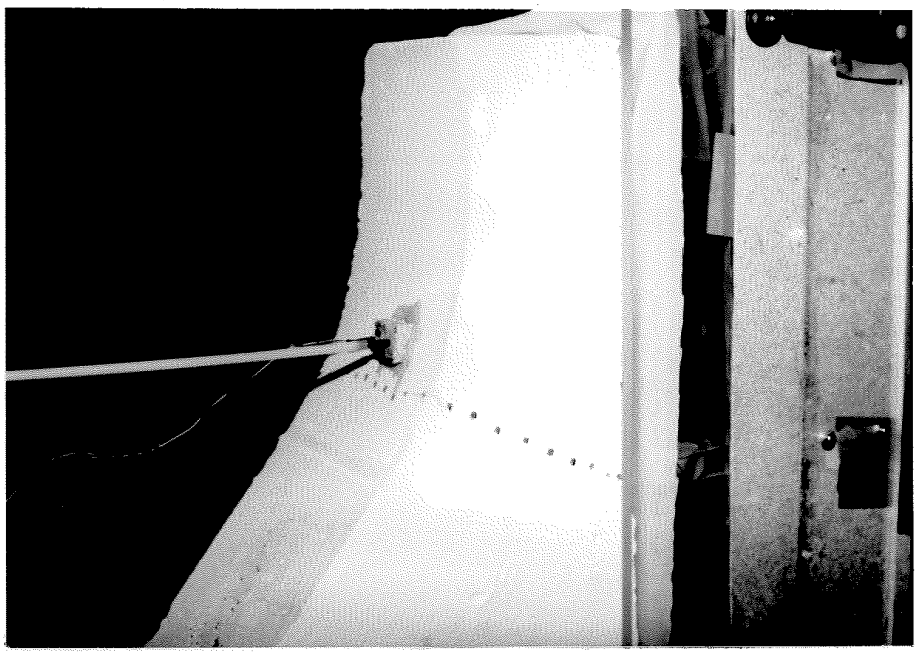

Figure 4.35: (a) Filmed side and downstream face of second composite after initial cracking earthquake test.

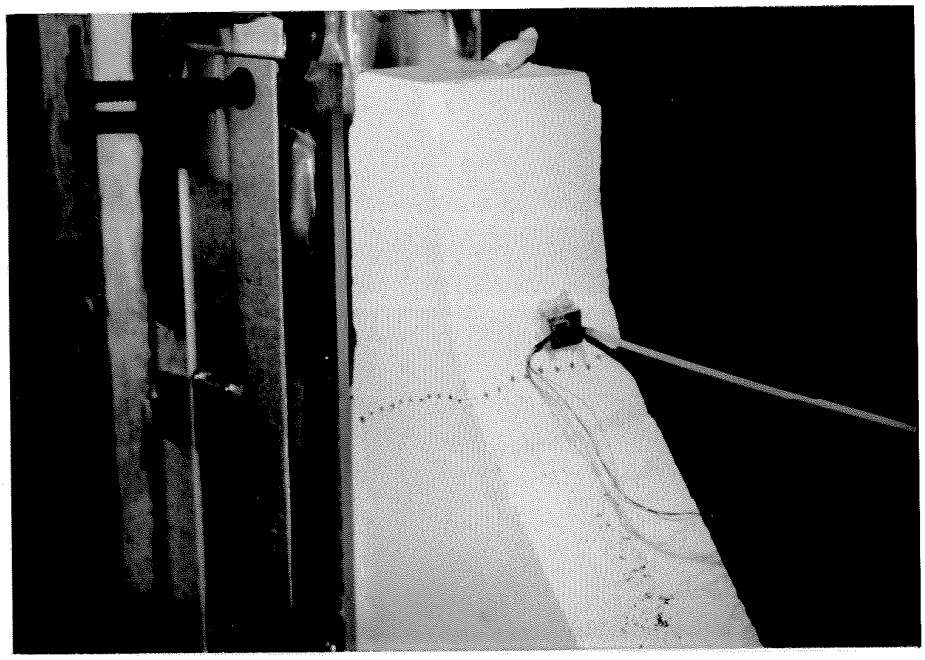

Figure 4.35: (b) Opposite side and downstream face of second composite after initial cracking earthquake test.

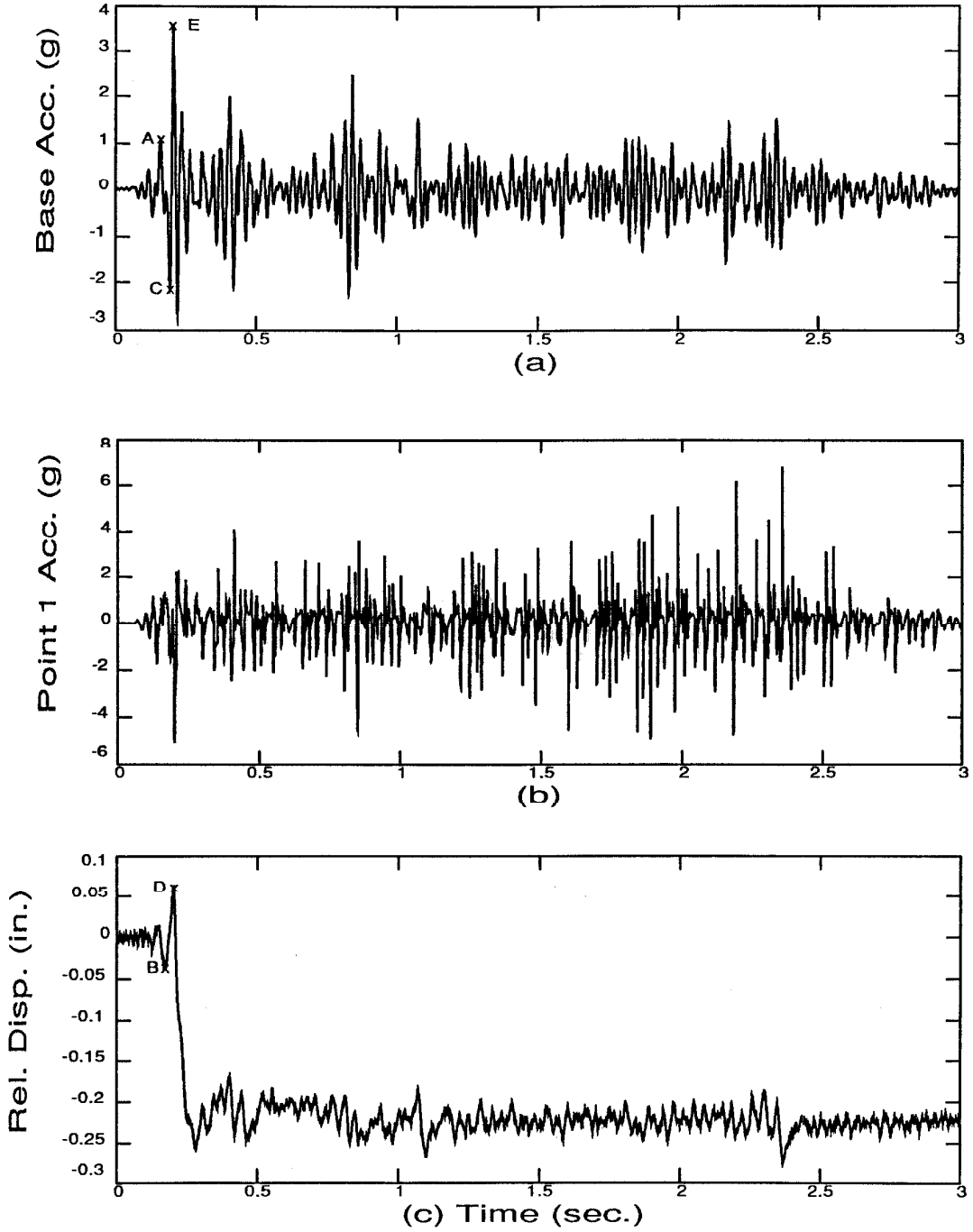

Figure 4.36: (a) Base acceleration, (b) acceleration response at point 1, and (c) displacement of point 1 relative to the base for the second earthquake test on the second composite model.

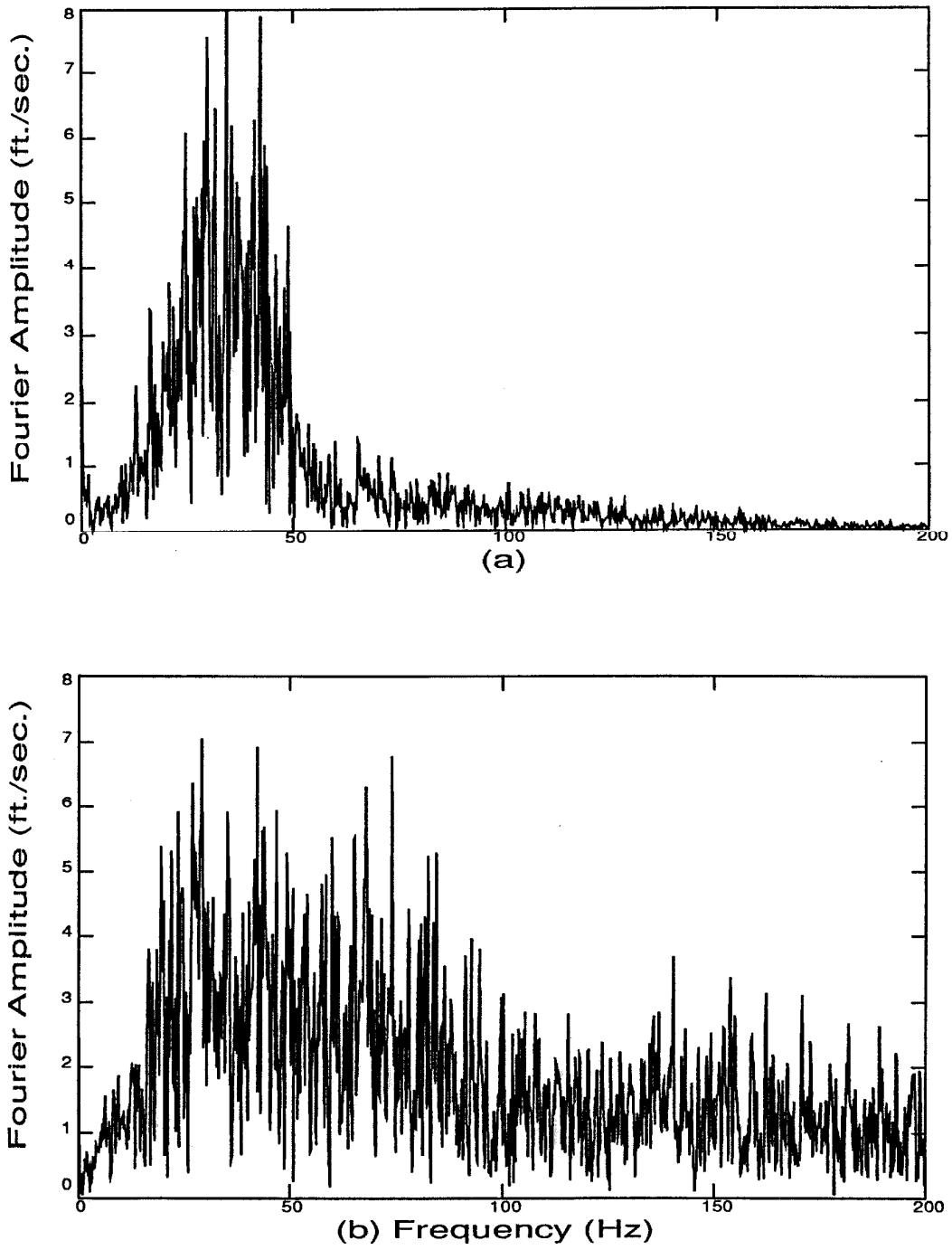

Figure 4.37: Fourier transforms of the base motion (a) and dam response at point 1 (b) for the second earthquake test on the second composite model.

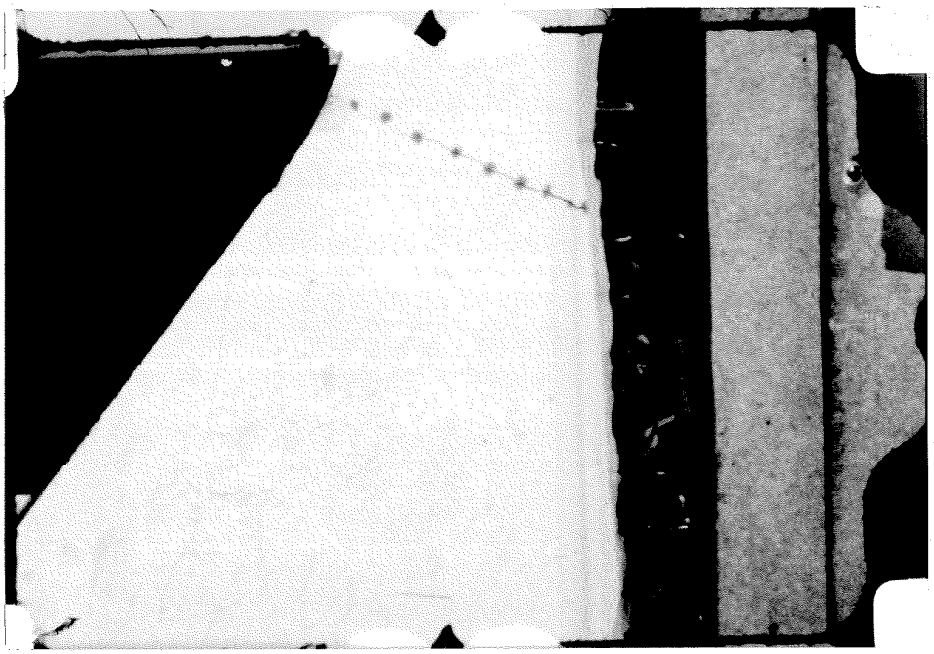

Figure 4.38: (a) t=0.173 sec.

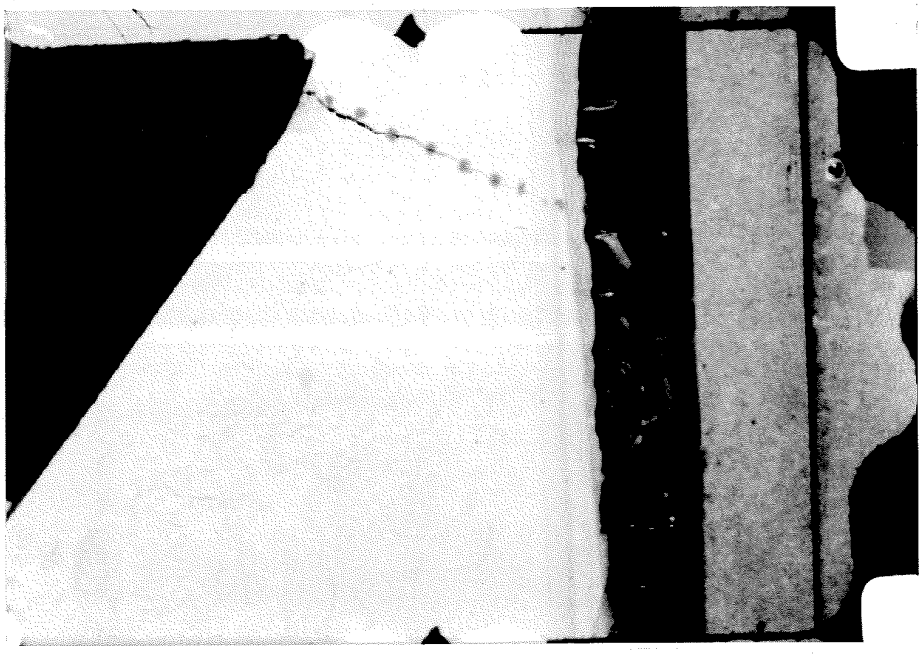

Figure 4.38: (b) t=0.20 sec.

Figure 4.38: Film frames at specific instants of time of the second earthquake test on the second composite model.

Figure 4.38: (c) t=0.21 sec.

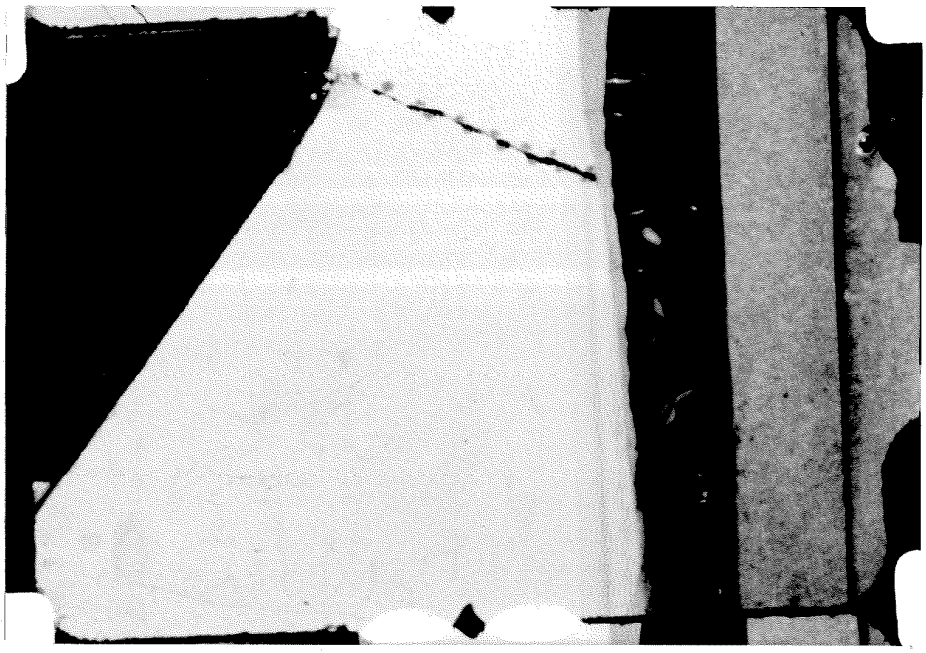

Figure 4.38: (d) t=0.24 sec.

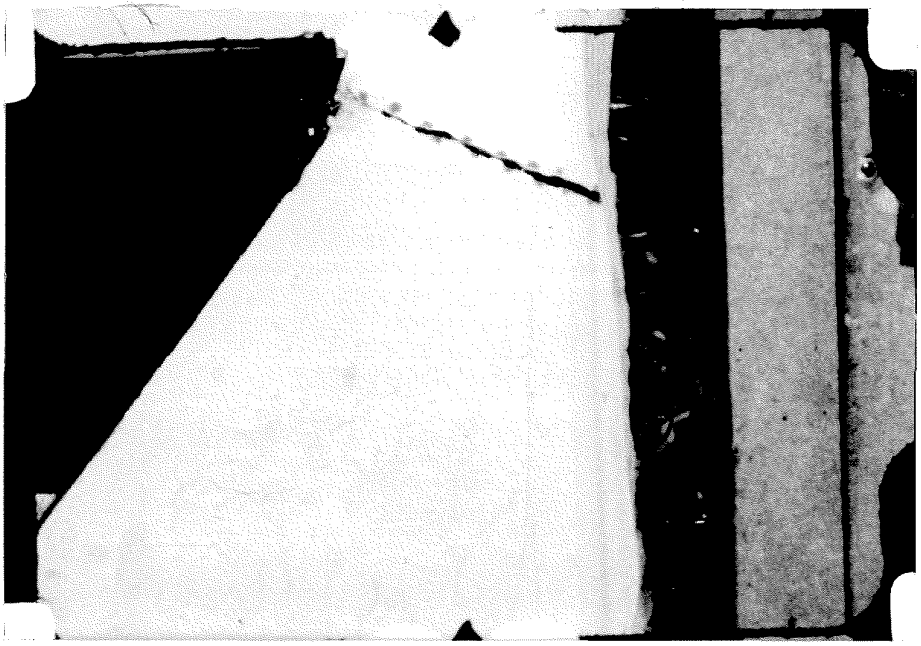

Figure 4.38: (e) t=0.25 sec.

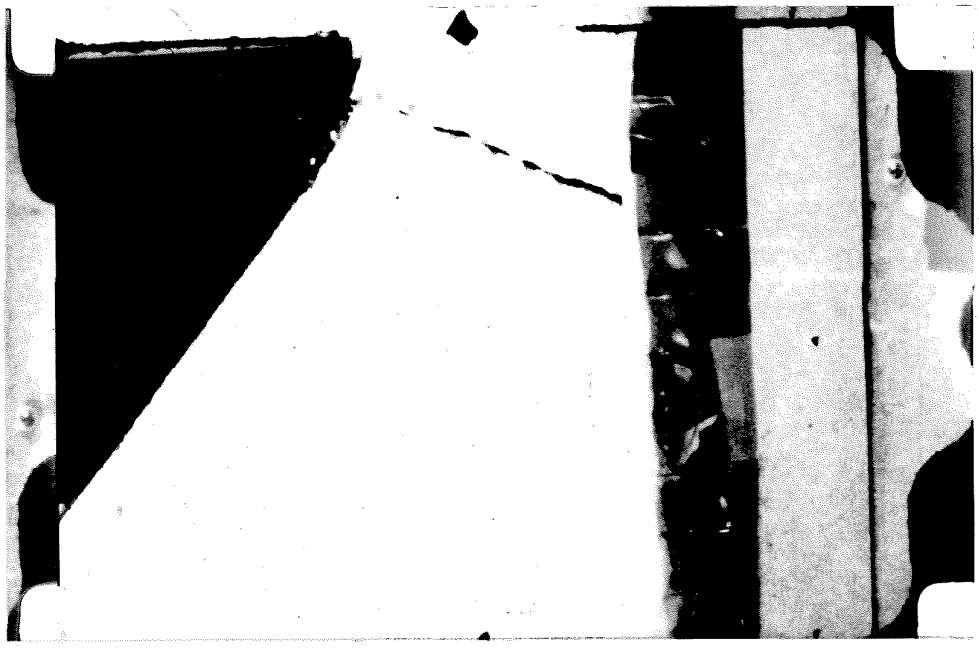

Figure 4.38: (f) t=0.27 sec.

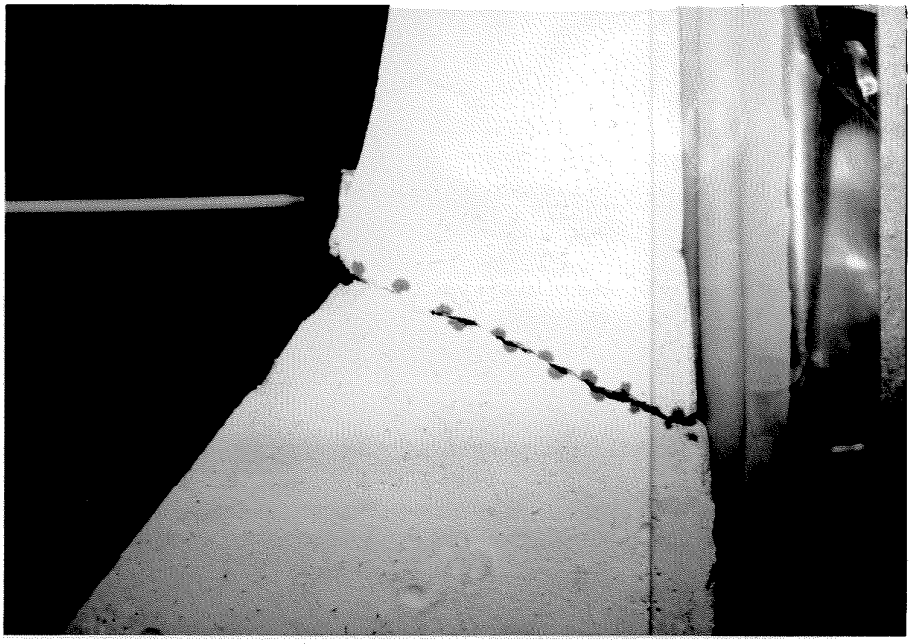

Figure 4.39: (a) Filmed side of second composite after second earthquake test.

Figure 4.39: (b) Opposite side of second composite after second earthquake test.

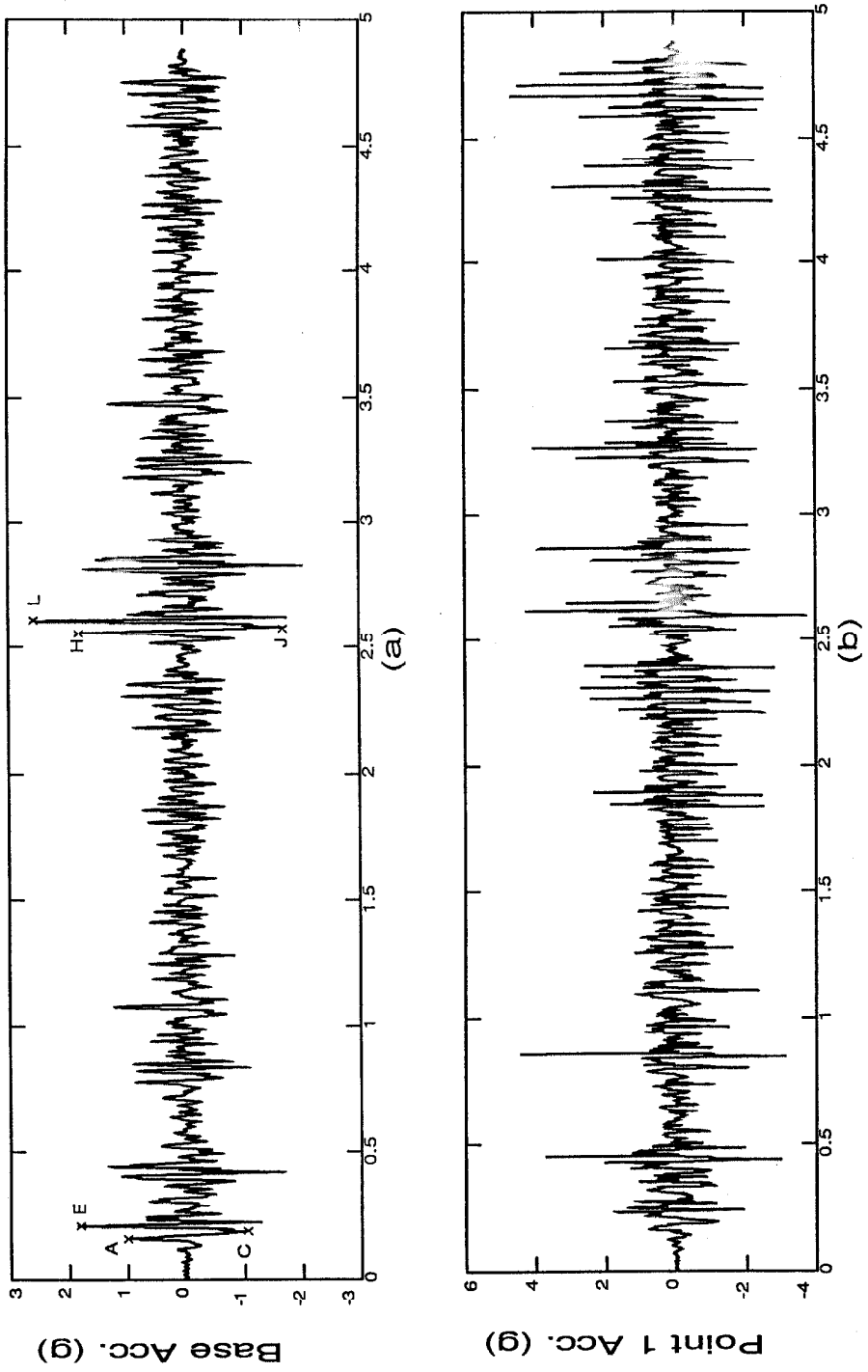

Figure 4.40: (a) Base acceleration and (b) acceleration response at point 1 for the third earthquake test on the second composite model.

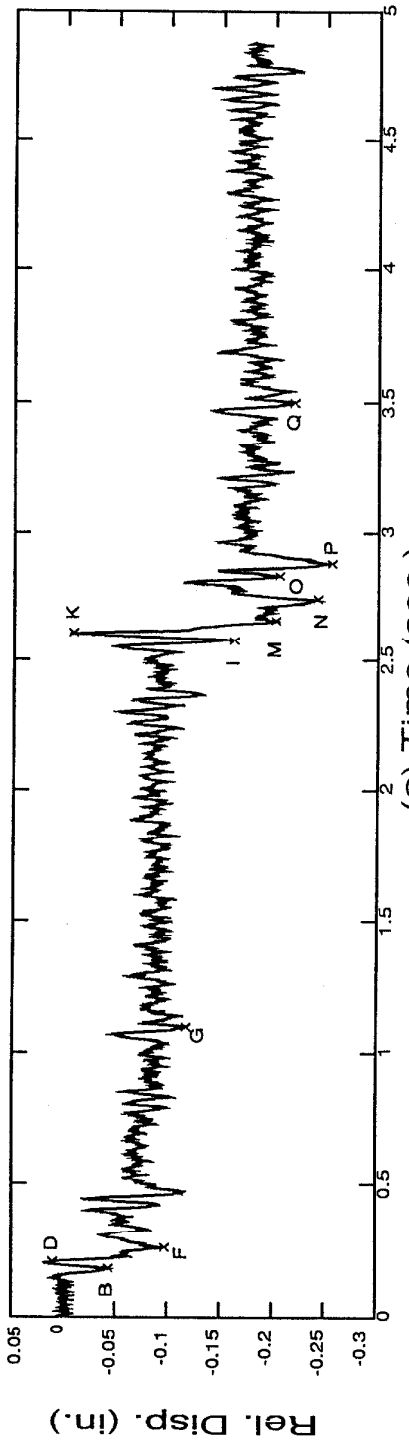

Figure 4.40: (c) Displacement at point 1 relative to the base for the third earthquake test on the second composite model.

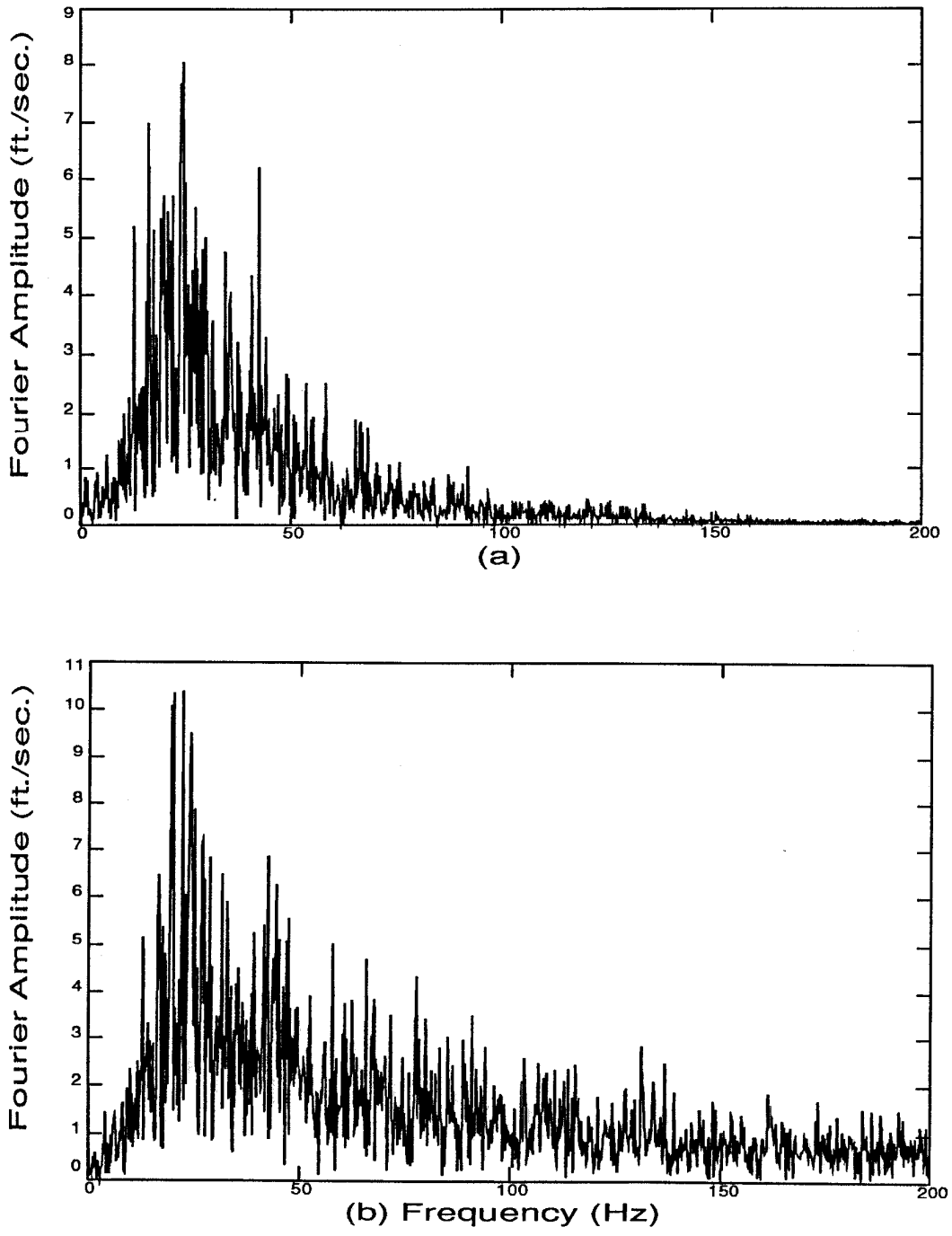

Figure 4.41: Fourier transforms of the base motion (a) and dam response at point 1 (b) for the third earthquake test on the second composite model.

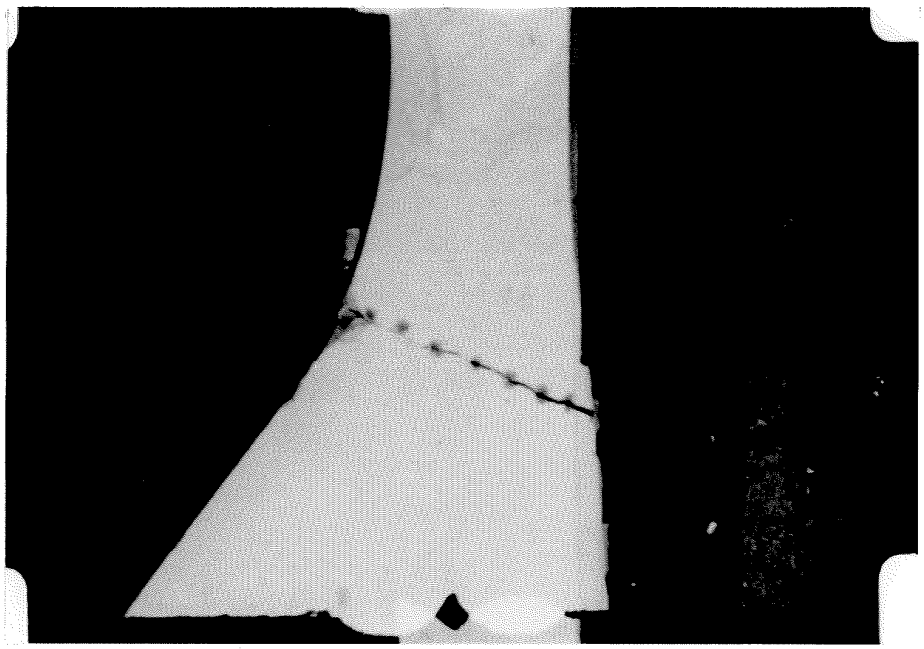

Figure 4.42: (a) t=0.175 sec.

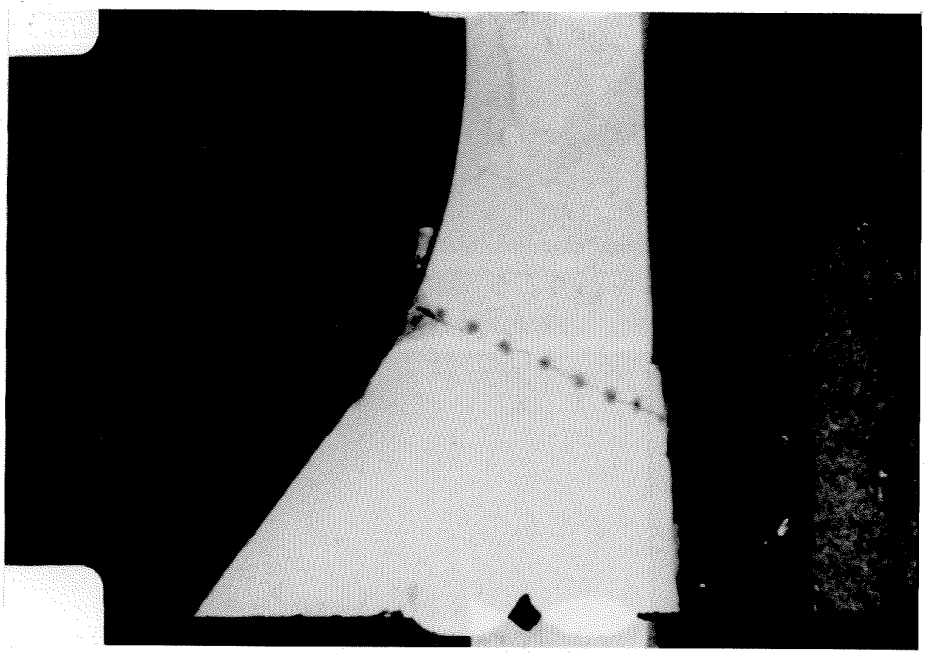

Figure 4.42: (b) t=0.21 sec.

Figure 4.42: Film frames at specific instants of time of the third earthquake test on the second composite model.

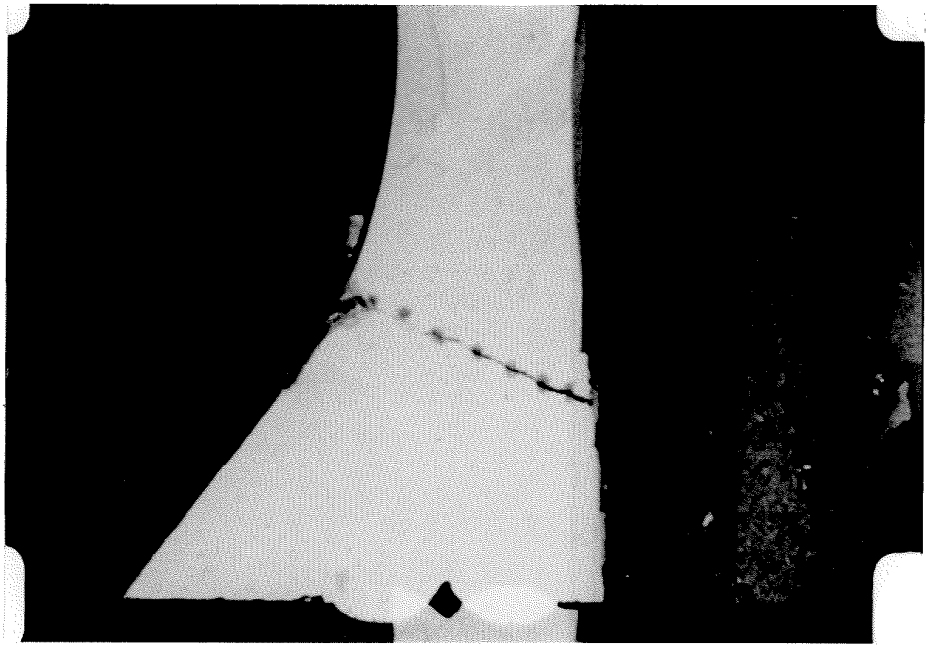

Figure 4.42: (c) t=0.26 sec.

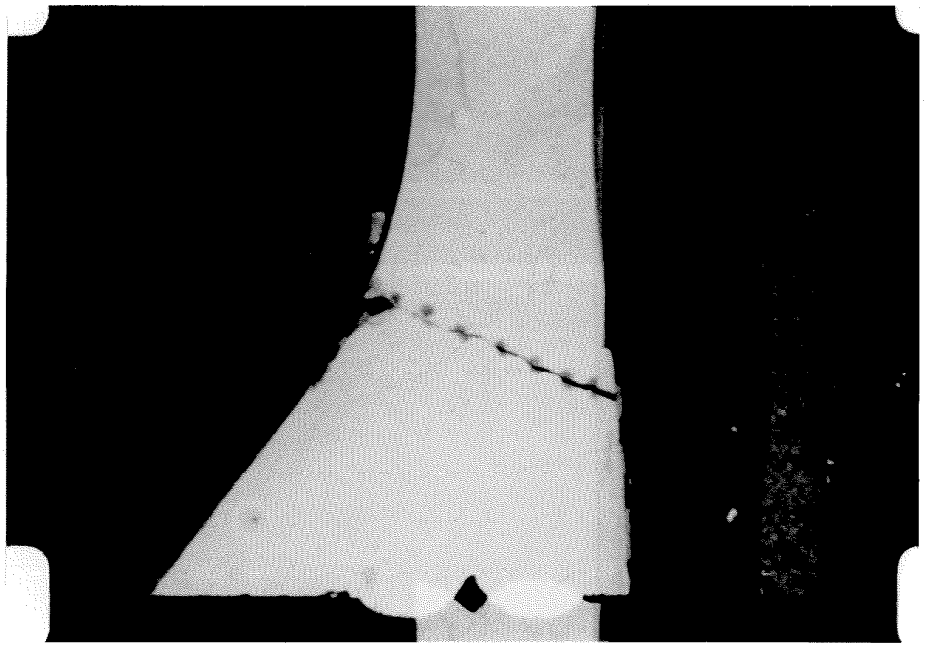

Figure 4.42: (d) t=1.12 sec.

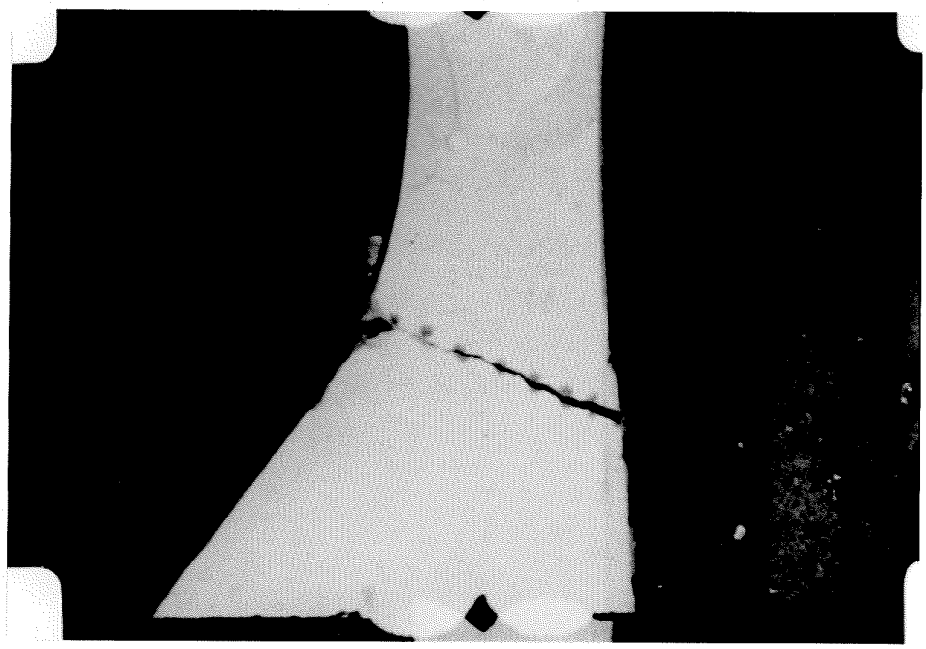

Figure 4.42: (e) t=2.59 sec.

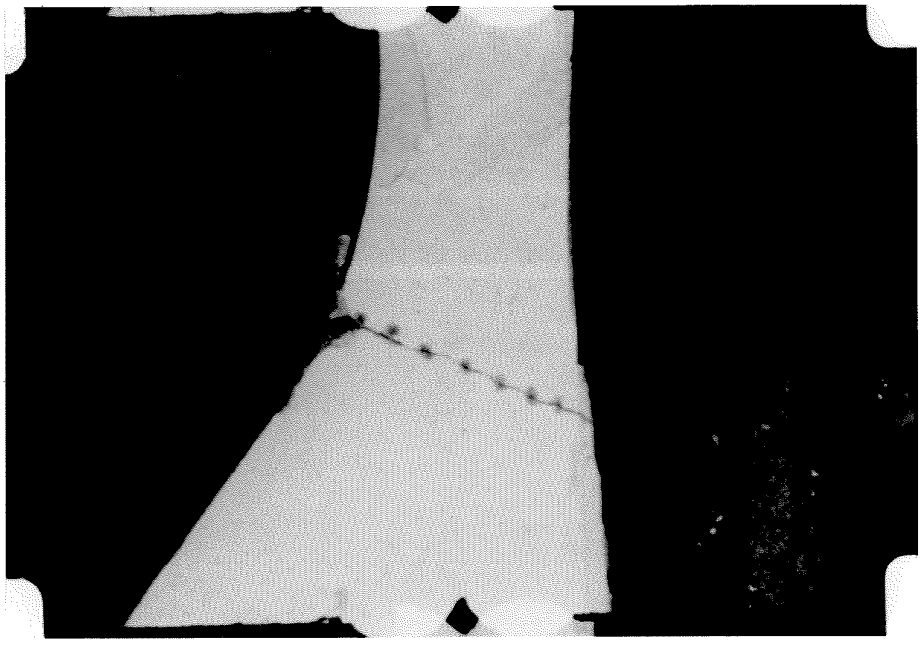

Figure 4.42: (f) t=2.61 sec.

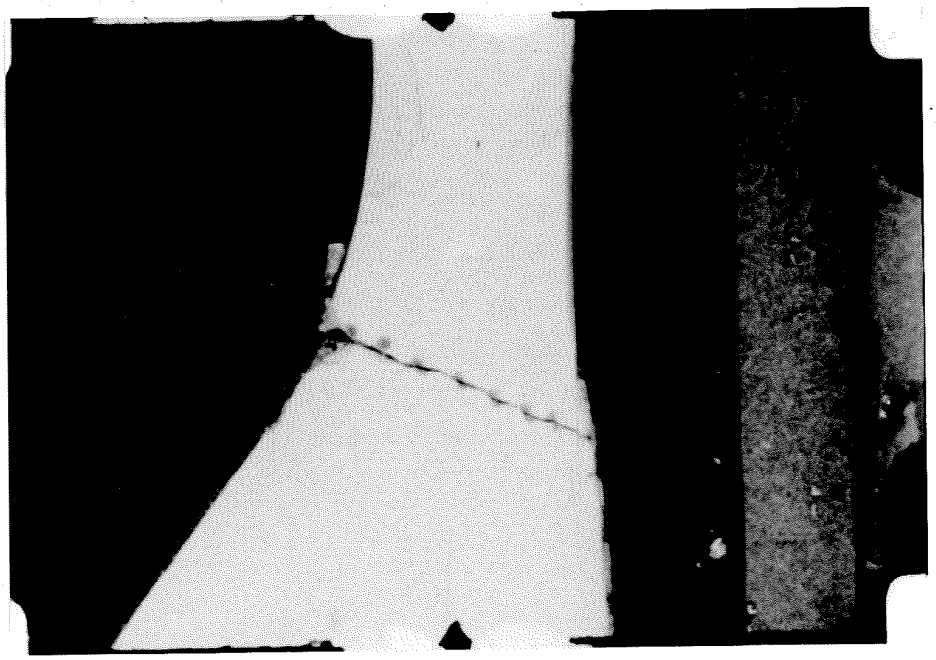

Figure 4.42: (g) t=2.62 sec.

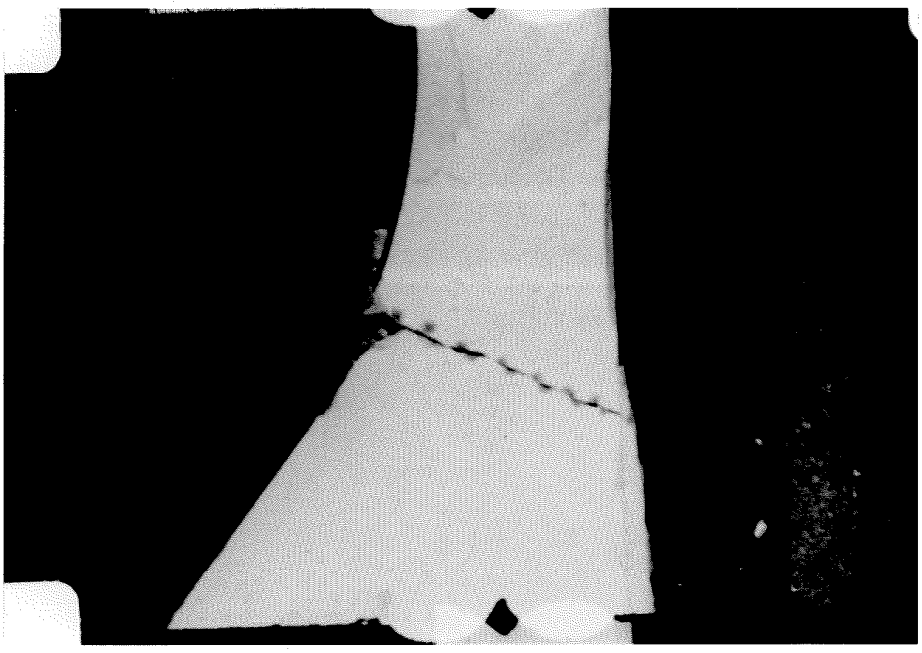

Figure 4.42: (h) t=2.63 sec.

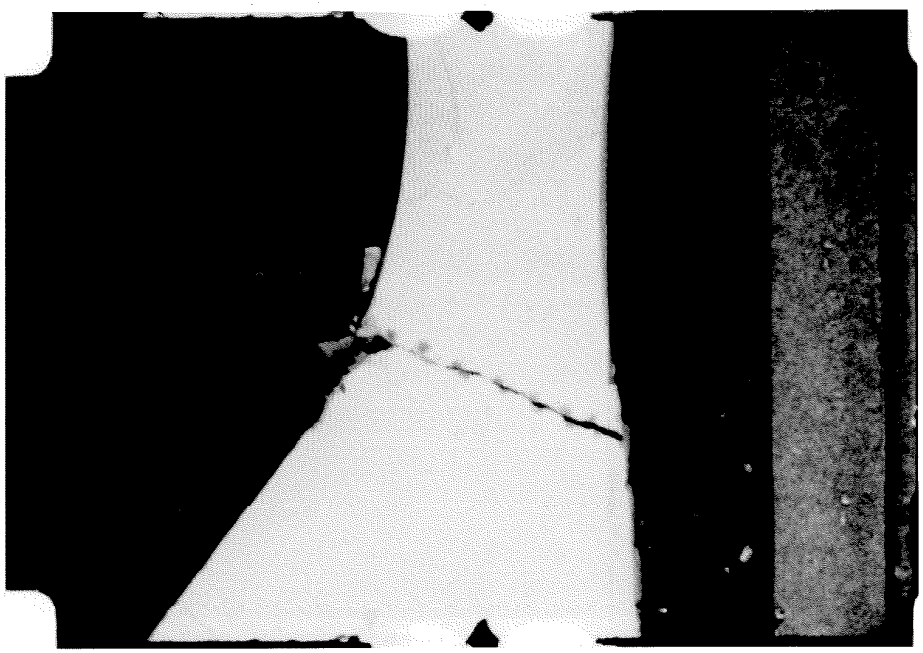

Figure 4.42: (i) t=2.67 sec.

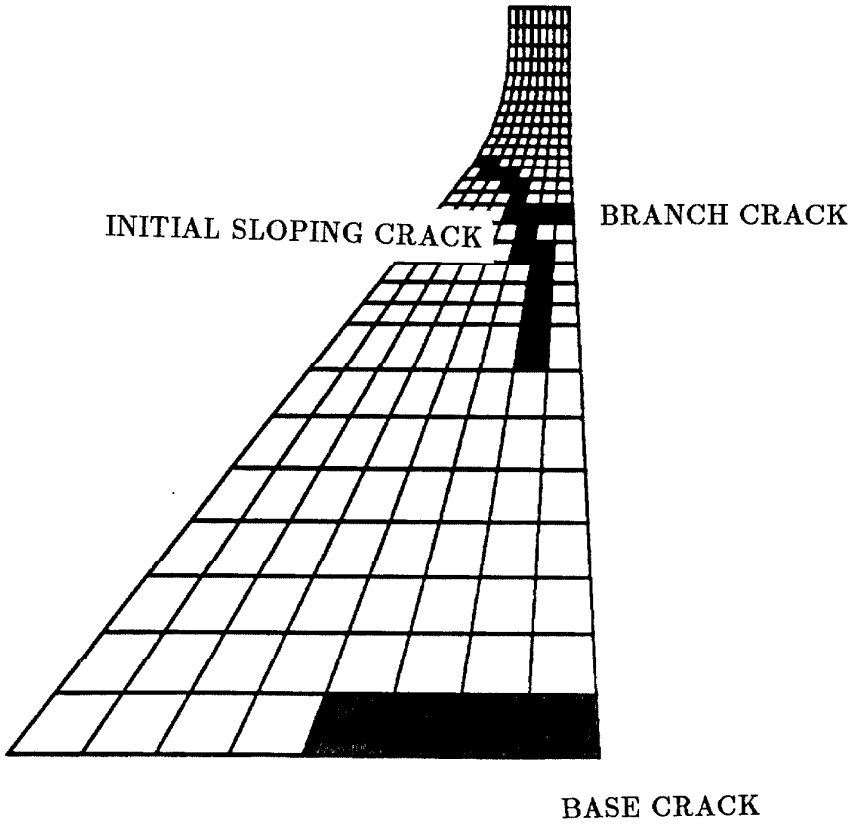

Figure 4.43: Cracking pattern from (8).

Chapter 5

Summary and Conclusions

5.1 Summary

The purpose of these experiments was to investigate the nonlinear seismic response of concrete gravity dams through the testing of small-scale models. The correct modeling of such a structure at a length scale of 115 places stringent requirements on the materials and excitation employed in the tests. Two plaster-based materials were developed to meet the density, strength, and stiffness requirements established by the laws of similitude, as was a polymer-based material which satisfied the density and stiffness requirements. Three models were constructed: a monolithic model made entirely of a plaster-based material and two composite models constructed of a polymer-based lower portion and a plaster- based upper half. Resonance tests were conducted to determine dynamic properties in the linear range. The excitation signal employed in the earthquake tests to study crack initiation and postcracking response was a modified version of the north-south component of the 1940 Imperial Valley earthquake ground motion, applied to the base of the dam model in the stream direction by means of a vibration table. Tests were conducted under full reservoir (height of reservoir = 95% of dam height) and no water conditions. The model geometry was that of Pine Flat Dam, a structure with dimensions typical of concrete gravity dams. The jointed construction

technique used for this class of structure provided some justification for modeling a single vertical monolith of the dam.

Acceleration and displacement transducers recorded the response of the model. In addition, the area of likely crack formation was filmed using high speed, 16 millimeter cameras. Frame by frame analysis of these films and correlation with the response time histories provided insight into the mechanisms of crack initiation and propagation as well as the motion of the top block after crack formation.

5.2 Conclusions and Discussion

1) The feasibility of developing plaster-based materials that approximately satisfy the strength, stiffness, and density requirements for small-scale models at length scales on the order of 1 to 100 was again shown. The density requirement was met by the addition of lead oxide powder in one case and small lead beads (1.6 mm diameter) in another case. Similitude for the critical stress intensity factor is also required but was not investigated; appropriate values for prototype dam concrete are not available.

2) Model construction is greatly hampered by the occurrence of shrinkage cracks that result from the large shrinkage strains experienced by the plaster-based materials upon drying coupled with their low tensile strengths. The material using lead oxide powder required a greater amount of water than the lead bead material and, consequently, suffered more from shrinkage cracks. Lead powder is also much more difficult to work with than the beads and requires extensive safety precautions and effort in cleanup.

3) The polymer-based material developed for use in the lower part of the

dam where cracking was not expected provided excessive damping, which is a significant disadvantage.

4) Tests on the models agreed with results from analyses that the neck region of a concrete gravity dam is most susceptible to cracking.

5) Only for the monolithic model did the high-speed photography provide conclusive evidence of the mechanism of crack propagation from one side of the dam to the other. Interestingly, this crack propagated into the interior on one swing of the dam and extended to the opposite face from the old tip on the other swing.

6) Resulting crack profiles from the three tests were very different. These differences can be attributed to variations among the models in material properties, construction techniques, flaws, excitations, etc. Perhaps this indicates that seismically induced crack profiles in prototype dams will be similarly sensitive. This is an important point due to the dependence of the seismic stability of the dam on the crack profile.

7) In spite of very strong excitations, many of which significantly exceeded typical strong earthquake motions, no failures of the dam models resulted. This was partly due to the favorable profiles of the main cracks: V-shaped for the monolithic model and sloped up in the downstream direction for the composite models. It should be emphasized that favorable profiles may not always result. For example, if the upstream crack in the monolithic model, which initiated horizontally but then turned down in the interior, had continued propagating to a point close to the downstream face, the top block would have been in a vulnerable position, especially with water in the reservoir. Further, it is possible that incorrect scaling of the critical stress intensity factor actually prevented such an occurrence.

8) The absence of any failure in the models should be considered without

forgetting that water penetration into open cracks was prevented by the plastic membrane. Although little is known about the capability of water under pressure to enter cracks during brief openings, a significant penetration would tend to destabilize the top block through uplift pressure. The test results showed that the presence of water tended to increase the openings at the upstream face and decrease them at the downstream face. Also, water penetration would be greatly facilitated by sliding along a rough crack due to dilation of the crack. The combination of an unfavorable crack profile with water penetration could lead to failure under much less intense excitation than used here.

9) Future work is needed to allow water penetration into open cracks. At present, this appears very difficult because the membrane is needed not only to prevent the water from deteriorating the plaster-based model (the upstream face of which could be water-proofed), but to prevent leakage around the model monolith. Of course, proper modeling of water penetration would add a number of fluid material parameters to the similitude requirements, so considerable difficulty could be encountered in the scaling.

10) The stability exhibited by the favorable crack profiles seen in this study suggests the use of a joint, say, with a location similar to the sloping crack that developed in the second composite model, as a defensive design measure against earthquakes. This joint would prevent an unfavorable crack profile from forming, and could be keyed to restrict sliding and sealed with a flexible cap at the upstream face to prevent water penetration. Formation of branch cracks as seen in tests on the monolithic and first composite models could be countered with selective use of steel reinforcement. Such a system could be accurately modeled mathematically and experimentally, without concern over possible water penetration and parameter sensitivity of a seismically induced crack. Of course, other schemes for

defensive design against earthquakes are also feasible, such as reshaping the dam cross-section in order to thicken the neck region, or the use of a light-weight crest structure.

REFERENCES

(1) "Koyna Earthquake December 11, 1967," *Report of the Committee of Experts (UNESCO)*, New Delhi, India, April 1968.

(2) Chopra, A. K. and Chakrabati, P., "The Koyna Earthquake of December 11, 1967 and the Performance of Koyna Dam," *Report No. EERC 71-1*, Earthquake Engineering Research Center, University of California, Berkeley, April 1971.

(3) Shen, C.-K., et. al., "Earthquakes Induced by Reservoir Impounding and their Effect on Hsinfengkiang Dam," *Scientia Sinica*, Volume 17, Number 2, April 1974.

(4) Agbabaian Associates, "Nonlinear Analysis of Norris Dam for Seismic Loads," El Segundo, California, June 1975.

(5) Mlakar, P. F., "Nonlinear Response of Concrete Gravity Dams to Strong Earthquake-Induced Ground Motion," *Computers and Structures*, Volume 26, Numbers 1-2, 1987.

(6) Pal, N., "Nonlinear Earthquake Response of Concrete Gravity Dams," *Report No. EERC 74-14*, Earthquake Engineering Research Center, University of California, Berkeley, December 1974.

(7) Vargas-Loli, L. M. and Fenves, G., "Nonlinear Earthquake Response of Concrete Gravity Dams," Department of Civil Engineering, University of Texas, Austin, December 1987.

(8) El-Aidi, B. "Nonlinear Earthquake Response of Concrete Gravity Dam Systems," *Report No. EERL 88-02*, Earthquake Engineering Research Laboratory, California Institute of Technology, Pasadena, 1988.

(9) Ayari, M. L. and Saouma, V. E., "A Fracture Mechanics Based Seismic Analysis of Concrete Gravity Dams Using Discrete Cracks," *International Conference on Fracture and Damage of Concrete and Rock*, Vienna, July 4-6, 1988.

(10) Droz, Patrice, "Modele numerique du comportement non-lineaire d'ouvrages massifs en beton non arme," *Thesis Number 682*, Department de Genie Civil, Ecole Polytechnique Federal de Lousanne, EPFL 1987.

(11) Skrikerud, P. E. and Bachmann, H., "Discrete Crack Modelling for Dynamically Loaded Unreinforced Concrete Structures," *Earthquake Engineering and Structural Dynamics*, Volume 14, Number 2, March-April 1986.

(12) Niwa, A. and Clough, R. W., "Shaking Table Research on Concrete Dam Models," *Report No. UCB/EERC-80-05*, Earthquake Engineering Research Center, University of California, Berkeley, September 1980.

(13) Norman, C. D., "Dynamic Failure Tests and Analysis of a Model Concrete Dam," *Technical Report SL-86-33*, U.S. Army Waterways Experiment Station, Vicksburg, Mississippi, September 1986.

(14) Raphael, J. M. "Properties of Plaster-Celite Mixtures for Models," *Symposium on Concrete Dam Models*, Paper Number 15, Lisbon, October 14-19, 1963.

(15) Yoshida, T. and Baba, K., "Dynamic Response of Dams," *Proceedings of the 3rd World Conference on Earthquake Engineering*, Volume 2, Auckland, 1965.

(16) Baba, K., "Model and Full-Scale Concrete Dam Studies in Japan," *Proceedings of the International Research Conference on Earthquake Engineering*, Skopje, Yugoslavia, 1980.

(17) Oberti, G. and Lauletta, E., "Dynamic Test on Models of Structures," *Proceedings of the 2nd World Conference on Earthquake Engineering*, Volume 2, Tokyo, 1960.

(18) Oberti, G. and Castoldi, A., "The Use of Models in Assessing the Behavior of Concrete Dams," *Dams and Earthquakes*, Institution of Civil Engineers, London, England, 1981.

(19) Bakhtin, B. M. and Dumenko, V. I., "Seismic Stability of a Concrete Gravity Dam Having a Lightweight Profile," *Gidrotekhnicheskoe Stroitel'stvo (Hydrotechnical Construction)*, Number 5, May 1979.

(20) Lyatkher, V. M., Kapstan, A. D., and Semenov, I.V., "Seismic Stability of the Toktogul Dam," *Gidrotekhnicheskoe Stroitel'stvo (Hydrotechnical Construction)*, Number 2, February 1977.

(21) Gutidze, P. A., "Model Investigations of Seismic Action on the Concrete Arch Dam of the Inguri Hydroelectric Station," *Gidrotekhnicheskoe Stroitel'stvo (Hydrotechnical Construction)*, Number 11, November 1985.

(22) Hall, J. F. "The Dynamic and Earthquake Behavior of Concrete Dams: Review of Experimental Behavior and Observational Evidence," *Soil Dynamics and Earthquake Engineering*, Volume 7, Number 2, April 1988.

(23) Oberti, G. and Lauletta, E., "Structural Models for the Study of Dam Earthquake Resistance," *Proceedings of the 9th International Congress on Large Dams*, Question 35, Istanbul, Turkey, 1967.

(24) Chapuis, J., Rebora, B., and Zimmerman, Th., "Numerical Approach of Crack Propagation Analysis in Gravity Dams During Earthquakes," *Commission Internationale Des Grands Barrages*, Question 57, Lausanne, 1985.

(25) Fanelli, M., Ferrara, G., and Giuseppetti, G., "The Fracture Mechanics Researches Applied to Concrete Coordinated by ENEL to Study the Dam Fracture Problem," *Commission Internationale Des Grands Barrages*, Question 57, Lausanne, 1985.

(26) Linsbauer, H. N., "Fracture Mechanics Models for Characterizing Crack Behavior in Concrete Gravity Dams," *Commission Internationale Des Grands Barrages*, Question 57, Lausanne, 1985.

(27) Rea, D., Liaw, C.-Y., and Chopra, A., "Mathematical Models for the Dynamic Analysis of Concrete Gravity Dams," *Earthquake Engineering and Structural Dynamics*, Volume 3, 1975.

(28) Duron, Z. H., "Experimental and Finite Element Studies of a Large Arch Dam," *Report No. EERL 87-02*, Earthquake Engineering Research Laboratory, California Institute of Technology, Pasadena, September, 1987.

(29) Chakrabati, P. and Chopra, A.K., "Earthquake Response of Gravity Dams Including Reservoir Interaction Effects," *Report No. EERC 72-6*, Earthquake Engineering Research Center, University of California, Berkeley, 1972.

(30) Fenves, G. and Chopra, A. K.,"Simplified Analysis for Earthquake Resistant Design of Concrete Gravity Dams," *Report No. UCB/EERC-85-10*, Earthquake Engineering Research Center, University of California, Berkeley, 1986.

CALIFORNIA INSTITUTE OF TECHNOLOGY

Reports Published
by
Earthquake Engineering Research Laboratory*
Dynamic Laboratory
Disaster Research Center

Note: Numbers in parenthesis are Accession Numbers assigned by the National Technical Information Service; these reports may be ordered from the National Technical Information Service, 5285 Port Royal Road, Springfield, Virginia, 22161. Accession Numbers should be quoted on orders for reports (PB — —). Reports without this information either have not been submitted to NTIS or the information was not available at the time of printing. An N/A in parenthesis indicates that the report is no longer available at Caltech.

1. Alford, J.L., G.W. Housner and R.R. Martel, "Spectrum Analysis of Strong-Motion Earthquake," 1951. (Revised August 1964). (N/A)

2. Housner, G.W., "Intensity of Ground Motion During Strong Earthquakes," 1952. (N/A)

3. Hudson, D.E., J.L. Alford and G.W. Housner, "Response of a Structure to an Explosive Generated Ground Shock," 1952. (N/A)

4. Housner, G.W., "Analysis of the Taft Accelerogram of the Earthquake of 21 July 1952." (N/A)

5. Housner, G.W., "A Dislocation Theory of Earthquakes," 1953. (N/A)

6. Caughey, T.K. and D.E. Hudson, "An Electric Analog Type Response Spectrum," 1954. (N/A)

7. Hudson, D.E. and G.W. Housner, "Vibration Tests of a Steel-Frame Building," 1954. (N/A)

8. Housner, G.W., "Earthquake Pressures on Fluid Containers," 1954. (N/A)

9. Hudson, D.E., "The Wilmot Survey Type Strong-Motion Earthquake Recorder," 1958. (N/A)

---

* To order directly by phone, the number is (703) 487-4650.

10. Hudson, D.E. and W.D. Iwan, "The Wilmot Survey Type Strong-Motion Earthquake Recorder, Part II," 1960. (N/A)

11. Caughey, T.K., D.E. Hudson and R.V. Powell, "The CIT Mark II Electric Analog Type Response Spectrum Analyzer for Earthquake Excitation Studies," 1960. (N/A)

12. Keightley, W.O., G.W. Housner and D.E. Hudson, "Vibration Tests of the Encino Dam Intake Tower," 1961. (N/A)

13. Merchant, H.C., "Mode Superposition Methods Applied to Linear Mechanical Systems Under Earthquake Type Excitation," 1961. (N/A)

14. Iwan, W.D., "The Dynamic Response of Bilinear Hysteretic Systems," 1961. (N/A)

15. Hudson, D.E., "A New Vibration Exciter for Dynamic Test of Full-Scale Structures," 1961. (N/A)

16. Hudson, D.E., "Synchronized Vibration Generators for Dynamic Tests of Full-Scale Structures," 1962. (N/A)

17. Jennings, P.C., "Velocity Spectra of the Mexican Earthquakes of 11 May and 19 May 1962," 1962. (N/A)

18. Jennings, P.C., "Response of Simple Yielding Structures to Earthquake Excitation," 1963. (N/A)

19. Keightley, W.O., "Vibration Tests of Structures," 1963. (N/A)

20. Caughey, T.K. and M.E.J. O'Kelly, "General Theory of Vibration of Damped Linear Dynamic Systems," 1963. (N/A)

21. O'Kelly, M.E.J., "Vibration of Viscously Damped Linear Dynamic Systems," 1964. (N/A)

22. Nielsen, N.N., "Dynamic Response of Multistory Buildings," 1964. (N/A)

23. Tso, W.K., "Dynamics of Thin-Walled Beams of Open Section," 1964. (N/A)

24. Keightley, W.O., "A Dynamic Investigation of Bouquet Canyon Dam," 1964. (N/A)

25. Malhotra, R.K., "Free and Forced Oscillations of a Class of Self-Excited Oscillators," 1964.

26. Hanson, R.D., "Post-Elastic Response of Mild Steel Structures," 1965.

27. Masri, S.F., "Analytical and Experimental Studies of Impact Dampers," 1965.

28. Hanson, R.D., "Static and Dynamic Tests of a Full-Scale Steel-Frame Structures," 1965.

29. Cronin, D.L., "Response of Linear, Viscous Damped Systems to Excitations Having Time-Varying Frequency," 1965.

30. Hu, P.Y.-F., "Analytical and Experimental Studies of Random Vibration," 1965.

31. Crede, C.E., "Research on Failure of Equipment when Subject to Vibration," 1965.

32. Lutes, L.D., "Numerical Response Characteristics of a Uniform Beam Carrying One Discrete Load," 1965. (N/A)

33. Rocke, R.D., "Transmission Matrices and Lumped Parameter Models for Continuous Systems," 1966. (N/A)

34. Brady, A.G., "Studies of Response to Earthquake Ground Motion," 1966. (N/A)

35. Atkinson, J.D., "Spectral Density of First Order Piecewise Linear Systems Excited by White Noise," 1967. (N/A)

36. Dickerson, J.R., "Stability of Parametrically Excited Differential Equations," 1967. (N/A)

37. Giberson, M.F., "The Response of Nonlinear Multi-Story Structures Subjected to Earthquake Excitation," 1967. (N/A)

38. Hallanger, L.W., "The Dynamic Stability of an Unbalanced Mass Exciter," 1967.

39. Husid, R., "Gravity Effects on the Earthquake Response of Yielding Structures," 1967. (N/A)

40. Kuroiwa, J.H., "Vibration Test of a Multistory Building," 1967. (N/A)

41. Lutes, L.D., "Stationary Random Response of Bilinear Hysteretic Systems," 1967.

42. Nigam, N.C., "Inelastic Interactions in the Dynamic Response of Structures," 1967.

43. Nigam, N.C. and P.C. Jennings, "Digital Calculation of Response Spectra from Strong-Motion Earthquake Records," 1968.

44. Spencer, R.A., "The Nonlinear Response of Some Multistory Reinforced and Prestressed Concrete Structures Subjected to Earthquake Excitation," 1968. (N/A)

45. Jennings, P.C., G.W. Housner and N.C. Tsai, "Simulated Earthquake Motions," 1968.

46. "Strong-Motion Instrumental Data on the Borrego Mountain Earthquake of 9 April 1968," (USGS and EERL Joint Report), 1968.

47. Peters, R.B., "Strong Motion Accelerograph Evaluation," 1969.

48. Heitner, K.L., "A Mathematical Model for Calculation of the Run-Up of Tsunamis," 1969.

49. Trifunac, M.D., "Investigation of Strong Earthquake Ground Motion," 1969. (N/A)

50. Tsai, N.C., "Influence of Local Geology on Earthquake Ground Motion," 1969. (N/A)

51. Trifunac, M.D., "Wind and Microtremor Induced Vibrations of a Twenty-Two Steel Frame Building," EERL 70-01, 1970.

52. Yang, I-M., "Stationary Random Response of Multidegree-of-Freedom Systems," DYNL-100, June 1970. (N/A)

53. Patula, E.J., "Equivalent Differential Equations for Non-linear Dynamic Systems," DYNL-101, June 1970.

54. Prelewicz, D.A., "Range of Validity of the Method of Averaging," DYNL-102, 1970.

55. Trifunac, M.D., "On the Statistics and Possible Triggering Mechanism of Earthquakes in Southern California," EERL 70-03, July 1970.

56. Heitner, K.L., "Additional Investigations on a Mathematical Model for Calculation of Run-Up of Tsunamis," July 1970.

57. Trifunac, M.D., "Ambient Vibration Tests of a Thirty-Nine Story Steel Frame Building," EERL 70-02, July 1970.

58. Trifunac, M.D. and D.E. Hudson, "Laboratory Evaluations and Instrument Corrections of Strong-Motion Accelerographs," EERL 70-04, August 1970. (N/A)

59. Trifunac, M.D., "Response Envelope Spectrum and Interpretation of Strong Earthquake Ground Motion," EERL 70-06, August 1970.

60. Keightley, W.O., "A Strong-Motion Accelerograph Array with Telephone Line Interconnections," EERL 70-05, September 1970.

61. Trifunac, M.D., "Low Frequency Digitization Errors and a New Method for Zero Baseline Correction of Strong-Motion Accelerograms," EERL 70-07, September 1970.

62. Vijayaraghavan, A., "Free and Forced Oscillations in a Class of Piecewise-Linear Dynamic Systems," DYNL-103, January 1971.

63. Jennings, P.C., R.B. Mathiesen and J.B. Hoerner, "Forced Vibrations of a 22-Story Steel Frame Building," EERL 71-01, February 1971. (N/A) (PB 205 161)

64. Jennings, P.C., "Engineering Features of the San Fernando Earthquake of February 9, 1971," EERL 71-02, June 1971. (PB 202 550)

65. Bielak, J., "Earthquake Response of Building-Foundation Systems," EERL 71-04, June 1971. (N/A) (PB 205 305)

66. Adu, R.A., "Response and Failure of Structures Under Stationary Random Excitation," EERL 71-03, June 1971. (N/A) (PB 205 304)

67. Skattum, K.S., "Dynamic Analysis of Coupled Shear Walls and Sandwich Beams," EERL 71-06, June 1971. (N/A) (PB 205 267)

68. Hoerner, J.B., "Model Coupling and Earthquake Response of Tall Buildings," EERL 71-07, June 1971. (N/A) (PB 207 635)

69. Stahl, K.J., "Dynamic Response of Circular Plates Subjected to Moving Massive Loads," DYNL-104, June 1971. (N/A)

70. Trifunac, M.D., F.E. Udwadia and A.G. Brady, "High Frequency Errors and Instrument Corrections of Strong-Motion Accelerograms," EERL 71-05, 1971. (PB 205 369)

71. Furuike, D.M., "Dynamic Response of Hysteretic Systems With Application to a System Containing Limited Slip," DYNL-105, September 1971. (N/A)

72. Hudson, D.E. (Editor), "Strong-Motion Instrumental Data on the San Fernando Earthquake of February 9, 1971," (Seismological Field Survey, NOAA, C.I.T. Joint Report), September 1971. (PB 204 198)

73. Jennings, P.C. and J. Bielak, "Dynamics of Building-Soil Interaction," EERL 72-01, April 1972. (PB 209 666)

74. Kim, B.-K., "Piecewise Linear Dynamic Systems with Time Delays," DYNL-106, April 1972.

75. Viano, D.C., "Wave Propagation in a Symmetrically Layered Elastic Plate," DYNL-107, May 1972.

76. Whitney, A.W., "On Insurance Settlements Incident to the 1906 San Francisco Fire," DRC 72-01, August 1972. (PB 213 256)

77. Udwadia, F.E., "Investigation of Earthquake and Microtremor Ground Motions," EERL 72-02, September 1972. (PB 212 853)

78. Wood, J.H., "Analysis of the Earthquake Response of a Nine-Story Steel Frame Building During the San Fernando Earthquake," EERL 72-04, October 1972. (PB 215 823)

79. Jennings, P.C., "Rapid Calculation of Selected Fourier Spectrum Ordinates," EERL 72-05, November 1972.

80. "Research Papers Submitted to Fifth World Conference on Earthquake Engineering, Rome, Italy, 25–29 June 1973," EERL 73-02, March 1973. (PB 220 431)

81. Udwadia, F.E. and M.D. Trifunac, "The Fourier Transform, Response Spectra and Their Relationship Through the Statistics of Oscillator Response," EERL 73-01, April 1973. (PB 220 458)

82. Housner, G.W., "Earthquake-Resistant Design of High-Rise Buildings," DRC 73-01, July 1973. (N/A)

83. "Earthquake and Insurance," Earthquake Research Affiliates Conference, 2-3 April, 1973, DRC 73-02, July 1973. (PB 223 033)

84. Wood, J.H., "Earthquake-Induced Soil Pressures on Structures," EERL 73-05, August 1973. (N/A)

85. Crouse, C.B., "Engineering Studies of the San Fernando Earthquake," EERL 73-04, March 1973. (N/A)

86. Irvine, H.M., "The Veracruz Earthquake of 28 August 1973," EERL 73-06, October 1973.

87. Iemura, H. and P.C. Jennings, "Hysteretic Response of a Nine-Story Reinforced Concrete Building During the San Fernando Earthquake," EERL 73-07, October 1973.

88. Trifunac, M.D. and V. Lee, "Routine Computer Processing of Strong-Motion Accelerograms," EERL 73-03, October 1973. (N/A) (PB 226 047/AS)

89. Moeller, T.L., "The Dynamics of a Spinning Elastic Disk with Massive Load," DYNL 73-01, October 1973.

90. Blevins, R.D., "Flow Induced Vibration of Bluff Structures," DYNL 74-01, February 1974.

91. Irvine, H.M., "Studies in the Statics and Dynamics of Simple Cable Systems," DYNL-108, January 1974.

92. Jephcott, D.K. and D.E. Hudson, "The Performance of Public School Plants During the San Fernando Earthquake," EERL 74-01, September 1974. (PB 240 000/AS)

93. Wong, H.L., "Dynamic Soil-Structure Interaction," EERL 75-01, May 1975. (N/A) (PB 247 233/AS)

94. Foutch, D.A., G.W. Housner and P.C. Jennings, "Dynamic Responses of Six Multistory Buildings During the San Fernando Earthquake," EERL 75-02, October 1975. (PB 248 144/AS)

95. Miller, R.K., "The Steady-State Response of Multidegree-of-Freedom Systems with a Spatially Localized Nonlinearity," EERL 75-03, October 1975. (PB 252 459/AS)

96. Abdel-Ghaffar, A.M., "Dynamic Analyses of Suspension Bridge Structures," EERL 76-01, May 1976. (PB 258 744/AS)

97. Foutch, D.A., "A Study of the Vibrational Characteristics of Two Multistory Buildings," EERL 76-03, September 1976. (PB 260 874/AS)

98. "Strong Motion Earthquake Accelerograms Index Volume," Earthquake Engineering Research Laboratory, EERL 76-02, August 1976. (PB 260 929/AS)

99. Spanos, P-T.D., "Linearization Techniques for Non-Linear Dynamical Systems," EERL 76-04, September 1976. (PB 266 083/AS)

100. Edwards, D.B., "Time Domain Analysis of Switching Regulators," DYNL 77-01, March 1977.

101. Abdel-Ghaffar, A.M., "Studies of the Effect of Differential Motions of Two Foundations upon the Response of the Superstructure of a Bridge," EERL 77-02, January 1977. (PB 271 095/AS)

102. Gates, N.C., "The Earthquake Response of Deteriorating Systems," EERL 77-03, March 1977. (PB 271 090/AS)

103. Daly, W., W. Judd and R. Meade, "Evaluation of Seismicity at U.S. Reservoirs," USCOLD, Committee on Earthquakes, May 1. (PB 270 036/AS)

104. Abdel-Ghaffer, A.M. and G.W. Housner, "An Analysis of the Dynamic Characteristics of a Suspension Bridge by Ambient Vibration Measurements," EERL 77-01, January 1977. (PB 275 063/AS)

105. Housner, G.W. and P.C. Jennings, "Earthquake Design Criteria for Structures," EERL 77-06, November 1977 (PB 276 502/AS)

106. Morrison, P., R. Maley, G. Brady and R. Porcella, "Earthquake Recordings on or Near Dams," USCOLD, Committee on Earthquakes, November 1977. (PB 285 867/AS)

107. Abdel-Ghaffar, A.M., "Engineering Data and Analyses of the Whittier, California Earthquake of January 1, 1976," EERL 77-05, November 1977. (PB 283 750/AS)

108. Beck, J.L., "Determining Models of Structures from Earthquake Records," EERL 78-01, June 1978 (PB 288 806/AS)

109. Psycharis, I., "The Salonica (Thessaloniki) Earthquake of June 20, 1978," EERL 78-03, October 1978. (PB 290 120/AS)

110. Abdel-Ghaffar, A.M. and R.F. Scott, "An Investigation of the Dynamic Characteristics of an Earth Dam," EERL 78-02, August 1978. (PB 288 878/AS)

111. Mason, A.B., Jr., "Some Observations on the Random Response of Linear and Nonlinear Dynamical Systems," EERL 79-01, January 1979. (PB 290 808/AS)

112. Helmberger, D.V. and P.C. Jennings (Organizers), "Strong Ground Motion: N.S.F. Seminar-Workshop," SL-EERL 79-02, February 1978.

113. Lee, D.M., P.C. Jennings and G.W. Housner, "A Selection of Important Strong Motion Earthquake Records," EERL 80-01, January 1980. (PB 80 169196)

114. McVerry, G.H., "Frequency Domain Identification of Structural Models from Earthquake Records," EERL 79-02, October 1979. (PB-80-194301)

115. Abdel-Ghaffar A.M., R.F.Scott and M.J.Craig, "Full-Scale Experimental Investigation of a Modern Earth Dam," EERL 80-02, February 1980. (PB-81-123788)

116. Rutenberg, A., P.C. Jennings and G.W. Housner, "The Response of Veterans Hospital Building 41 in the San Fernando Earthquake," EERL 80-03, May 1980. (PB-82-201377)

117. Haroun, M.A., "Dynamic Analyses of Liquid Storage Tanks," EERL 80-04, February 1980. (PB-81-123275)

118. Liu, W.K., "Development of Finite Element Procedures for Fluid-Structure Interaction," EERL 80-06, August 1980. (PB 184078)

119. Yoder, P.J., "A Strain-Space Plasticity Theory and Numerical Implementation," EERL 80-07, August 1980. (PB-82-201682)

120. Krousgrill, C.M., Jr., "A Linearization Technique for the Dynamic Response of Nonlinear Continua," EERL 80-08, September 1980. (PB-82-201823)

121. Cohen, M., "Silent Boundary Methods for Transient Wave Analysis," EERL 80-09, September 1980. (PB-82-201831)

122. Hall, S.A., "Vortex-Induced Vibrations of Structures," EERL 81-01, January 1981. (PB-82-201849)

123. Psycharis, I.N., "Dynamic Behavior of Rocking Structures Allowed to Uplift," EERL 81-02, August 1981. (PB-82-212945)

124. Shih, C.-F., "Failure of Liquid Storage Tanks Due to Earthquake Excitation," EERL 81-04, May 1981. (PB-82-215013)

125. Lin, A.N., "Experimental Observations of the Effect of Foundation Embedment on Structural Response," EERL 82-01, May 1982. (PB-84-163252)

126. Botelho, D.L.R., "An Empirical Model for Vortex-Induced Vibrations," EERL 82-02, August 1982. (PB-84-161157)

127. Ortiz, L.A., "Dynamic Centrifuge Testing of Cantilever Retaining Walls," SML 82-02, August 1982. (PB-84-162312)

128. Iwan, W.D. (Editor) "Proceedings of the U.S. National Workshop on Strong-Motion Earthquake Instrumentation, April 12-14, 1981, Santa Barbara, California," California Institute of Technology, Pasadena, California, 1981.

129. Rashed, A., "Dynamic Analysis of Fluid-Structure Systems, " EERL 82-03, July 1982. (PB-84-162916)

130. National Academy Press, "Earthquake Engineering Research—1982."

131. National Academy Press, "Earthquake Engineering Research—1982, Overview and Recommendations."

132. Jain, S.K., "Analytical Models for the Dynamics of Buildings," EERL 83-02, May 1983. (PB-84-161009)

133. Huang, M.-J., "Investigation of Local Geology Effects on Strong Earthquake Ground Motions," EERL 83-03, July 1983. (PB-84-161488)

134. McVerry, G.H. and J.L. Beck, "Structural Identification of JPL Building 180 Using Optimally Synchronized Earthquake Records." EERL 83-01, August 1983. (PB-84-162833)

135. Bardet, J.P., "Application of Plasticity Theory to Soil Behavior: A New Sand Model," SML 83-01, September 1983. (PB-84-162304)

136. Wilson, J.C., "Analysis of the Observed Earthquake Response of a Multiple Span Bridge," EERL 84-01, May 1984. (PB-85-240505/AS)

137. Hushmand, B., "Experimental Studies of Dynamic Response of Foundations," SML 83-02, November 1983. (PB-86-115383/A)

138. Cifuentes, A.O., "System Identification of Hysteretic Structures," EERL 84-04, 1984. (PB-240489/AS14)

139. Smith, K.S., "Stochastic Analysis of the Seismic Response of Secondary Systems," EERL 85-01, November 1984. (PB-85-240497/AS)

140. Maragakis, E., "A Model for the Rigid Body Motions of Skew Bridges," EERL 85-02, December 1984. (PB-85-248433/AS)

141. Jeong, G.D., "Cumulative Damage of Structures Subjected to Response Spectrum Consistent Random Process," EERL 85-03, January 1985. (PB-86-100807)

142. Chelvakumar, K., "A Simple Strain-Space Plasticity Model for Clays," EERL 85-05, 1985. (PB-87-234308/CC)

143. Pak, R.Y.S., "Dynamic Response of a Partially Embedded Bar Under Transverse Excitations," EERL 85-04, May 1985. (PB-87-232856/A06)

144. Tan, T.-S., "Two Phase Soil Study: A. Finite Strain Consolidation, B. Centrifuge Scaling Considerations," SML 85-01, August 1985. (PB-87-232864/CC)

145. Iwan, W.D., M.A. Moser and C.-Y. Peng, "Strong-Motion Earthquake Measurement Using a Digital Accelerograph," EERL 84-02, April 1984.

146. Beck, R.T. and J.L. Beck, "Comparison Between Transfer Function and Modal Minimization Methods for System Identification," EERL 85-06, November 1985. (PB-87-234688/A04)

147. Jones, N.P., "Flow-Induced Vibration of Long Structures," DYNL 86-01, May 1986. (PB-88-106646/A08)

148. Peek, R., "Analysis of Unanchored Liquid Storage Tanks Under Seismic Loads," EERL 86-01, April 1986. (PB-87-232872/A12)

149. Paparizos, L.G., "Some Observations on the Random Response of Hysteretic Systems," EERL 86-02. 1986. (PB-88235668/CC)

150. Moser, M.A., "The Response of Stick-Slip Systems to Random Seismic Excitation," EERL 86-03, September 1986. PB-

151. Burridge, P.B., "Failure of Slopes," SML 87-01, March 1987. PB-

152. Jayakumar, P., "Modeling and Identification in Structural Dynamics," EERL 87-01, May 1987. PB-

153. Dowling, M.J., "Nonlinear Seismic Analysis of Arc Dams," EERL 87-03, September 1987. PB-

154. Duron, Z.H., "Experimental and Finite Element Studies of a Large Arch Dam," EERL 87-02, September 1987. PB-

155. Whirley, R.G., "Random Response of Nonlinear Continuous Systems," EERL 87-04, September 1987. PB-

156. Peng, C.-Y., "General Model Identification of Linear and Nonlinear Dynamic Systems," EERL 87-05, September 1987. PB-

157. Levine, M.B., J.L. Beck, W.D. Iwan, P.C. Jennings and R. Relles, "Accelerograms Recorded at Caltech During the Whittier Narrows Earthquakes of October 1 and 4, 1987: A Preliminary Report," EERL 88-01, August 1988. PB-

158. Nowak, P.S., "Effect of Nonuniform Seismic Input on Arch Dams," EERL 88-03, September 1988. PB-

159. El-Aidi, B., "Nonlinear Earthquake Response of Concrete Gravity Dam Systems," EERL 88-02, August 1988. PB-

160. Smith, P.W., Jr., "Considerations for the Design of Gas-Lubricated Slider Bearings," DYNL 89-01, January 1988. PB-